APPLICATION OF SURROGATE MODELING METHOD IN HYBRID SIMULATION FOR UNCERTAINTY PROPAGATION

A Thesis submitted to the faculty of
San Francisco State University
In partial fulfillment of
the requirements for
the Degree

Master of Science

In

Engineering: Structural/Earthquake Engineering

by

Yifeng Xu

San Francisco, California

August 2018

CERTIFICATION OF APPROVAL

I certify that I have read *Application of Surrogate Modeling Method in Hybrid Simulation for Uncertainty Propagation* by Yifeng Xu, and that in my opinion this work meets the criteria for approving a thesis submitted in partial fulfillment of the requirement for the degree Master of Science in Engineering: Structural/Earthquake at San Francisco State University.

Cheng Chen, Ph.D.
Associate Professor

Wensheng Pong, Ph.D.
Professor

APPLICATION OF SURROGATE MODELING METHOD IN HYBRID SIMULATION FOR UNCERTAINTY PROPAGATION

Yifeng Xu
San Francisco, California
2018

Hybrid simulation combines physically tested experimental substructures and numerically modeled numerical substructures that works as an effective solution for structural response prediction under earthquake excitations. The uncertainties from numerical and experimental substructures can lead to large variance on the system response, and it raise the challenge of using full potential of this advanced simulation technique. In this study, Particle Swarm Optimization, Markov Chain Monte Carlo simulation and surrogate modeling techniques are applied for uncertainty propagation. Also, a procedure of experiment design of hybrid simulation is proposed. With the presentation of proposed procedure, good estimation on the uncertainty of system response can be reached with a relatively small number of experiments.

I certify that the Abstract is a correct representation of the content of this thesis.

Chair, Thesis Committee

12/08/2018

Date

ACKNOWLEDGEMENTS

The author appreciatively acknowledges the support from Dr. Cheng Chen, and Dr. Wenshen Pong of San Francisco State University.

TABLE OF CONTENTS

LIST OF TABLES

Table Page

LIST OF FIGURES

Figures Page

Chapter 1: Introduction

1.1 Background on Hybrid Simulation

System-level structural response (e.g. roof displacement, and inter-story drifts) plays an important role in defining system dynamic characteristics. The response of structural system depends on many factors such as seismic characteristics, structure materials, structure systems, soil properties and others. One popular way to simulate the structural response under seismic excitation is to conduct shake table tests.

It can, however, be very expensive to conduct a shake table test. The size and weight of shake table test can raise significant challenges on the space and servo-hydraulic systems in the laboratories. One solution, proposed by researchers to overcome these limitations, is the quasi-static test. This type of test provides a more economical way for laboratories with conventional equipment to perform tests on structures. While on the other hand, the quasi-static test may not fully represent the conditions of seismic excitations, which can lead to the inaccurate system response.

To address this challenge, a new experimental technique named hybrid simulation (hybrid testing) has been developed trying to combine the advantages from economic quasi-static and realistic shake table tests together. Hybrid simulation is an effective solution for structural response prediction under earthquake excitations. It integrates physically-built experimental substructures with numerically modeled analytical substructures thus enables large-scale experiments in size-limited laboratories. The responses of physically tested experimental substructures are measured and feed back to numerical substructures, where computational algorithms are applied for numerical integration.

Figure 1-1 shows the basic framework of a hybrid simulation. In a hybrid simulation, the numerical substructure sends the displacement output to the experimental substructure, and experimental substructure feedbacks the restoring force to the numerical substructure.

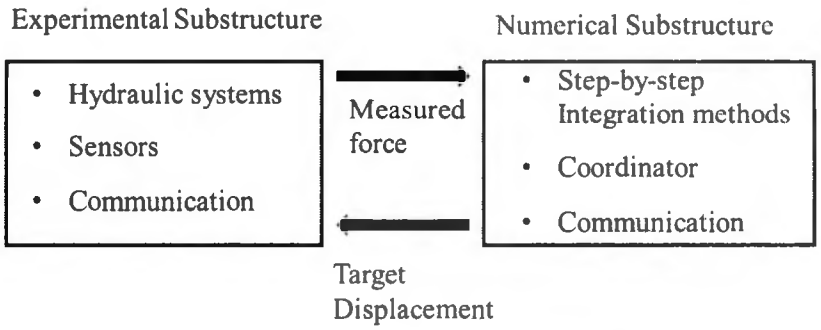

Figure 1-1: Basic frame of a hybrid simulation

1.1.1 History of Hybrid Simulation

This history of hybrid simulation started around 1970 (Takanashi 1975, Hakuno et al. 1969 and Takanashi 1980), with the technique named pseudo-dynamic test. At that time, researchers in Japan proposed the pseudo-dynamic algorithm for experimental evaluation of steel and concrete structural components.

The pseudo-dynamic test focused to solve the equation below:

$$M\ddot{x}(t) + C\dot{x}(t) + r(t) = f_g(t) \qquad (1\text{-}1)$$

In Eq. (1-1), M is the mass matrix; C is the damping matrix; $\ddot{x}(t), \dot{x}(t), r(t), f_g(t)$ are the acceleration, velocity and restoring force of structure and seismic excitation force due to ground motion at time instant t. The pseudo-dynamic test applies the estimate displacement on structure and measure the restoring force. The integration algorithm is applied to the displacement and measured restoring force to modify the displacement.

During that time, experimental facilities have been developed and these facilities allowed the full-scale tests on multi-story structures. Good agreements have been found between the outcome of the pseudo-dynamic tests and the shake table tests (Okada 1980).

More tests have been conducted in U.S. and Japan in the following years, and researchers have paid attentions on verifying the reliability of the test, the improvement of algorithms, the development of control systems, and the experimental error propagation (Shing and Mahin 1983, McClamroch et al. 1981 and Mahin and Williams 1981).

More recently, Dermitzakis and Mahin (1985) introduced the concept of substructures into the pseudo-dynamic test, which leads to the substructure pseudo-dynamic test also known as the substructure test. For the substructure pseudo-dynamic tests, the equation of motion in Eq. (1-1) can be revised as:

$$M\ddot{x}(t) + C\dot{x}(t) + K_a x(t) + r(t) = f_g(t) \qquad (1\text{-}2)$$

In Eq. (1-2),M is the mass matrix, C is the damping matrix and $K_a$is the stiffness matrix of numerical substructure. $\ddot{x}(t), \dot{x}(t), r(t), f_g(t)$ stand for the acceleration, velocity and restoring force of structure and force from ground motion input at time instant t. The difference between the pseudo-dynamic test and the substructure pseudo-dynamic test is that in the substructure pseudo-dynamic test, the restoring force is the sum of $K_a x(t)$ and $r(t)$, and $K_a x(t)$ is calculated and $r(t)$ is measured.

Following that, the development of the energy dissipation device raises the challenge to the hybrid simulation. For example, the viscous damper, rubber bearing, friction damper, and other velocity or acceleration depended components challenges the hybrid simulation with the needs of the tests to be conducted with respect to the time domain. Nakashima et al. (1992) proposed the Real-Time Hybrid Simulation (RTHS) to address the challenge of running simulation in the time domain.

From the studies done by researches, it is concluded that hybrid simulation is a reliable method under the investigation of appropriate experimental and numerical techniques.

1.1.2 Recent Developments in Hybrid Simulation

In recent years, researchers show their interests to develop the hybrid simulation in the fields of the numerical integration algorithms, the time delay compensation for real-time hybrid simulation and the geographically distributed hybrid simulation. Sections below give a brief review of these fields.

1.1.2.1 Geographically Distributed Hybrid Simulation

The geographically distributed hybrid simulation is based on the substructure technique and internet communication, and it enables the distribution of a hybrid simulation into different laboratories (Pan et al. 2006). The geographically distributed hybrid simulation enables the test of large and complex systems. Through the substructure technique, large scale hybrid simulation can be divided and performed in laborites word wide. Also, the fast internet communication enables the data transformation been different laborites in time. Through the presentation of geographically distributed hybrid simulation technique, the cost of hybrid simulation can be reduced as well.

Today, there are many geographically distributed the hybrid simulation platform available worldwide, for example, Network for Earthquake Engineering Simulations (Spencer et al. 2004). The Parallel Pseudo-Dynamic Testing System with the Internet and the Internet-based Simulation for Earthquake Engineering (Pan et al. 2005, Yang et al. 2007 and Wang et al. 2007).

1.1.2.2 Integration Algorithm for Hybrid Simulation

In hybrid simulation, the computer calculates the target displacement and send the displacement to actuators. To calculate the target displacement, the integration algorithms are applied to solve the equation of motion. The numerical integration algorithm used in the hybrid simulation can often be divided into the implicit algorithm and explicit algorithms. A variety of implicit and explicit algorithms can be chosen; however, due to the requirement of iteration, the explicit algorithms are preferred compare to the implicit algorithms. The hybrid simulation conducted by Nakashima et al. (1992), where the central difference method which is an explicit algorithm was selected. Explicit Newmark method also has been applied by researchers, examples can be found in Nakashima et al. (1990) and Magonette (2001). There are also limitations on applying the explicit algorithm, such as the stability limit. One solution is using a smaller integration step to overcome this limitation. Another solution is the development of unconditionally stable explicit algorithms. Chen and Ricles (2008) developed an unconditionally stable explicit algorithm (referred to as CR algorithm hereafter) based on discrete control theory. Also, the approach involves the non-iterative implicit-explicit predictor correct scheme (Hughes et al. 1979) like the Operator Splitting (OS) method developed by Nakashima et al. (1990) can be applied as well.

Explicit methods are preferred in hybrid simulation since no iterations as well as the tangential stiffness or initial stiffness matrix are required. While in some cases, the explicit methods cannot be adapted, the implicit algorithms are preferred. For example, when explicit algorithms cannot be applied due to unstable or the high model frequency. In these scenarios, the implicit algorithms are introduced. The first implicit algorithm is proposed by Thewalt and Mahin (1987) based on HHT $-\alpha$ algorithm (Hilbert et al. 1977). Later, Shin et al. (1991) proposed a scheme based on the method developed by Hilber et al. (1977) and Hughes (1983). More recently, Chen and Ricles (2011) proposed a modified HHT $-\alpha$ algorithm to improve its performance toward nonlinearity. Other applications

based on implicit Newmark method are developed as well, examples can be found by Dorka (2002), Bayer et al. (2005) and Schellenberg et al. (2009).

1.1.2.3 Time Delay Compensation for Real-Time Hybrid Simulation

For time delay compensation, Horiuchi et al. (1999) proposed that time-delay on actuator cab be equivalent to be negative damping on the system. Mercan and Ricles (2007) discussed the impact of time-delay on system stability. Chen and Ricles (2009) developed an inverse method for compensation.

The development of hybrid simulation increases the capability of laboratories for testing. However, there still challenges on hybrid simulation of high-rise building or long-span bridges. Future researches need to be conducted to make this advanced technique reach its full potential.

1.1.3 Research Needs for Hybrid Simulation

There are still the needs of researcher on variety filed to make hybrid simulation the advanced structure testing technique to reach its full potential, for example the uncertainty quantification of hybrid simulation, the development of numerical integration algorithms, the error analysis, the development of control systems, the time-delay compensation of real-time hybrid simulation, and the development of modeling numerical substructures.

1.2 Uncertainty Quantification

1.2.1 Uncertainty in Earthquake Engineering

In recent years, uncertainty quantification becomes an import topic in a variety of disciplines. Many researchers from different background (e.g. structural engineering, mechanical engineering, hydrology, control) have realized the importance of uncertainty quantification. Therefore, researchers have developed a variety of methods that can be used

for uncertainty quantification, including the Monte Carlo Sampling (MCS) method and its variants, perturbation methods, moment equations, Operator-Based Methods, and surrogate modeling methods (Xiu 2010).

In earthquake engineering, the uncertainty the uncertainties from ground motions and uncertainties in structural properties are usually been considered. Uncertainty quantification aims to quantitatively characterize the uncertainties in systems and their effects on system responses. Through this procedure, researches can have access to more information of structural response under earthquakes. With this information, researcher can give more reliable evaluating on structural performance; therefore, the cost of the structure and be reduced, and the safety of the structure can be increased.

1.2.1.1 Uncertainties in Ground Motions

The uncertainties in ground motion can be the record-to-record variability or the synthetic ground motion modal parameters (Deng et al. 2018). For different method of generating synthetic ground motion, the parameters can be different, for example, the method proposed by Hwang et. al (2001) accounts for the seismic source characteristics, local soil conditions and path attenuations, and the method proposed by Rezaeian and Kiureghian (2010) accounts for the evolving intensity, predominant frequency, and bandwidth of the acceleration time-history.

1.2.1.2 Uncertainties in Structural Properties

The structural response uncertainty also coupled with the uncertainties from structural properties (Deng et al. 2018 and Yu and Lu 2012). From Wang's (2012) work, 5 types of structural uncertainties are take into consideration namely (1) material properties, (2) From geometric dimensions, (3) boundary conditions, (4) the complexity of system, (5) applied loads. On example from Yu and Lu's work, a reinforced concrete frame is been used. The

reinforced concrete frame is numerically developed using OpenSees, model parameters including the live load, unit weight of reinforced concrete, concrete strain at maximum strength, concrete cursing strength concrete strain at cursing strength, yield strength and Young's modules of steel component and viscous damping coefficients are considered the structural properties with uncertainties.

1.2.2 Numerical Methods for Uncertainty Quantification

1.2.2.1 Monte Carlo Simulation (MCS)

For uncertainty quantification, Monte Carol simulation is a classic approach; however, this approach requires sampling from high dimensional space, which may lead to the high cost in computation time (Mooney 1997).

Monte Carlo simulation is a class of simulation and has a bunch of variants. This type of simulation depends on the random samples to process numerical results; however, the random samples here always generated through pseudorandom sample generators in computer. Monte Carlo simulation can be applied for any problems with probability interpretation through the approximate numerical integrations through the equation below:

$$\int f(u)du \approx \frac{1}{n}\sum_{i=1}^{n} f(x_i) \qquad (1\text{-}3)$$

where $f(u)$ is the function; n is the number of samples; x_i is the pseudorandom sequence and $f(x_i)$ is the target function.

1.2.2.2 Quasi-Monte Carlo Method (QMCM)

Quasi-Monte Carlo method solves problems and numerical integrations using low-discrepancy sequence. Monte Carol simulation and Quasi-Monte Carlo method both

approximate numerical integrations through the Eqs. (1-3). The difference between MCS and QMCM is that the data set x_i is low-discrepancy sequence for the latter. Through the usage of low-discrepancy, the convergence rate is increased for Quasi-Monte Carlo method, while it has convergence rate around $O(\frac{1}{n})$ and Monte Carlo simulation has convergence rate around $O(\sqrt{n})$ [2]. Two commonly used low-discrepancy sequences are Sobol Sequence (Sobol 1967) and Halton Sequence (Halton 1964).

1.2.2.3 Meta-Modeling Method

1.2.2.3.1 Kriging Method

Another technique that is often applied for uncertainty quantification is the surrogate modelling method, which is also known as meta-modelling method. When applying surrogate modelling methods, good estimation of uncertainty of system outputs can be achieved by smaller number of tests compared with that of Monte Carlo based approach. For example, when evaluating the mean and variance of a system output, different estimations can be found if multiple MC simulations are conducted, while surrogate modelling method can give more consistent estimations.

Kriging method, also known as Gaussian process regression method is first proposed by Krige (1951) and originally designed for mine valuation and later been applied to geo-statistics. Kriging method is a stochastic interpolation method that can give unbiased estimation under given points. Later, Mathero (1963) developed the Kriging method, and following Mathero's work, Sack et al. (1989) extended Kriging method to other fields. Following Sack's work, in recent years, Kriging method has been applied in many fields of study including geo-statistics, meteorology, engineering optimization problems and structural reliability analysis.

1.2.2.3.2 Polynomial Chaos Expansion (PCE) Method

Polynomial Chaos Expansion (PCE) is a popular surrogate modeling method, which is based on Wiener's homogenous chaos theory (Wiener 1938). Isukapalli et al. (1998) proposed that PCE method has higher efficacy than that of MCS method when UQ is conducted under limited sample space. Abbiati et al. (2015) proposed a PCE based approach for uncertainty quantification of the dynamic response from a hybrid simulation accounting for uncertainty from numerical substructures. Sudret and Mai (2013) proposed a PCE based approach for uncertainty quantification for dynamic response of a steel frame structure, and the uncertainty from ground motion characteristics are considered.

1.3 Objectives of This Study

1.3.1 Uncertainties Quantification for Dynamic Response Analysis of SDOF Structures

In current practice, an integration algorithm is utilized to compute the structural response based on deterministic properties of analytical substructures. The value of parameters of the analytical substructures are deterministic based on the simplifications of actual structure by ignoring uncertainties from structural properties; however, the uncertainty from structural properties can be significant, and it can lead to large variance of the system outputs. How to quantify these uncertainties through hybrid simulation with a relatively small amount of experiments presents a challenge to utilize this advanced experimental technique to its full potential.

In this study, Polynomial Chaos Expansion has been applied for uncertainty quantification for the structural maximum, restoring force and acceleration response of a single-degree-of-freedom (SDOF) system under earthquakes. Following that, the influence from different nonlinearities to the performance of Polynomial Chaos Expansion is discussed. Three types

of nonlinearity (Linear Perfect Plastic, Linear Plastic with Harding, Flag Shape Plastic) are considered here.

1.3.2 Experimental Design of Hybrid Simulation of SDOF Structures to Account for Structural Uncertainties

A common approach to account for uncertainties of system output is MC simulation, and the accuracy of estimation highly rely to the number of simulations. However, the cost of conduct one hybrid simulation can be expensive, which make MC simulation not suitable for uncertainty quantification for system response of hybrid simulations. Under the goal of minimized the test cost, or in other word, minimize the required number of tests, an algorithm for guiding experiment design is proposed with the presentation of Low-discrepancy sampling, Particle Swamp Optimization (PSO) and Markov Chain Monte Carlo (MCMC) simulation.

1.3.3 A Framework of Hybrid Simulation to Account for Uncertainties

As shown in Figure 1-2, this study will be part of a framework of hybrid simulation to account for uncertainties from structures and earthquake characters.

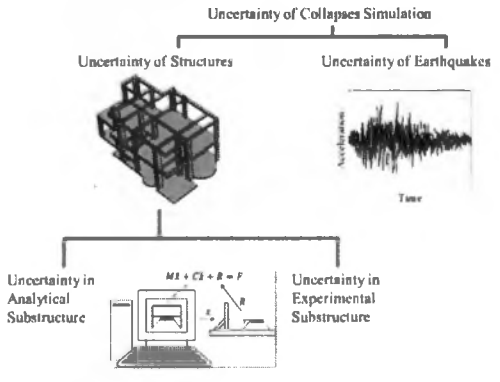

Figure 1-2: Scheme of hybrid simulation account for uncertainties

Nomenclature

In this section, the variables used in Chapter 6 and Chapter 7 are nomenclated here.

NS	Numerical Substructure
PS	Experimental Substructure
NSP	Numerical Substructure Parameter
PSP	Experimental Substructure Parameter
PDF	Probability of Density Function
CDF	Cumulative Distribution Function
$NSP_k^{i(j)}$	The j^{th} parameter of the i^{th} numerical substructure for the k^{th} hybrid simulation
$PSP_k^{i(j)}$	The j^{th} parameter of the i^{th} experimental substructure.
$PSP_{k,PDF}^{i(j)}$	PDF developed through MCMC results of the i^{th} experimental Substructure j^{th} parameter, and k^{th} sample
$PSP_{k,CDF}^{i(j)}$	CDF developed through MCMC results of the i^{th} experimental Substructure j^{th} parameter, and k^{th} sample
$PSP_{k,PSO}^{i(j)}$	PSO result of i^{th} experimental Substructure j^{th} parameter and k^{th} hybrid simulation
$PSP_{k,HC,1}^{i(j)}$	Experimental substructure i, j^{th} parameter in k^{th} hybrid simulation [0,1] based on $PSP_{k,PDF}^{i(j)}$
$PSP_{k,HC,0}^{i(j)}$	Experimental substructure i, j^{th} parameter in k^{th} hybrid simulation [0,1] based on $PSP_{n,PDF}^{i(j)}(n = k - 1)$
$NSP_{k,HC}^{i(j)}$	Numerical substructure i, j^{th} parameter in k^{th} hybrid simulation [0,1] based on $PSP_{k,PDF}^{i(j)}$

Chapter 2: Meta-Modelling through Polynomial Chaos Expansion and Kriging

2.1 Meta-Modeling Background

Numerical simulation plays an important role for seismic risk assessment of structural, and Nonlinear Time History Analysis (NLTHA) is the common solution selected by researchers to get system-level structural response prediction. Through the application of NLTHA, significant computational burden may get involved if the system is complex or the required number of simulations is large. To address this challenge from computational burden, meta-modeling technique is introduced in this study. The meta-modeling technique (i.e., surrogate modeling technique) gives an approximate functional relationship between the target input parameters and system outputs; therefore, replace the time-consuming analysis of the original model. In this chapter, two meta-modeling techniques, Polynomial Chaos Expansion (PCE) and Kriging are introduced, and their performance are evaluated through on example.

2.1.1 History of Meta-Modeling

2.1.1.1 Polynomial Chaos Expansion

PCE is a popular surrogate modeling technique, which based on Wiener's homogenous chaos theory (Wiener 1938). Isukapalli et al. (1998) supports that PCE method has higher efficacy compared to MCS method when UQ is conducted under limited sample space.

Original PCE method uses Hermite polynomial as the basis; therefore, often called Hermite polynomial, and has high performance for systems with random inputs in Gaussian distribution. Cameron and Martin (1947) showed that Hermite polynomial can converge with any arbitrary process with finite second moments. Ghanem (1999) further indicated that Hermite polynomial has an exponential type of optimal convergence rate towards random variables with the Gaussian distribution. For random variables with distribution

type close to Gaussian distribution, they can be transferred to Gaussian distribution through equal probability method, and then treated with Hermite polynomial. However, original PCE method has difficulty dealing with some situations. Therefore, researchers proposed variants of original PCE method to address these challenges. For random variables other than Gaussian distribution, Xiu and Karniadakis (2002) proposed a generalized PCE (gPCE) method, which extends Wiener's approach from Hermite polynomial to continuous and discrete polynomials. Wan and Karniadakis (2006) proposed multi-element generalized PCE (ME-gPCE) for problems involving long-term integration, or problems with discontinuous random space. Lucor and Karniadakis (2004) proposed an adaptive generalized PCE approach for problems require a high order or high dimensionality PCE.

Marelli and Sudre (2017) indicated that the PCE uses representation of a system on a properly selected basis to make functional approximation, which can be shown below:

$$\mathrm{y}(\mathrm{x}) \approx y^{pc}(x) = \sum_{a \in A} c_a \psi_a(x) \qquad (2\text{-}1)$$

where $y^{pc}(x)$ is the PCE meta-model; $\mathrm{y}(x)$ is the original system; c_a is the coefficients of PCE; $\psi_a(x)$ is the multivariate orthonormal polynomials. Table 2-1 shows some commonly used orthogonal polynomials with respect to different types of input variables.

Table 2-1: Commonly used orthogonal polynomials

Type of variable	Orthogonal polynomials
Uniform	Legendre
Gaussian	Hermite
Gamma	Laguerre
Beta	Jacobi

After the multi-index of multivariate polynomials is selected based on the distribution type of training set, the corresponding coefficients are computed based on either intrusive or non-intrusive approach.

2.1.1.2 Kriging

Kriging is a method that use the Gaussian process indexed by the system input to approximate the output of the system (Schobi et al. 2017). Kriging, also known as Gaussian process modeling, is a stochastic interpolation algorithm to estimate a variable at an unmeasured location from observed values at surrounding locations based on the regression on the observations.

The theoretical basis of the Kriging method was developed by Matheron (1951). Based on Matheron's work, Sack et al. (1989) proposed a Kriging model with a regression part and a random process in order to attain higher accuracy. Lophaven et al. (2002) developed a Matlab toolbox DACE for applying the Kriging method to computer models. Kaymaz (2015) pointed out that for problems involving experimental design with small sample space, or Kriging model with improperly select coefficients, the Kriging method does not show the higher accuracy of the results when compared with the response surface method. In order to address this challenge, Li (2013) proposed a variant of the original Kriging method, and other researchers proposed different optimizations for Kriging coefficients selection, such as Liu et al. (2013), Li et al. (2014), and Richad et al. (1997).

2.1.2 Application of Meta-Modeling for Engineering Analysis

PCE and Kriging method has received the attention from researches and are applied to different disciplines in engineering. The application of PCE methods includes reliability analysis and uncertainty propagation. For example, Sudret and Mai (2013) applied PCE to compute the seismic fragility of a steel frame structure subjected to earthquakes. Abbiati et. al (2015) applied PCE for uncertainty propagation and global sensitivity analysis in

hybrid simulation. The application of Kriging method ranges from mine valuation to many other engineering displaces. For example, Kriging method has been applied to reliability analysis (Kaymaz 2005, Wang and Shafieezadeh 2018 and Xie et al. 2007). The application of Kriging method for design optimization for aircraft and trains (Liu et al. 2012, Hang et al. 2007 and Yao et al. 2013) and reliability-based design optimization (Doh et al. 2018). Gidaris et al. (2015) use Kriging for seismic assessment.

PCE and Kriging method shows high accuracy on predicting nonlinear behavior; therefore, became one of the popular meta-modeling techniques.

2.2 Meta-Modeling through PCE

2.2.1 Calculation of PCE Coefficients

Two types of methods are commonly used for PCE coefficients calculation, namely the intrusive method and non-intrusive method. Sections below gives an overview of these two methods.

2.2.1.1 Intrusive Methods

Galerkin projection is an intrusive method for PCE coefficient calculation. This method requires the reformation of governing equations to determine the PCE coefficients, and it is used for original PCE (Onorato et al. 2010). However, this method is not suitable for problems involving significant nonlinearity (Crestaux et al. 2009). Therefore, in this study the intrusive method will not be applied to calculate PCE coefficients.

2.2.1.2 Non-Intrusive Methods

Intrusive approach requires the reformation of the equations and has difficulty dealing with problems involving high nonlinearity. Therefore, this study will mainly focus on using non-intrusive method to calculate PCE coefficients. Two commonly used non-intrusive

methods are projection method and regression method. The projection method can be expressed as:

$$c_a = \mathrm{E}[\psi_a(\mathrm{x}) \cdot \mathrm{y}(\mathrm{x})] \qquad (2\text{-}2)$$

Based on the orthonormality of the polynomial basis, the computation of corresponding coefficients reduces to the expectation values in Eq. *(2-2)*.

The PCE coefficients computation using regression method can be expressed as below:

$$c_a = \arg min \frac{1}{N} \sum_{i=1}^{N} (y(x^i) - \sum_{a \in A} c_a \psi_a(x^i))^2 \qquad (2\text{-}3)$$

The coefficients can be obtained by minimizing the Eq. *(2-3)*, where x is the samples of random inputs.

2.2.2 Determination of PCE Order for Meta-Modelling

2.2.2.1 Global Sensitivity Analysis

The order of PCE can be selected based on multiple criterions, and global sensitivity analysis result is one of them. Besides the mean value and variance of the system output, it is often important to analyze the contributions from stochastic input random variables to the variance of system outputs as well. This is also known as global sensitivity analysis (GSA). GSA helps identify the influence of individual input variable on the output variance. In this study, Sobol indices are selected for GSA.

2.2.2.2 Total and First Order Sobol Index

For the evaluation of the influence from variables to the system output, the Sobol' index (Sobol 2001) is selected in this study.

The Sobol' decomposition is defined by:

$$f(:x) = f_0 + \sum_{s=1}^{n} \sum_{i_1 < \cdots < i_s}^{n} f_{i_1 \ldots i_s}(x_{i_1}, \ldots, x_{i_s}) \quad (2\text{-}4)$$

where $1 \leq i_1 .. i_s \leq n$. The constant D and $D_{i_1 \ldots i_s}$ are calculated as following:

$$\mathrm{D} = \int f(x)^2 dx - f_0^2 \quad (2\text{-}5)$$

$$D_{i_1 \ldots i_s} = \int f^2_{i_1 \ldots i_s}(x_{i_1}, \ldots, x_{i_s}) dx_{i_1} \ldots dx_{i_s} \quad (2\text{-}6)$$

where f_0 is defined as

$$f_0 = \int f(x) dx \quad (2\text{-}7)$$

The Sobol indices $S_{i_1 \ldots i_s}$ can be calculated as

$$S_{i_1 \ldots i_s} = \frac{D_{i_1 \ldots i_s}}{D} \quad (2\text{-}8)$$

All the Sobol indices are nonnegative and their sum is equal to 1. The higher S value is, the more influence from this variable to the system output is. In this study, both first order and total Sobol indices were used to evaluate the performance of PCE technique. Using Monte Carlo based method to calculate Sobol indices estimation often requires large number of samples (Sobol 1993). A PCE based method (Sudret 2008) gives effective solution for Sobol indices calculation. By post-processing of the polynomial coefficients, the Sobol indices can be calculated without the need of extra samples.

The total Sobol index is the measure of the influence of x_{i_s} under the presentation of all other variables. It can help researchers to have an overall view of the influence of variables on the variance of system output. The sum of total Sobol indices can be greater than 1.

The first order Sobol' index is the measure of the influence of x_{i_s} alone on the system output. The sum of first to higher order Sobol' index is equal to 1.

2.3 Meta-Modeling though Kriging

Kriging methods start with the assumption that output $y(x) \equiv M(x)$ is a sample path of a Gaussian stochastic process Y (Dubourg et al. 2011). The Y has unknown mean value and covariance function that will be determined by input $X = [x^i, i = 1,2 \dots n]$ and output $Y = [y^i = M(x^i), i = 1,2 \dots n]$.

A Kriging surrogate model can be written as:

$$y(x) \approx y^K(x) = \sum_{i=1}^{P} \beta_i f_i(x) + Z(x) = f(x)^T \beta + \sigma^2 Z(x, w) \qquad (2\text{-}9)$$

where $f(x)^T \beta$ is the regression part with coefficients $\beta_i, i = 1,2 \dots n$, and selected basis functions $f_i, i = 1,2 \dots, n$; $Z(x, w)$ is a stationary Gaussian process with zero mean, constant variance σ^2, and its probability space is represented by w, which is determined by a correlation function R, and its hyper-parameters θ. The correlation function can be described as below:

$$R = R(x, x'; \theta) \qquad (2\text{-}10)$$

Lataniotis et al. (2017) pointed out that obtaining a Kriging model is the process of selecting basis functions, regression coefficients, correlation function, and its hyper-parameters. These values can be computed by maximum likelihood method, which is shown below:

$$L(y|\beta,\sigma^2,\theta) = \frac{\det(R)^{-\frac{1}{2}}}{(2\pi\sigma^2)^{\frac{l}{2}}} \exp\left[-\frac{1}{2\sigma^2}(y - F\beta)^T R^{-1}(y - F\beta)\right] \qquad (2\text{-}11)$$

Similar to PCE model formation, UQLab is used for to format the Kriging model.

2.4 Software Framework UQLab

In this study, a Matlab based uncertainty quantification frame work named UQLab is used for PCE analysis and Kriging analysis (Marelli and Sudret 2014). UQLab is a platform that offers build-in analysis and algorithms. It supports the analysis using surrogate-modeling, rare even estimation, global sensitivity analysis and Bayesian technique for invers problem. The features of using surrogate-modeling and global sensitivity analysis are used in this study.

2.5 Meta-Modelling of a Structure Subjected to Earthquakes

In this section, the meta-modeling techniques are applied to estimate the maximum system response, maximum restoring force and maximum system acceleration of a structure subjected to selected ground motion. Figure below shows the structure developed in OpenSees (OpenSees 2010).

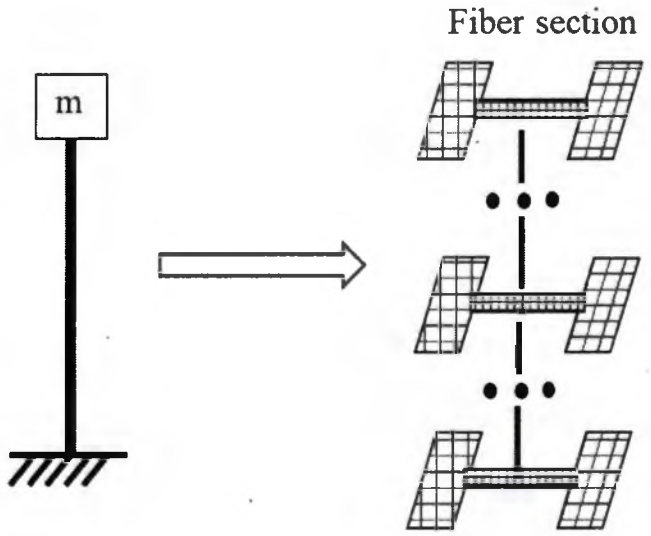

Figure 2-1: Schematic of the OpenSees Model

The target structure is developed in OpenSees by fiber section approach using the Bouc-Wen material (Baber and Noori 1985). The α and β value, which control the shape of hysteresis behavior of the Bouc-Wen material are selected to be the input parameters for meta-modeling procedure. The fiber section size is selected to be the geometry size of the W36X150 and W30X108 steel section, and the mass is assigned to locate at the top of the column. Also, the Rayleigh damping is assigned to the column. The number of fibers is 8 along the web depth, 2 along the web thickness, 8 along the flange width and 2 along the web thickness.

2.5.1 PCE Modelling

In this section, PCE method is applied to predict the maximum displacement, restoring force and acceleration response of the structure developed in previous section. The structure is subject to the 1994 Northridge earthquake recorded at Beverly Hills-12520 Mulhol station with the peak ground acceleration of 0.516g. The sample number of PCE training set is defined to be 64, and Sobol sequence-based sampling procedure is used.

2.5.1.1 PCE Modelling of Maximum Structural Response

Figure below shows the comparison between PCE perdition results and OpenSees simulation results.

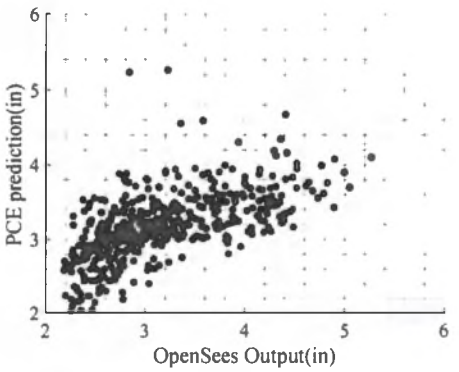

Figure 2-2: PCE prediction of maximum structural response

From figure above, it can be observed that PCE can predict the maximum structural response while the accuracy of the prediction on maximum structural response is lower compare to the prediction on maximum structural response and restoring force from the following sections. It can be explained that under the same training set of input x, the training set y which are the maximum acceleration, maximum structural response and restoring force are different, and PCE method is a sample-based method. The performance of PCE on different structural response can be different.

2.5.1.2 PCE Modelling of Maximum Restoring Force

In this section, PCE method is applied to predict the maximum restoring force of the structure. Figure below shows the comparison between PCE perdition results and OpenSees simulation results.

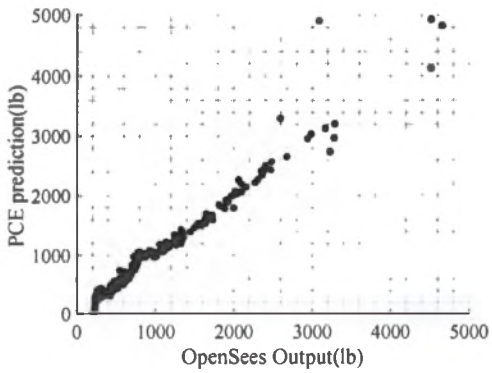

Figure 2-3: PCE prediction of maximum restoring force

From the figure, good agreement can be observed on maximum restoring force of the structural under selected earthquake can be observed. Also, it can be observed that PCE model can give more accurate prediction of maximum restoring force than maximum structural response by comparing to Figure 2-2.

2.5.1.3 PCE Modelling of Maximum Acceleration Response

In this section, PCE method is applied to predict the maximum acceleration response of the system. Figure below shows the comparison between PCE perdition results and OpenSees simulation results.

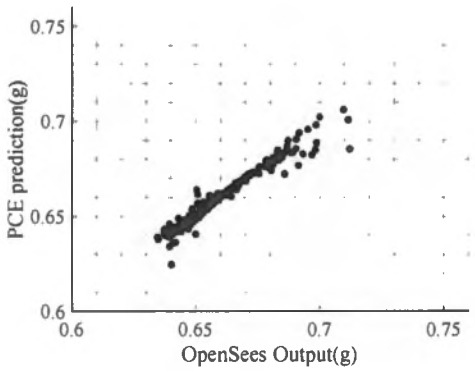

Figure 2-4: PCE prediction of maximum acceleration response

Similar to the prediction on maximum restoring force, the PCE model has good performance on predicting the maximum structural response.

2.5.2 Kriging Modelling

2.5.2.1 Kriging Modelling of Maximum Structural Response

In this section, the kriging method is been applied to predict the maximum structural response of the SDOF system under seismic excitation.

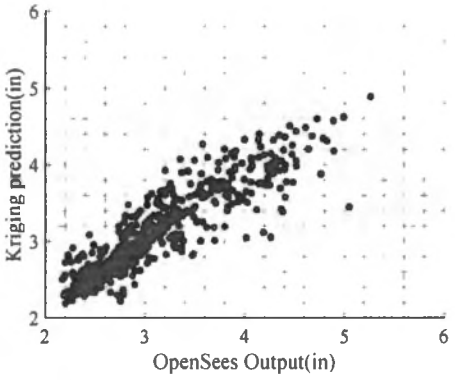

Figure 2-5: Kriging prediction of maximum structural response

It can be observed that kriging can be applied to predict the maximum structural response. Also, from the comparison between Figure 2-2 and Figure 2-5, it can be observed that under the same number of training sample, Kriging model has better performance on predicting the maximum structural response compare to PCE model.

2.5.2.2 Kriging Modelling of Maximum Restoring Force

In this section, the kriging method is applied to predict the maximum restoring force of the SDOF system under seismic excitation.

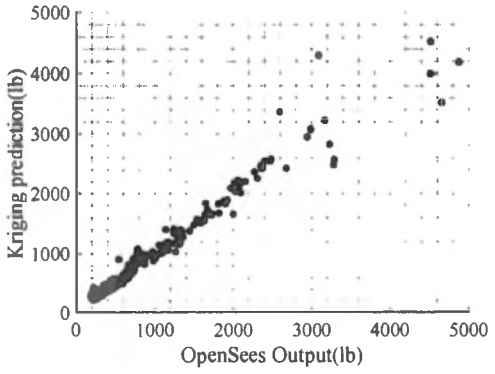

Figure 2-6: Kriging prediction of maximum restoring force

From figure above, it can be observed that with the 64 training samples, the developed Kriging model can give accurate prediction on the maximum restoring force of the system. Also, by comparing Figure 2-3 and Figure 2-6, it can be observed that both Kriging model and PCE model has good accuracy on predicting the maximum restoring force.

2.5.2.3 Kriging Modelling of Maximum Acceleration Response

In this section, the kriging method is applied to predict the maximum acceleration response of the SDOF system under seismic excitation.

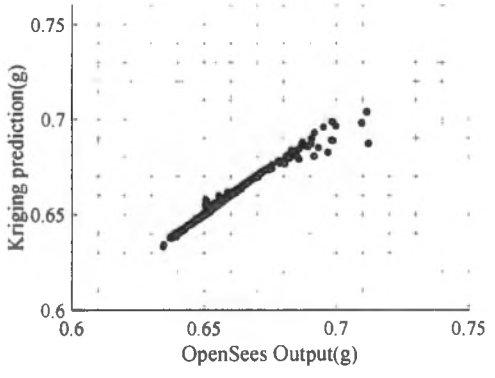

Figure 2-7: Kriging prediction of maximum acceleration response

From the figure above and the comparison between Figure 2-4 and Figure 2-7, similar observation can be made as Kriging model and PCE model both has good accuracy on predicting the maximum acceleration response.

2.6 Summary

In this chapter, two meta-modeling technique are introduced. To validate the performance of PCE method and kriging method, a structure is developed in OpenSees using fiber section and Bouc-Wen material. This SDOF structural is then subjected to 1991 Northridge earthquake, and the system output of interest are the maximum structural response, maximum restoring force, and the maximum acceleration response. 64 samples are selected based on Sobol' sequence, and the dynamic analyses using these 64 samples are conducted. The system parameters are the mass, damping coefficient, α and β value for Bouc-Wen model, and the combination of system parameters with the system outputs generate the train-set of meta-modeling process using PCE and Kriging methods. Three PCE models and three Kriging models are developed using the training sets. The accuracies of the meta-models are validated using another 500 samples generated using Monte Carlo sampling method. For the newly generated 500 samples, from the comparison between PCE and Kriging model predictions and dynamic analysis results using OpenSees, good agreement can be observed. However, for different system outputs, the performance of PCE and Kriging can be different. Both PCE and Kriging method shows better performance on predicting maximum restoring force and maximum acceleration response. Also, comparing to PCE model, Kriging model shows better performance on predicting maximum structural response. Through the comparison, it supports that PCE and Kriging method can be applied to predict the maximum structural response, maximum restoring force, maximum acceleration response.

Chapter 3: Sampling for Uncertainty Quantification

3.1 Introduction

In this chapter, several sample methods are introduced for uncertainty quantification, and the performance of these sampling methods are evaluated through the estimation on the mean and standard deviation of the maximum structural response of the structure developed in Chapter 2 under earthquake excitation. This chapter focusses on two types of sampling methods namely sequential sampling and adaptive sampling. For sequential sampling, a pre-defined sample number is required to generate the sample and one cannot give information of the samples at any dimensions. For adaptive sampling, the sample set is generated through greedy enrichment, and one can give information of samples at any dimensions.

3.1.1 Definition of Sampling

Sampling is a process of taking sets from a statistical population. Under the same sample size, difference samples can be obtained by using different sampling methods. In this chapter, different sampling methods based on different criterion are introduced, and the performance of samples selected through different sample methods are evaluated using a SDOF structural.

3.1.2 Definition of Discrepancy

Discrepancy can be considered as a measurement of the "uniform level" of samples. A sequence has discrepancy has the discrepancy closer to zero means the sequence is more equally distributed in the space. Researchers proposed different types of discrepancy including star discrepancy, F discrepancy and GF discrepancy. Regardless the types of different discrepancy, the sequence with low discrepancy ensure the level of uniform is high. To get sample set with low discrepancy, there are sequence available with low discrepancy nature, for example, Sobol sequence and Halton sequence. Also, there are

algorithms to enrich sequence with new samples to make the updated sequence has lowest discrepancy, for example, the space-filling Max-min algorithm (Pronzato 2017) and other sampling greedy algorithms focus on minimize the discrepancy.

3.1.3 Types of Discrepancy used in Engineering Research

For the usage of discrepancy in engineering research, for example, structural and mechanical engineering, the most common application is in quasi-Monte Carlo simulation. Once again, as mentioned before, Quasi-Monte Carlo method is a method using low-discrepancy sequence to solve problem. The only difference between normal Monte Carlo simulation and quasi-Monte Carlo simulation is that quasi-Monte Carlo using low-discrepancy sequence as samples selected from sample space. It helps increasing the convergence rate from $O(\sqrt{n})$ to $O(\frac{1}{n})$ (Asmussen and Glynn 2007). The performance of quasi-Monte Carlo method is studied (Morokoff and Caflisch 1995) using different low discrepancy sequence, for example Sobol sequence and Halton sequence. It shows that Halton sequence has good performance when the dimension of variables is below 6, and Sobol sequence has better performance when the dimension of variables is high comparing when the dimension is low.

Also, low discrepancy sequence also been used for the construction of meta-modeling techniques. For example, the selection of training data set for PCE coefficient calculation. Through the presentation of training sets selected using low-discrepancy samples, better accuracy of the constructed meta-model can be overserved. In computer engineering, the low discrepancy sequence serves an important character in many disciplines, for example, the image rendering algorithms in design and movie industry. These example shows that the low discrepancy nature of a sequence can enables many applications to engineering researches.

3.1.3.1 Star Discrepancy

The definition of discrepancy follows Niederreiter's (1992) notation is shown below:
Giving a set P = $\{x_1, x_2, \ldots, x_n\}$,

$$D_N(P) = sup_{B \in J} \left| \frac{A(B;P)}{N} - \lambda_s(B) \right| \quad (3\text{-}1)$$

Where λ_s is the s-dimensional Lebesgue measure, $A(B;P)$ is the number of samples in P fall in to B; J is in the form below:

$$\prod_{i=1}^{s} [a_i, b_i) = \{x \in R^s : a_i \leq x_i \leq b_i\}, 0 \leq a_i \leq b_i \leq 1 \quad (3\text{-}2)$$

Eq. (3-2) can be used for the calculation of discrepancy for different sets of samples. The supremum of the difference between the s-dimensional Lebesgue measure, and the ratio of the number of samples fall into that area to the total number of samples is taken as the discrepancy. Table below shows the calculated discrepancy of 64 samples generated using MCS, Sobol sequence, Halton sequence and Max-min approaches.

3.1.3.2 F Discrepancy

Fang and Wang (1993) proposed the F discrepancy taking account for the distribution information from variables, and the F discrepancy is defined as:

$$D_F(N) = \sup_{x \in H^s} |F_n(x) - F(x)| \quad (3\text{-}3)$$

$F(x)$ is the joint cumulative distribution function (CDF), and $F_n(x)$ is empirical distribution function as:

$$F_n(x) = \frac{1}{n} \sum_{q=1}^{n} I\{x_q < x\} \quad (3\text{-}4)$$

where $I\{\cdot\}$ is the indicator function, $I\{ture\} = 1\ and\ I\{false\} = 0$. It can be observed that when the input variables are in uniform distribution, equation *(3-3)* becomes equation *(3-1)*.

3.1.3.3 GF Discrepancy

From equation, it can be observed that all points are assigned to have the same assigned probability of 1/n instead of giving different assigned probability. Therefore, based on Fang and Wang's work, Chen et al. (2016) extended the F discrepancy to GF discrepancy.

$$D_{GF}(N) = \max_{1 \le i \le s} \{ \sup_{x \in H^s} |F_{n,i}(x) - F_i(x)| \} \quad (3\text{-}5)$$

Where $F_i(x)$ is the marginal CDF of i^{th} variable X_i, and $F_{n,i}(x)$ is empirical distribution function as:

$$F_{n,i}(x) = \frac{1}{n} \sum_{q=1}^{n} p_q I\{x_{q,i} < x\} \quad (3\text{-}6)$$

where $x_{q,i}$ is the q^{th} point of i^{th} variable X_i; I is the indicator function p_q is the assigned probability which can be calculated using Voronoi cell.

$$p_q = \int_0^{V_q} \rho(x) dx \quad (3\text{-}7)$$

Where V_q is the representative volume which can be calculated as equation below:

$$V_q = \{x \in R^s : \left|\left|x - x_q\right|\right| \le \left|\left|x - x_j\right|\right|, \forall x_j \in N, j \ne q\} \quad (3\text{-}8)$$

where N is the sample set.

It can be observed from the equations above that the computation burden for F discrepancy increase exponentially with the increase of the number of variables.

3.2 Non-adaptive Sampling

In this section, four types of non-adaptive sampling technique are introduced. The term of non-adaptive stands for that the sample set is generated according to a pre-defined number and cannot be enriched with given value of one or more dimensions.

3.2.1 Monte Carlo Sampling

MCS is a sampling procedure that based on pseudo-random variable generator, to generate pseudo-random variables. Many different computer software has pseudo-random variables generator available, and in this study Matlab is used to generate the MCS samples. The figure below shows when the location of samples drawn in the 2-D space.

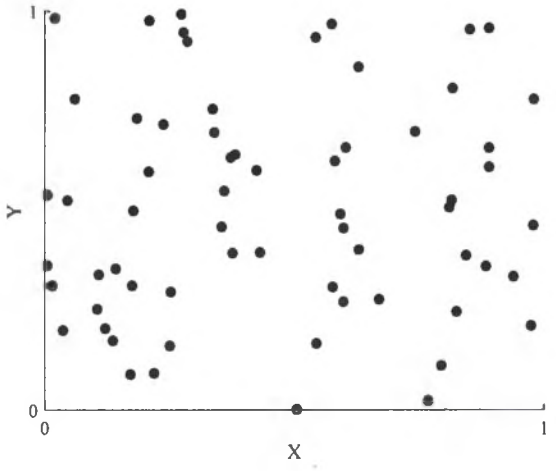

Figure 3-1: MCS of 64 samples

It can be overserved in Figure 3-1 that there are clusters and gaps between the samples. Therefore, it can lead to the missing of statistical analysis of the data between the gap regions and overemphasize of the data from the cluster regions. Using Equation *(3-1)*, the discrepancy of the 64 MCS samples is 0.095.

3.2.2 Sobol Sequence

To introduce Sobol and Halton sequence, the radical inversion and Van der Corput sequence will be first introduced (Halton 1960).

The radical inversion can be expressed as below:

$$\mathrm{i} = \sum_{l=0}^{M-1} a_l(i) b^l \tag{3-9}$$

$$\Phi_{b,C}(i) = (b^{-1} \ \ldots \ b^{-M}) \left[C \begin{pmatrix} a_0(i) \\ \ldots \\ a_{M-1}(i) \end{pmatrix} \right] \tag{3-10}$$

Where b is a positive constant, and stands for the position notation, for example $\mathrm{b} = 2$ stands for binary and $\mathrm{b} = 10$ stands for decimal; $a_l(i)$ is a vector contains all numbers at positions; i is postie integers; C is called generator matrix.

When C is an identify matrix, it constructs the Van der Corput sequence, and it can be expressed as below:

$$\Phi_b(i) = (b^{-1} \ \ldots \ b^{-M}) \begin{pmatrix} a_0(i) \\ \ldots \\ a_{M-1}(i) \end{pmatrix} \tag{3-11}$$

The Van der Corput sequence is also considered to be the simplest case of radical inversion. Below is an example shows how radical works.

Given $i = 1, \mathrm{b} = 2$, C is an identify matrix. The value of $i = 1$ in binary system is 1; therefore $\Phi_2(1) = 0.5$. Table below shows $\Phi_2(i)$ values when $i = 1,2 \ldots 6$.

Table 3-1: Example of radical inversion under b=2, and C is an identify matrix

i	b = 2	$\Phi_2(i)$
1	1	$(0.1)_2 = 0.5$
2	10	$(0.01)_2 = 0.25$
3	11	$(0.11)_2 = 0.75$
4	100	$(0.001)_2 = 0.125$
5	101	$(0.101)_2 = 0.625$
6	110	$(0.110)_2 = 0.375$
…	…	…

The construction of Sobol sequence can be expressed as below:

$$S_{Sobol,i} = (\Phi_{2,C_1}(i) \dots \Phi_{2,C_n}(i)) \quad (3\text{-}12)$$

Where i a positive integer, and C_n stands for different generator matrix.

Figure below shows the 2-D plot of the 64 samples Sobol sequence.

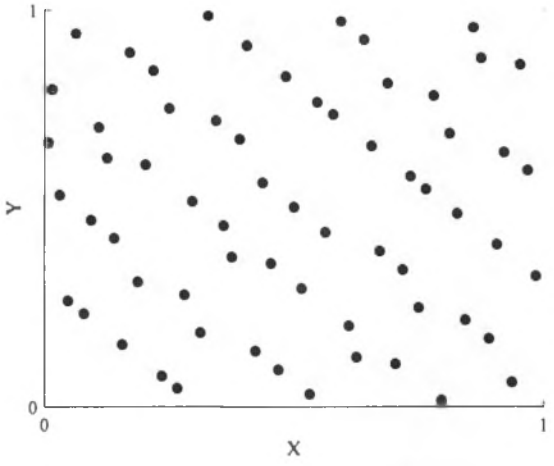

Figure 3-2: Sobol Sequence of 64 samples

From the figure above, it can be observed that the samples from Sobol sequence distributed more evenly in the space comparing to the MCS samples with same sample number, and also it can be observed that the clusters and gaps are avoid. Using Eq. *(3-1)*, the discrepancy of the 64 MCS samples is 0.034.

3.2.3 Halton Sequence

The Halton sequence is generated based on Van der Corput sequence. The samples in Halton sequence can be expressed as (Halton 1960):

$$S_{Halton,i} = (\Phi_{b_1}(i) \dots \Phi_{b_n}(i)) \quad (3\text{-}13)$$

Where i a positive integer, and the samples in each dimension is constructed based on different bases b_n, and the bases are relatively prime to each other. Figure below shows the 2-D plot the 64 samples Sobol sequence.

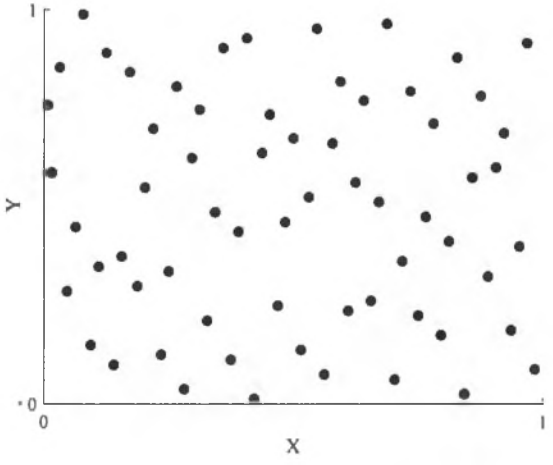

Figure 3-3: Halton Sequence of 64 samples

From the figure above, it can be observed that like Sobol sequence, the samples from Halton sequence also distributed more evenly in the space comparing to the MCS samples with same sample number. Using Eq. *(3-1)*, the discrepancy of the 64 MCS samples is 0.032.

3.2.4 GF-discrepancy based Sequential Sampling

For GF-discrepancy based sequential sampling (Chen et al. 2016), the initial points set are selected through Sobol sequence and then the initial point set is rearranged to reduce its GF discrepancy and therefore, a new point set is developed. The rearrangement involves two steps of transformation as below:

First, the initial samples are generated though the Sobol sequence is transformed in each dimension to make the assigned probability close to each other.

$$x'_{m,i} = F_i^{-1}(\sum_{q=1}^{n} \frac{1}{n} * I\{x_{q,i} < x_{m,i}\} + \frac{1}{2} * \frac{1}{n}) \quad (3\text{-}14)$$

The m is the points and i is the dimension, and F_i^{-1} is the inverse CDF for i-th dimension.

$$x''_{m,i} = F_i^{-1}(\sum_{q=1}^{n} p_q * I\{x'_{q,i} < x'_{m,i}\} + \frac{1}{2} * \frac{1}{n}) \quad (3\text{-}15)$$

Following that, the assigned probability is calculated, and the equation above is applied to reduce the GF-discrepancy, and $x''_{m,i}$ is the selected final samples.

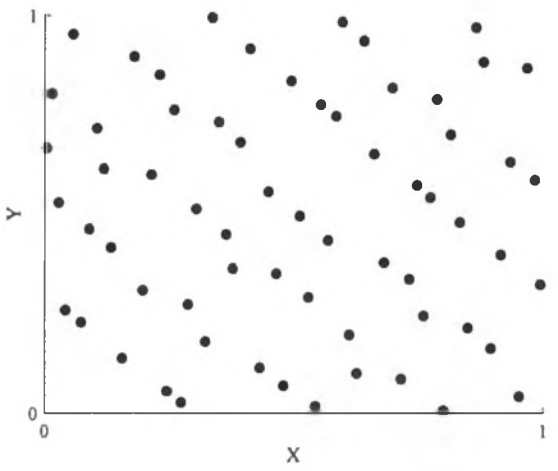

Figure 3-4: GF-Discrepancy based Sequential Sampling

From figure above, it can be observed that with the GF-Discrepancy based sequential sampling, the samples are uniformly selected in the sample space, and since uniform distribution is considered, these samples are similar to the samples generated by Sobol Sequence approach.

3.3 Adaptive Sampling

3.3.1 Max-Min Space Filling

For adaptive sampling, the samples can be enriched adaptively, and first method introduced here is the space filling technique which focus on maximize the minimum distance between selected sample points.

The procedure of maximize the minim distance (Max-min Procedure) is as below:

(1) Define the sample size of interest and generate a sample pool namely the experiment design (ED) by divide n-dimensional hypercube space into equally divide space in each dimension or use MCS.

(2) Generate initial sample set N according to Sobol sequence.

(3) Select a new sample from the ED, with

$$N^* = \max\left(\min(||ED - N||)\right), N^* \in ED.$$

(4) Add the new sample to $N_{new} = N \cup N^*$ *and* $ED \backslash N^*$.

(5) Return to procedure (3) if predefined sample size is not reached.

Figure below shows the 2-D plot the 64 samples selected using Max-min procedure with divided n-dimensional hypercube.

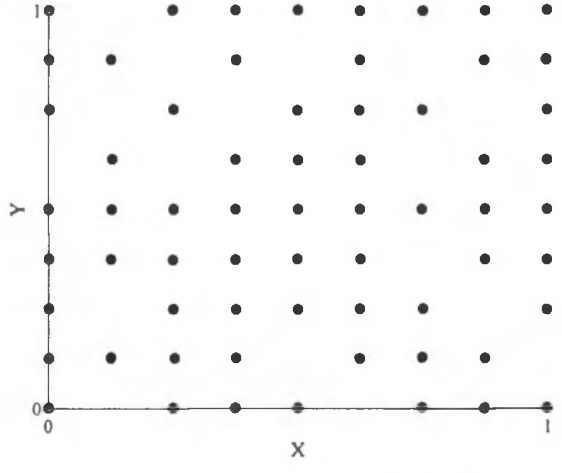

Figure 3-5: Max-min procedure selected 64 samples

Using Eq. *(3-1)*, the discrepancy of the 64 MCS samples is 0.038.

3.3.2 S-optimal

S-Optimal is proposed by Shin and Xiu (2016). Fajraoui et. al (2017) applied this method for PCE experiment design optimization. Through presentation of S-optimal technique, a small sample set X_s can be selected from a sample set X_L with sample size around $10^5 \sim 10^6$ that can construct PCE model with high accuracy. Consider X_s be a N $\times$ M matrix, where N is the sample number and M is the number of variables, and X_s is formed by N rows in X_L. The selected of X_s should satisfy the criterion below, where eq. *(3-16)* is the minimization of X_s and eq. *(3-17)* is the minimization of X_L:

$$c_a(X_s) = \arg min \frac{1}{N} \sum_{i=1}^{N} (M(x_s^i) - \sum_{a \in A} c_a \psi_a(x_s^i))^2 \quad (3\text{-}16)$$

$$c_a(X_L) = \arg min \frac{1}{N} \sum_{i=1}^{N} (M(x_L^i) - \sum_{a \in A} c_a \psi_a(x_L^i))^2 \quad (3\text{-}17)$$

The goal is minimized the difference between the PCE coefficient calculated on X_s andX_L, and it can be written as:

$$X^{\dagger} = \text{argmin}(||c_a(X_s) - c_a(X_L)||) \quad (3\text{-}18)$$

It can be re-written as following:

$$R^{\dagger} = \text{argmin}(||c_a(RX_L) - c_a(X_L)||) \quad (3\text{-}19)$$

Where R is the row selection matrix; QR decomposition is then applied here as$A_L = Q_L R_L$, where A_L is the PCE modal matrix under X_L, and then the equation below can be applied:

$$||c_a(X_L) - c_a(X_s)|| \leq ||R^{-1}|| \cdot ||g|| \quad (3\text{-}20)$$

where g is the least square solution as:

$$RQ_L g = RP^{\perp} c_a(X_L) \quad (3\text{-}21)$$

$$P^{\perp} = (I - Q_L Q_L^T) \quad (3\text{-}22)$$

From equations above, it can be observed that minimize $||g||$ can reduce the difference between PCE coefficient calculated by X_s and X_L. Therefore, the point selection criterion is (1) maximize the determine of RQ_L or (2) maximize the column orthogonality of RQ_L. For the sake of these two objects, Shi and Xiu proposed an evaluation variable named S-value is defined as below, and the norm used in this section is vector 2-norm.:

$$S(A) = \left(\frac{\sqrt{detA^T A}}{\prod_{i=1}^{card(A)} ||A^i||}\right)^{\frac{1}{card(A)}} \quad (3\text{-}23)$$

In PCE, A is the modal matrix as mentioned before. Also, $S(A) = 0$ if $m < p$. In order to calculate the case when $m < p$, which happens when initial selection is a small size. The truncation can be applied, assume the size of initial point set is k, A is truncated to be a $k \times k$ square matrix in the calculation of $S(A)$ value.

Since the columns in the modal matrix A are orthonormal under the presentation of PCE, the QR decomposition can be omit and the equation can be re-written as below:

$$x = arg\max_{x \in \mathbb{X}}(S(x)) \quad (3\text{-}24)$$

Then the equation is equivalent to below:

$$x = arg\max_{x \in \mathbb{X}}(S(x)) \quad (3\text{-}25)$$

Through the presentation of equation above the PCE training sample set can be selected adaptively.

It worth mention that, this sample selection technique may involve challenge including very expensive computational cost in high dimension case.

3.3.3 Discrepancy Based Adaptive Techniques

For discrepancy based adaptive techniques, the concept is similar to Max-min space filling technique, but instead of focus on maximize the minimum distance between points, the focus change to minimize the discrepancy of the sample set.

The procedure of discrepancy based adaptive technique is as below:

(1) Define the sample size of interest and generate a sample pool namely the experiment design (ED) by divide n-dimensional hypercube space into equally divide space in each dimension or use MCS.

(2) Generate initial sample set N according to Sobol sequence.

(3) Select a new sample from the ED, with

$$N^* = \min\left(D_{Star\ or\ F\ or\ GF}(N \cup N^*)\right), N^* \in ED.$$

(4) Add the new sample to $N_{new} = N \cup N^*\ and\ ED \backslash N^*$.

(5) Return to procedure (3) if predefined sample size is not reached.

Figures below shows the samples generated through star-discrepancy adaptive and GF-discrepancy based adaptive procedures.

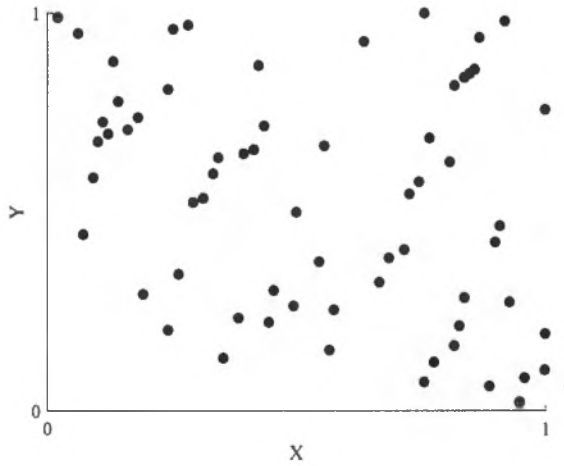

Figure 3-6: Star Discrepancy based Adaptive sampling

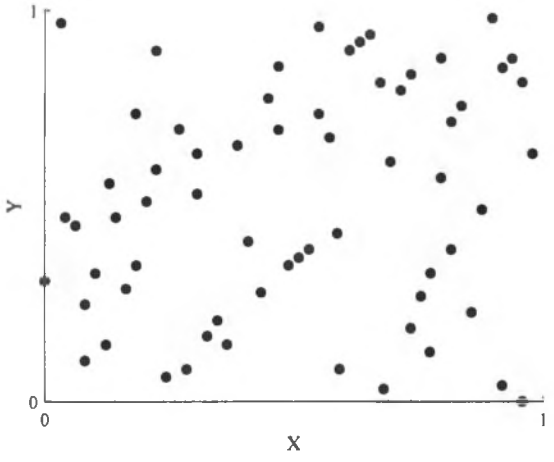

Figure 3-7: GF-Discrepancy based Adaptive sampling

From the figures above, it can be observed that still there are clusters and gaps exist; however, based on the size of ED these clusters and gaps be reduced.

3.4 Comparison between Different Sampling Techniques

3.4.1 Sampling from Distribution with Explicit Probability Density Function

In this chapter, an example of sampling from normal distribution with the presentation of a sequence in hyper cube is described. Since the points generate in previous section is under $U(0,1)$, so these points need to be converted into given distributions through calculating the value from inverse of the cumulative distribution function (CDF) given the value of points in all dimensions. Matlab is used to find the inverse of the CDF.

3.4.2 Sampling from Distribution with Implicit Probability Density Function

To get samples from distribution with implicit probability density function, the Markov Chain Monte Carlo (MCMC) can be applied, and detailed description of MCMC method can be found in Chapter 5.

3.4.3 Effect of Different Sampling Technique for Uncertainty Quantification

In this section, the effect of different sampling technique for uncertainty quantification is discussed. The structure developed in Chapter 2 is used here. To get samples for uncertainty quantification, for sequential sampling, the MCS, Sobol sequence, Halton sequence and GF discrepancy-based sequence are applied, and for adaptive sampling, the space-filling max-min and S-Optimal sampling are applied. In this example, involves four-dimension sampling. and due to the computational burden, the discrepancy based adaptive methods are not performed.

A total of 32 samples are generated through different sampling methods. The samples generated through different sampling methods are then conduct the dynamic analysis, and the mean and standard deviation estimation based on the maximum structural response from these sample are calculated. For S-Optimal sample, since it is based on the PCE basis, therefore, the PCE models are developed based on the samples selected through enrichment. Figures below show the mean and standard deviation estimation from the applied different sampling methods.

From the figures below, it can be observed that comparing to other sampling methods, the estimation from MCS method has lowest accuracy, it can be explained that the samples generated by MCS is random and cluster and gap may occur. Also, from the figures, it can be observed that comparing to the estimation on standard deviation, the estimations on the mean value have higher accuracy. For the estimation for standard deviation by the GF-discrepancy based sequence selection, Sobol sequence, Halton sequence, S-Optimal sampling and space-filling max-min sampling has similar performance. Therefore, to reduce the computational burden, different sampling method should be selected for different problems. For problems need given sample number, the sequence sampling methods may apply, and for problems need greedy enriched samples, the adaptive sampling methods may apply.

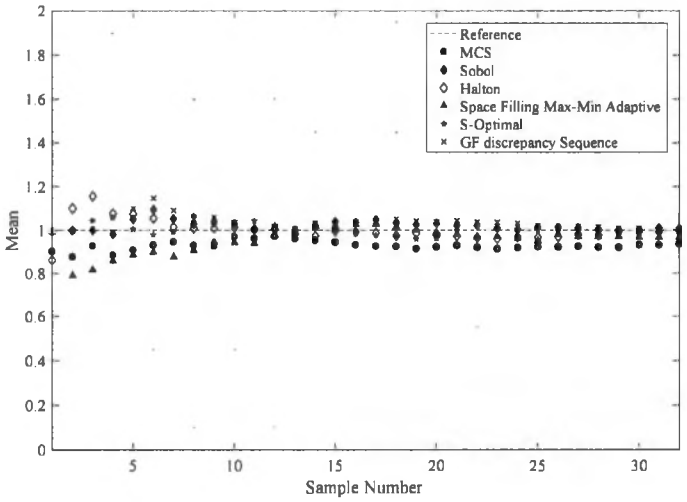

Figure 3-8: Mean estimation from different sampling methods

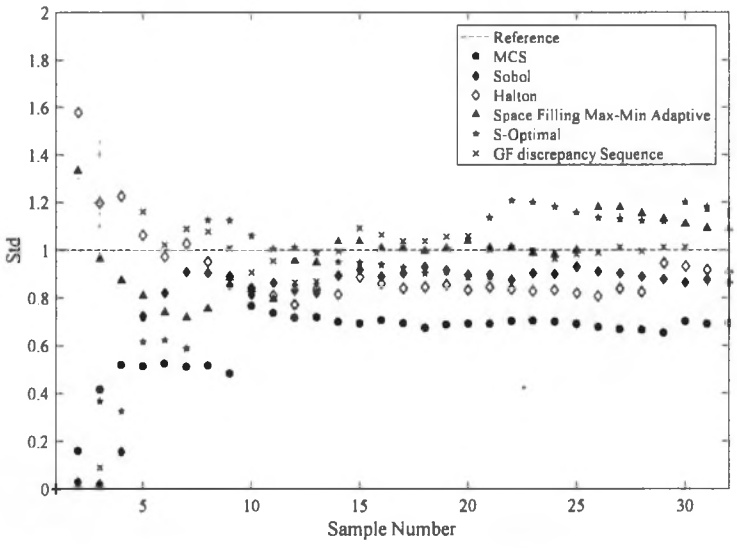

Figure 3-9: Standard deviation estimation from different sampling methods

3.5 Summary and Conclusion

In this chapter, different sampling techniques are discussed. A review of different discrepancy definition is conducted. Comparing to MCS, Sobol sequence, Halton sequence and space-filling max-min sampling and discrepancy based adaptive sampling can generate

samples distributed more uniformly in the sampling space without the exiting of gaps and clusters. For S-optimal sampling the focus change to get the samples to train PCE model with minimum difference between the PCE model trained based on large sample sets. The performance of uncertainty quantification using the samples generated are evaluated using the structure developed in Chapter 2. It can be observed that with a relatively smaller training sample size, the samples generated by Sobol sequence, Halton sequence, space-filling max-min sampling, S-Optimal sampling, GF discrepancy-based sequence has higher the accuracy on the estimation of mean and variance on the maximum structural response comparing to samples generated by MCS. Also, the computational burden for each sampling methods differs as well. It is essential to select the sampling method for problem solving to save the costs. For problem with given required sample, the sequence sampling methods can be applied since they have lower computational burden comparing to adaptive method, and the adaptive method may apply when the sequence approach is cannot meet the requirement. In conclusion, with the same sample size, the accuracy of uncertainty quantification can be significantly influence by the sampling method, with the properly selected sampling method, the accuracy of uncertainty quantification can be increased.

Chapter 4: Effect of Nonlinear Behavior on Uncertainty Quantification of Hybrid Simulation

4.1 Introduction

Researchers have developed varies of models to simulate different nonlinear behaviors from structural components. When doing uncertainty quantification, the different nonlinearities can influence the estimation accuracy. Therefore, it is essential to take account for the effect of nonlinearities. In this chapter, the PCE technique are applied to evaluate the mean, variance and the Sobol indices of the simulation output. The influence from different nonlinearities from experimental substructures (e.g. linear perfectly plastic, Linear plastic with hardening and the flag shape plastic) are then discussed.

Figure 4-1 shows the single-degree-of-freedom (SDOF) system selected for uncertainty quantification. The spring k_e is taken as the experimental substructure and the rest of the SDOF system is modeled numerically as analytical substructures. The spring k_a is assumed to be linear elastic while the spring k_e is assumed to be nonlinear. The equation of motion of the SDOF system can be expressed as:

$$m\ddot{x}(t) + c\dot{x}(t) + k_a x(t) + r(t) = m\ddot{x}_g(t) \qquad (4\text{-}1)$$

where m, c, k_a are the mass, viscous damping coefficient, and linear elastic stiffness of the SDOF system respectively. Three types of nonlinear behavior of experimental substructure are considered in this study for the experimental substructure including linear perfect elastic (LPE), linear plastic with hardening (LHP) and flag shape plastic (FSP).

The SDOF systems with different nonlinearities are then subject to the 1989 Loma Prieta earthquake recorded at Gilroy Array #3 station with the peak ground acceleration of 0.559g, and the 1994 Northridge earthquake recorded at Beverly Hills-12520 Mulhol station with the peak ground acceleration of 0.516g and 1992 Landers earthquake reordered at Lucerne

station with the peak ground acceleration of 0.725g. The time histories of the ground motions are shown in Figure 4-2.

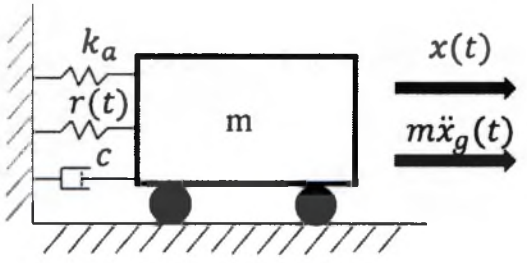

Figure 4-1: The scheme of the SDOF system

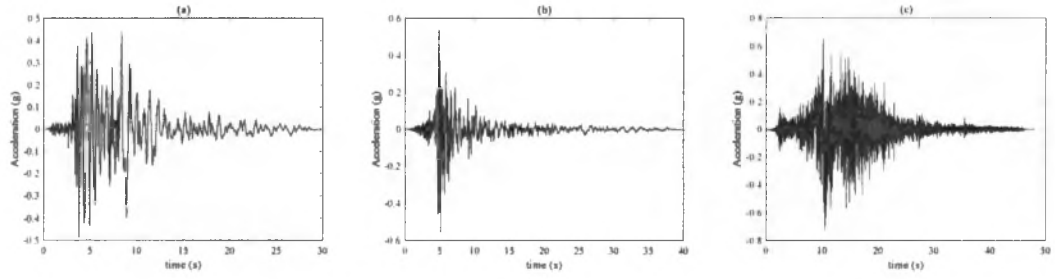

Figure 4-2: Earthquake time history, (a) Northridge, (b) Loma Prieta, (c) Lander

4.2 Types of Nonlinear Behavior

4.2.1 Linear Elastic (LE)

In this section, a model with LE behavior is developed, working as a benchmark to evaluate the performance of PCE when there is no nonlinearity in the system. K_e the initial elastic stiffness is the parameter control the behavior of this model. Figure below shows the displacement and force relationship of the LE type behavior. It can be observed from the figure that the force is proportional to the displacement.

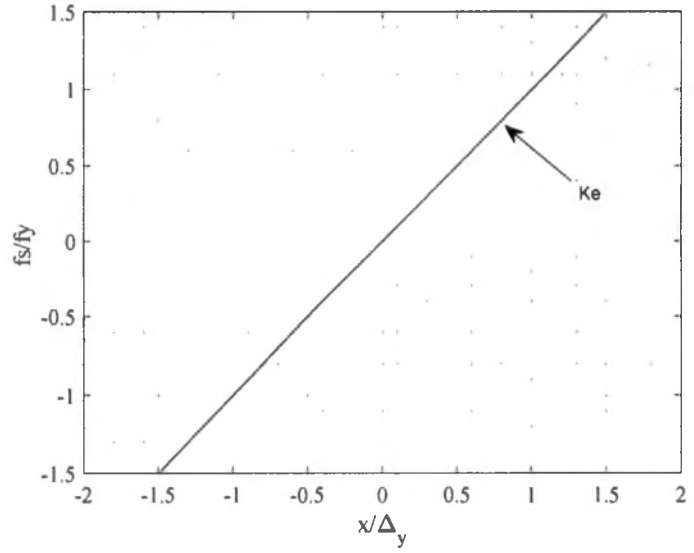

Figure 4-3: LE model

4.2.2 Linear Perfectly Plastic (LPP)

Two parameters are used to develop the LPP type behavior, namely K_e the initial elastic stiffness and α the post-yielding stiffness ratio. For LPP type behavior, the value of α is always take as 0. Figure below shows the displacement and force relationship of the LPP type behaviour. It can be observed that after the structural reaches its yield point, the initial elastic stiffness will switch to post yielding stiffness, which is 0. This type of behavior usually applied to represent the elastic to plastic behavior of structural components.

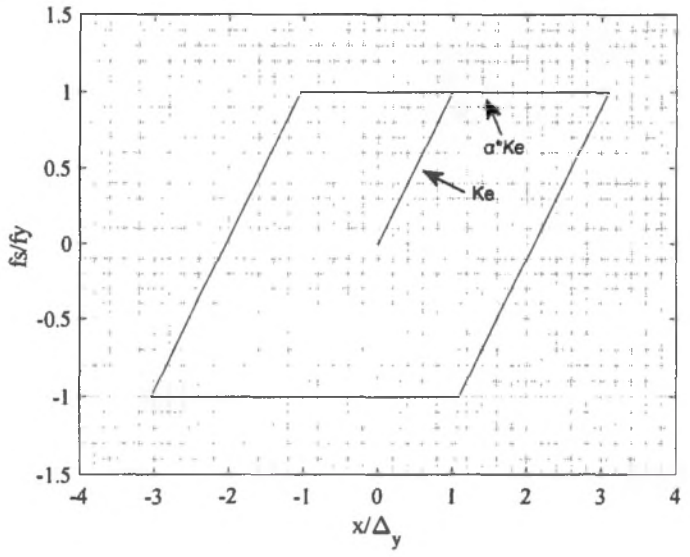

Figure 4-4: LPP model

4.2.3 Linear Plastic with Hardening (LHP)

Like LPP type behavior, two parameters are used to develop the LHP type behavior, namely K_e the initial elastic stiffness and α the post-yielding stiffness ratio. For LHP type behaviour, the value of α is always greater than 0. Figure below shows the displacement and force relationship of the LPP type behavior. It can be observed that after the structural reaches its yield point, the initial elastic stiffness will switch to post yielding stiffness. This type of behavior usually applied to represent the elastic to plastic behavior of structural components.

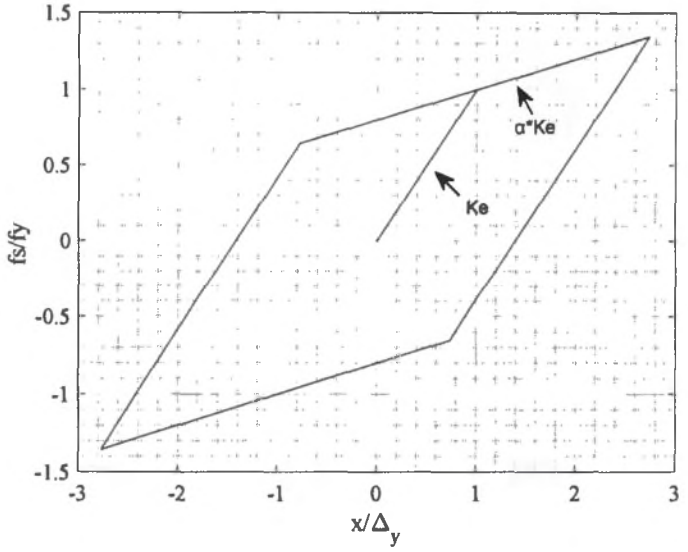

Figure 4-5: LHP model

4.2.4 Flag Shape Plastic (FSP)

For FSP type behavior three parameters are used, namely K_e the initial elastic stiffness, α the post-yielding stiffness ratio and β the energy dissipation coefficient. The value of β is usually taken from 0 to 1. Figure below shows the displacement and force relationship of the LPP type behavior. It can be observed from the figure that the self-centering behavior, which make this model suitable to simulate the behavior of structural components have self-centering behavior.

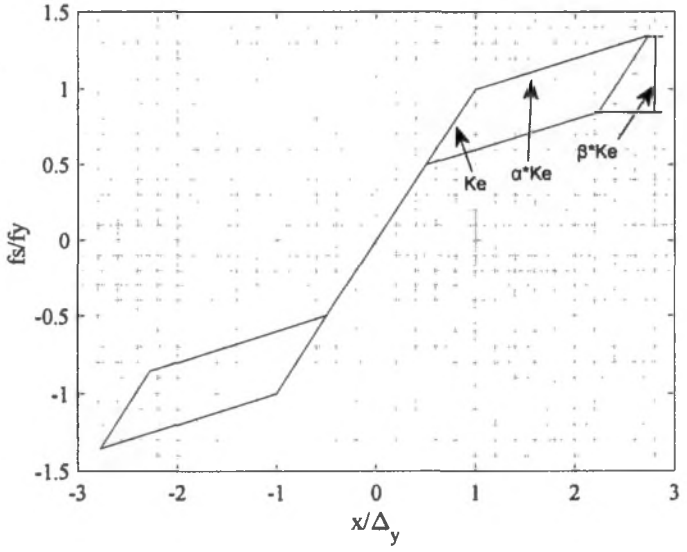

Figure 4-6: FPS model

4.3 Analysis Results and Discussion

To evaluate the performance of PCE technique on uncertainty quantification of hybrid simulation with experimental substructure with different types of nonlinearity behaviors, the uncertainty from numerical substructure is introduced first. To find the effect from nonlinear behavior, natural frequency, damping ration, ground motion and its scale.

A MATLAB based framework UQLab is utilized for generating input stochastic variables of the m, c, and k_a. Tables below show the mean and variance of these stochastic variables.

Table 4-1: Mean and standard deviation of mass, damping ratio and stiffness

Case	m		c		k_a	
	Mean	Std	Mean	Std	Mean	Std
(a)	1.00	0.20	0.63	0.13	39.48	7.90
(b)	1.00	0.20	0.63	0.13	39.48	7.90
(c)	1.00	0.20	0.63	0.13	39.48	7.90
(d)	1.00	0.20	0.63	0.13	39.48	7.90
(e)	1.00	0.20	0.63	0.13	39.48	7.90

(f)	1.00	0.20	0.63	0.13	39.48	7.90
(g)	1.00	0.20	1.26	0.25	157.91	31.58
(h)	1.00	0.20	0.42	0.08	17.55	3.51
(i)	1.00	0.20	1.26	0.25	39.48	7.90
(j)	1.00	0.20	0.63	0.13	39.48	7.90
(k)	1.00	0.20	0.63	0.13	39.48	7.90
(l)	1.00	0.20	0.63	0.13	39.48	7.90
(m)	1.00	0.20	0.63	0.13	39.48	7.90

The tables below show the nonlinearities parameters, ground motion selection, ground motion scale, natural period and damping ratio of these systems.

Table 4-2: Nonlinearities parameters, ground motion selection, ground motion scale, natural period and damping ratio of these systems

Case	Type	α	β	Period	Damping Ration	GM	$S_a(T_1)$
(a)	FSP	0.1	0.25	1	0.05	(a)	/
(b)	FSP	0.1	0.5	1	0.05	(a)	/
(c)	FSP	0.1	0.75	1	0.05	(a)	/
(d)	LHP	0.05	/	1	0.05	(a)	/
(e)	LHP	0.1	/	1	0.05	(a)	/
(f)	LPP	0	/	1	0.05	(a)	/
(g)	FSP	0.1	0.5	0.5	0.05	(a)	/
(h)	FSP	0.1	0.5	1.5	0.05	(a)	/
(i)	FSP	0.1	0.5	1	0.1	(a)	/
(j)	FSP	0.1	0.5	1	0.05	(a)	1 g
(k)	FSP	0.1	0.5	1	0.05	(b)	1 g
(l)	FSP	0.1	0.5	1	0.05	(c)	1 g
(m)	FSP	0.1	0.5	1	0.05	(a)	0.5 g
(n)	FSP	0.1	0.5	1	0.05	(a)	1.5 g

MC simulation of the SDOF (a) to (m) are then conducted using MATLAB. The values from MC simulation are considered as the reference and will be applied to evaluate the performance of PCE with different orders.

Figures below show the histogram of MC simulation results of maximum displacement of the systems under different cases.

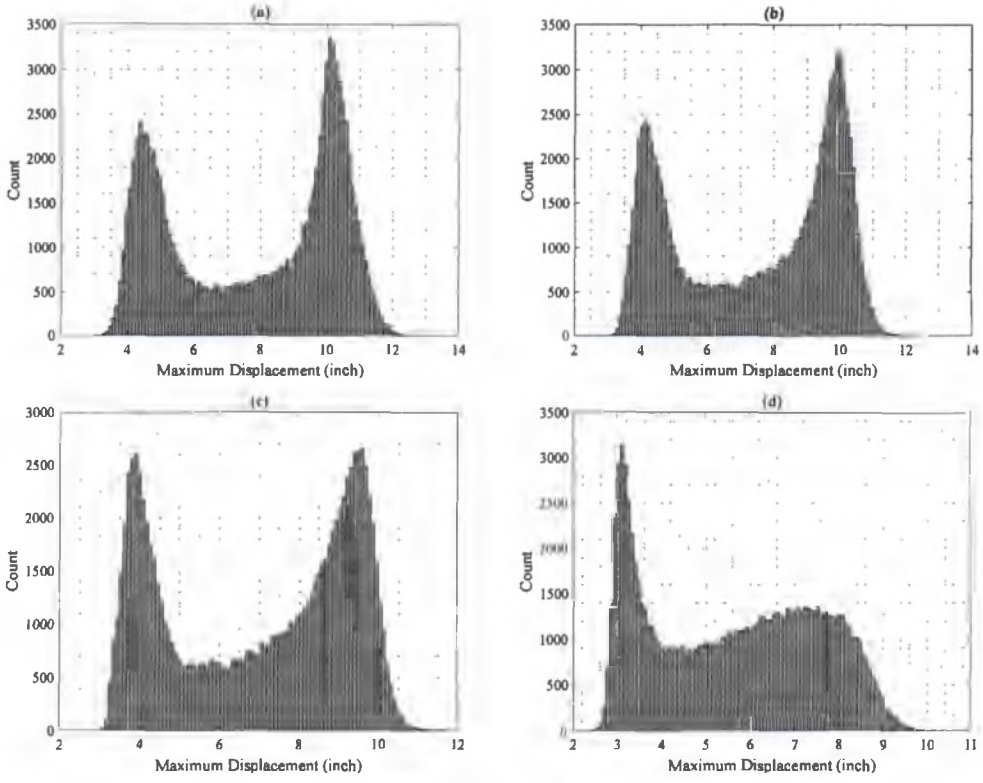
(a)
Count
Maximum Displacement (inch)
(b)
Count
Maximum Displacement (inch)
(c)
Count
Maximum Displacement (inch)
(d)
Count
Maximum Displacement (inch)

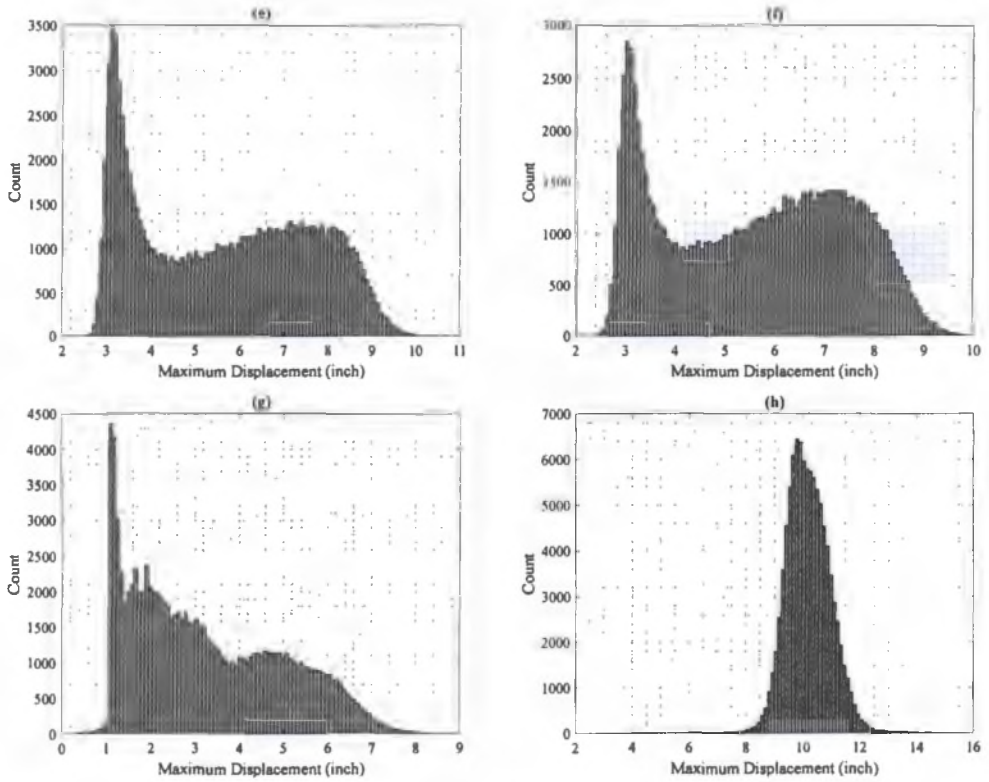
(e)
Count
Maximum Displacement (inch)
(f)
Count
Maximum Displacement (inch)
(g)
Count
Maximum Displacement (inch)
(h)
Count
Maximum Displacement (inch)

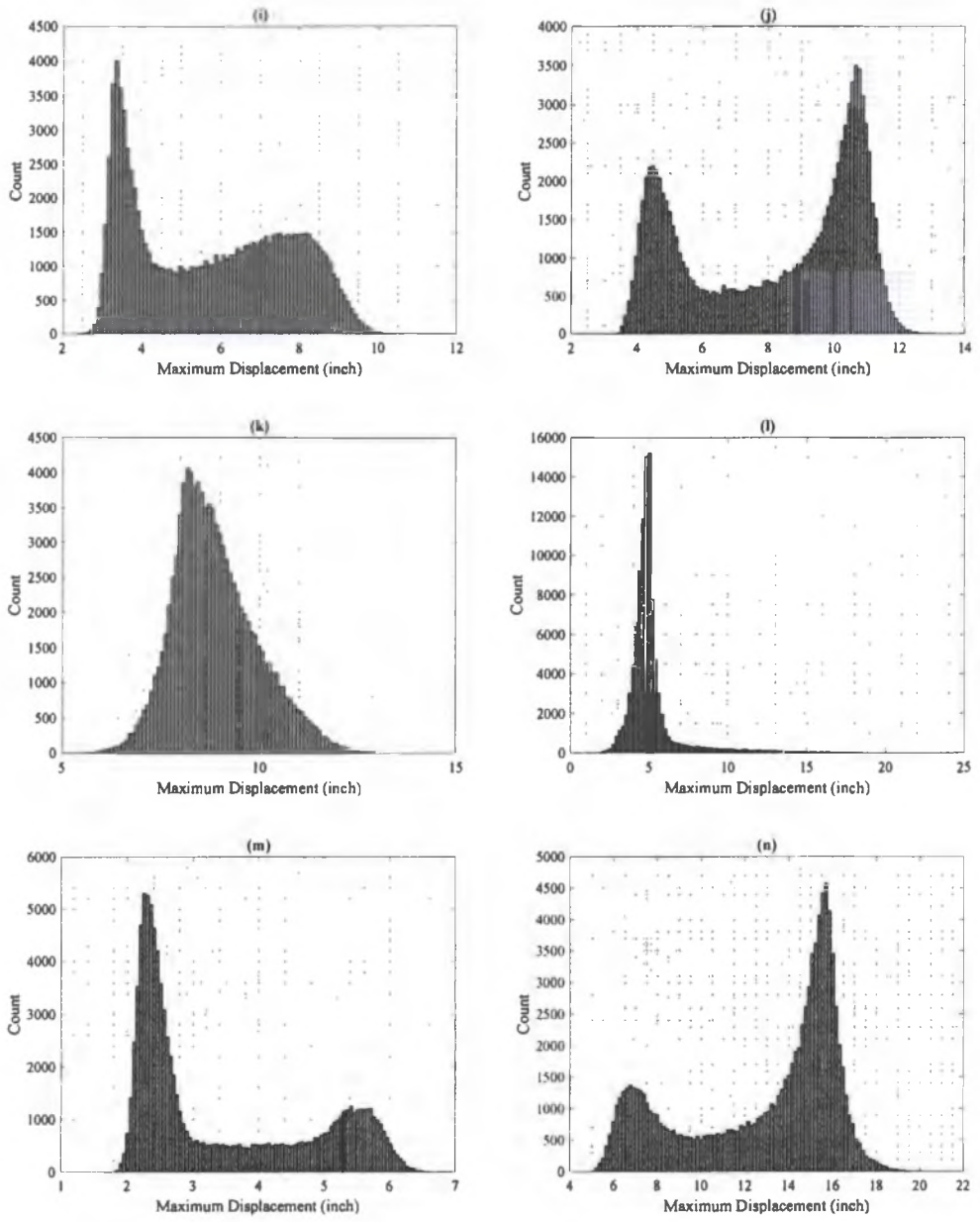

Figure 4-7: Histogram of MC simulation results

From figure above, large variance can be observed while systems are under different nonlinearities, different system properties and ground motion properties. Table below shows the mean and standard deviation of the maximum displacement as well as the first

order and total Sobol indices for all systems. The results present in the table is used as benchmark to evaluate the performance of PCE method.

Table 4-3: Mean, standard deviation, coefficient of variance, first order Sobol indices and total Sobol indices of MC simulation results

Case	Mean	Std	C.O.V	First Order Sobol			Total Sobol		
				m	c	k_a	m	c	k_a
(a)	7.85	2.54	32%	0.612	0.042	0.168	0.788	0.045	0.342
(b)	7.52	2.45	33%	0.636	0.038	0.166	0.794	0.041	0.323
(c)	7.06	2.30	33%	0.664	0.033	0.161	0.804	0.037	0.298
(d)	5.63	1.90	34%	0.767	0.024	0.113	0.858	0.029	0.202
(e)	5.64	1.95	34%	0.759	0.022	0.121	0.853	0.027	0.212
(f)	5.59	1.84	33%	0.775	0.027	0.102	0.866	0.031	0.192
(g)	3.26	1.68	52%	0.630	0.018	0.230	0.746	0.030	0.342
(h)	10.19	0.81	8%	0.487	0.291	0.015	0.691	0.310	0.216
(i)	5.76	1.96	34%	0.636	0.038	0.166	0.794	0.041	0.323
(j)	8.19	2.59	32%	0.632	0.039	0.170	0.789	0.042	0.325
(k)	8.88	1.07	12%	0.022	0.358	0.334	0.300	0.409	0.612
(l)	5.11	1.70	33%	0.515	0.036	0.105	0.856	0.049	0.461
(m)	3.45	1.34	39%	0.660	0.021	0.112	0.860	0.031	0.307
(n)	12.85	3.48	27%	0.617	0.047	0.183	0.769	0.050	0.335

After the mean, standard deviation, first order Sobol indices and total Sobol indices are analyzed, PCE analyses are the conduct to each case. The mean standard deviation, first order Sobol indices and total Sobol indices are also calculated through PCE method with a smaller training sample set compare to MC simulation; however, the difference in nonlinear behavior, natural frequencies, damping ratio and selection of ground motion as well as its scale may have influence on the performance of PCE method. Therefore, these properties are taking into account, and been analyzed and discussed in the following sections. The effect of nonlinear behavior, the effect of natural frequencies, the effect of damping ration and the effect of the selection of ground motion and its scale are discussed.

4.3.1 Effect of Nonlinear Behavior

In this section, the effect of nonlinear behavior of system to the performance to the PCE estimation of mean, variance, first order and total Sobol indices is discussed. Since a pre-defined sampling size is selected, the Sobol sequence sampling technique is applied in in this chapter. The optimal number of regression points is taken empirically by (M-1) multiplied by P (Crestaux et al. 2009), where M is the number of variables, and $P=(p+M)!/(p!M!)$ where p is the PCE degree. From the equation provided to estimate the optimal number of regression points, it can be found that the sample number will increase dramatically with the increasement of PCE degree. Also, with higher PCE degree, the computational effort for PCE coefficients increase as well. Therefore, it is essential to find an efficient PCE degree where the balance between the computational burden and estimation accuracy can be reached. Figure below shows the mean value estimation of six different nonlinearities case (a), (b), (c), (d), (e), (f). In the figures, the red dash line stands for the value calculated from Table 4-3.

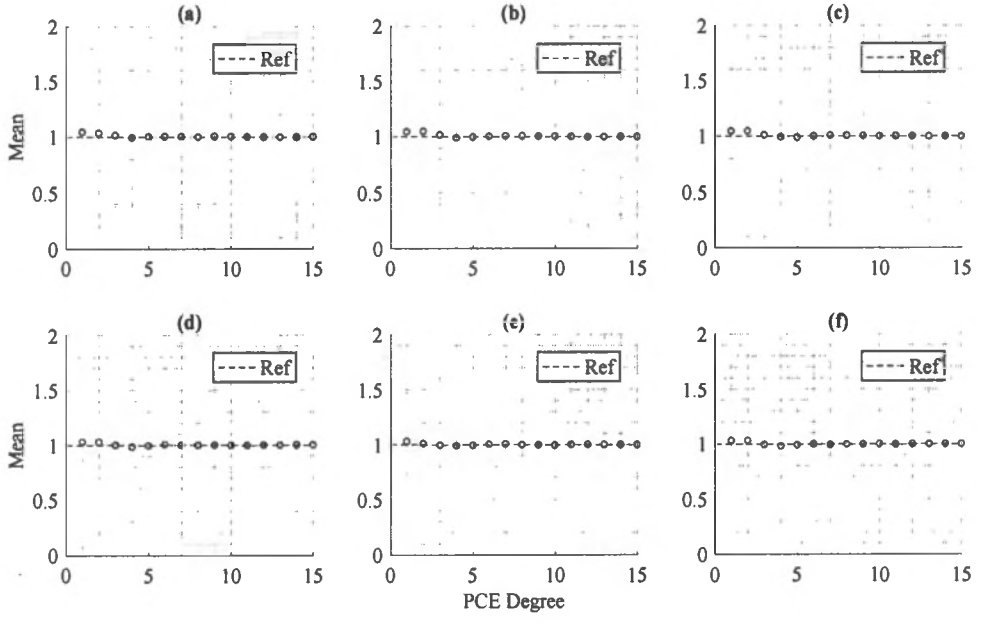

Figure 4-8: Mean value estimation

From figure above, it can be observed that with small PCE order, the accuracy of estimation on mean value of the maximum structural response is high. Also, from figure above, it can be observed that the accuracy of estimation on mean value of maximum structural response are similar when the systems have different nonlinearities. For LHP and LPP cases (d), (e), (f), the mean value reaches convergence around PCE degree of 3, while FSP cases (a), (b), (c), the mean value reaches convergence around PCE degree of 5. For the same type nonlinearity with different parameters, for example, FSP and LPP with different α and β do not have significant impact on the performance of the PCE estimation, while similar trend of mean value can be observed from figure above.

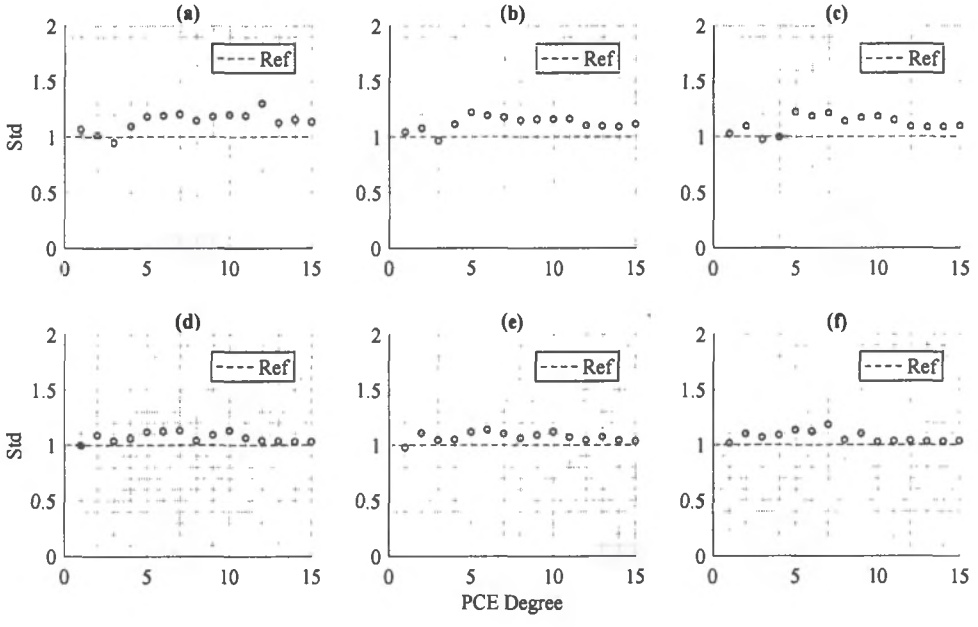

Figure 4-9: Standard deviation estimation

Figure above shows the PCE estimation on standard deviation of maximum structural response. From figure above, it can be observed that For FSP cases, PCE reaches convergence around PCE degree of 5 and for LHP and LPP cases around degree 3. Also,

similar observation on the influence from different nonlinearity type to the estimation accuracy can be observed. PCE has higher accuracy of standard deviation estimation for LHP and LPP cases compare to FSP cases.

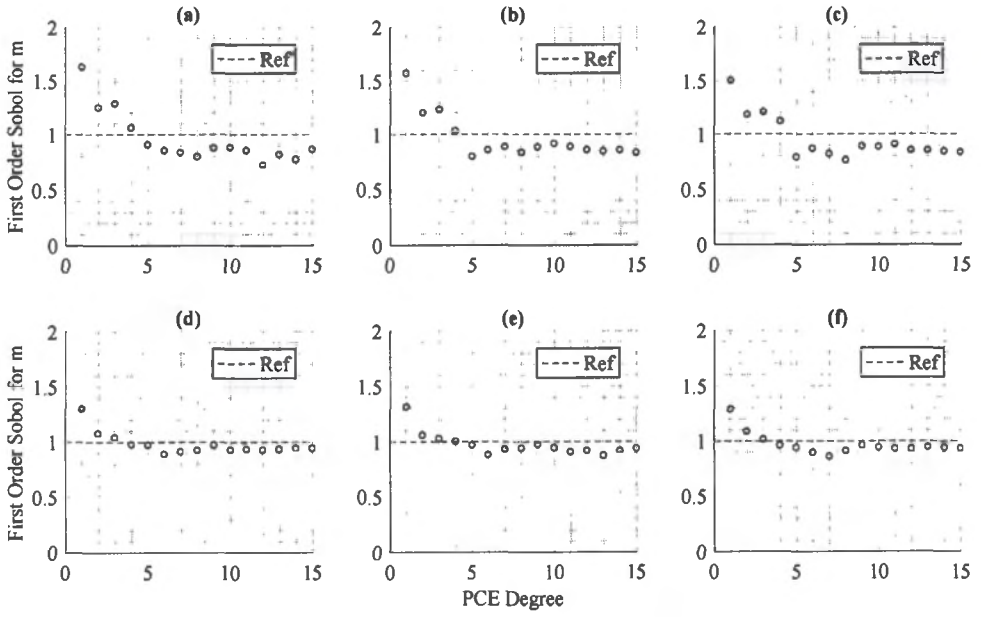

Figure 4-10: First order Sobol indices estimation on m

Figure 4-11: First order Sobol indices estimation on c

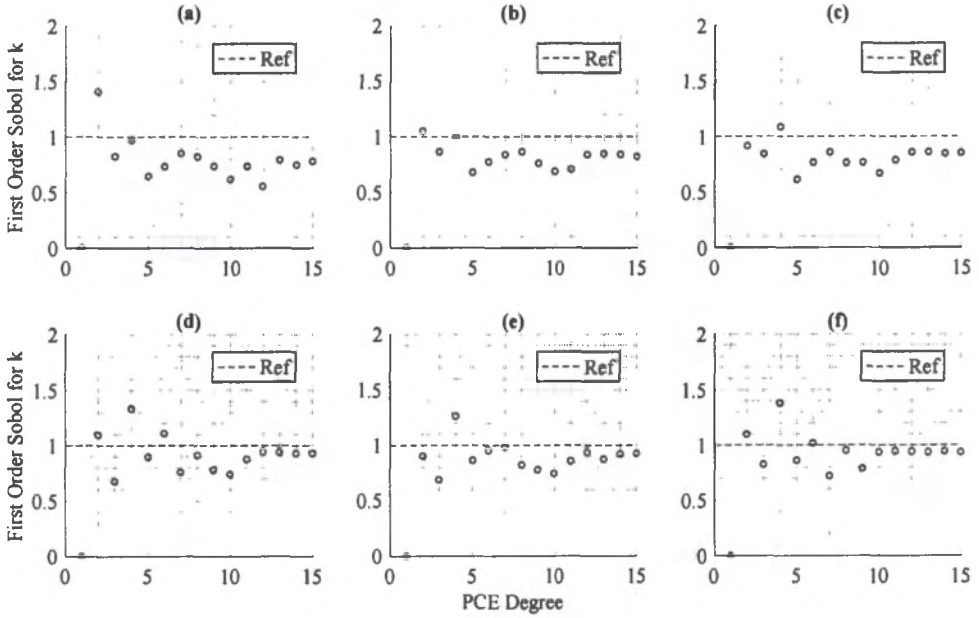

Figure 4-12: First order Sobol indices estimation on k

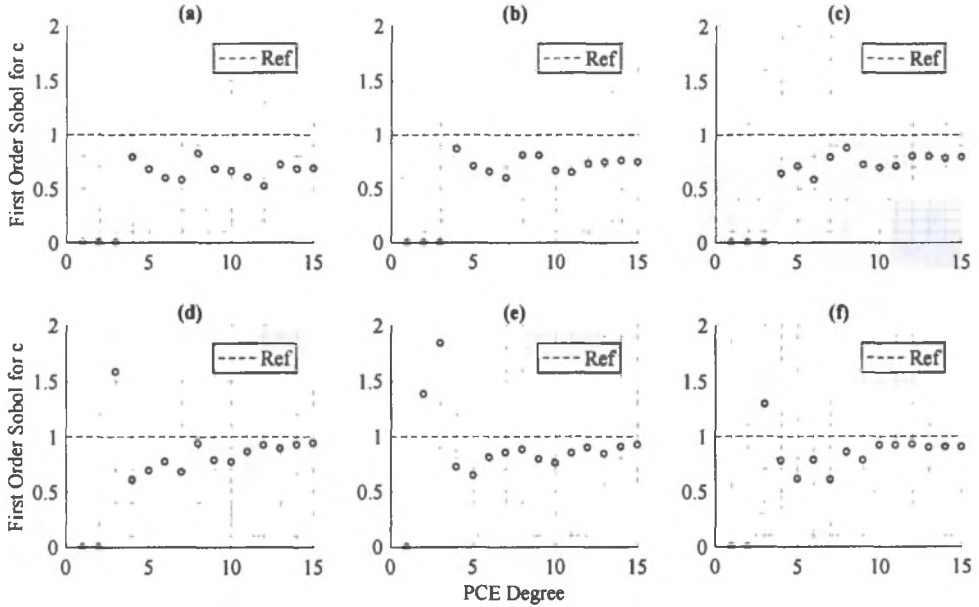
(a)
(b)
(c)
(d)
(e)
(f)
Ref
First Order Sobol for c
PCE Degree

From the figures above on first order Sobol indices estimation, it can be observed that compare to mean and standard deviation estimation, the estimation on first order Sobol indices reaches convergence with higher PCE order than the mean and standard deviation estimation, when the PCE order are higher than 10. Also, for some cases, the estimation did not reach convergence, for example, case (a) for the first order Sobol indices estimation of m, c and k. Another observation can be made is that for the estimation on first order Sobol indices, the PCE has better accuracy on LHP and LPP type of nonlinearities then FSP type of nonlinearity. Following the estimation of first order Sobol indices, is the estimation on total Sobol indices.

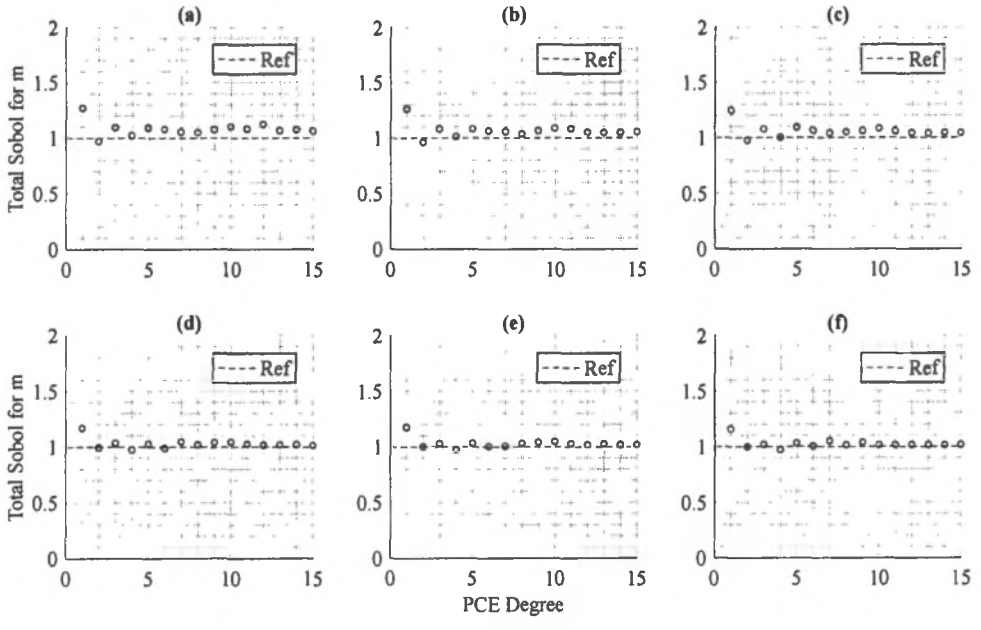

Figure 4-13: Total Sobol indices estimation on m

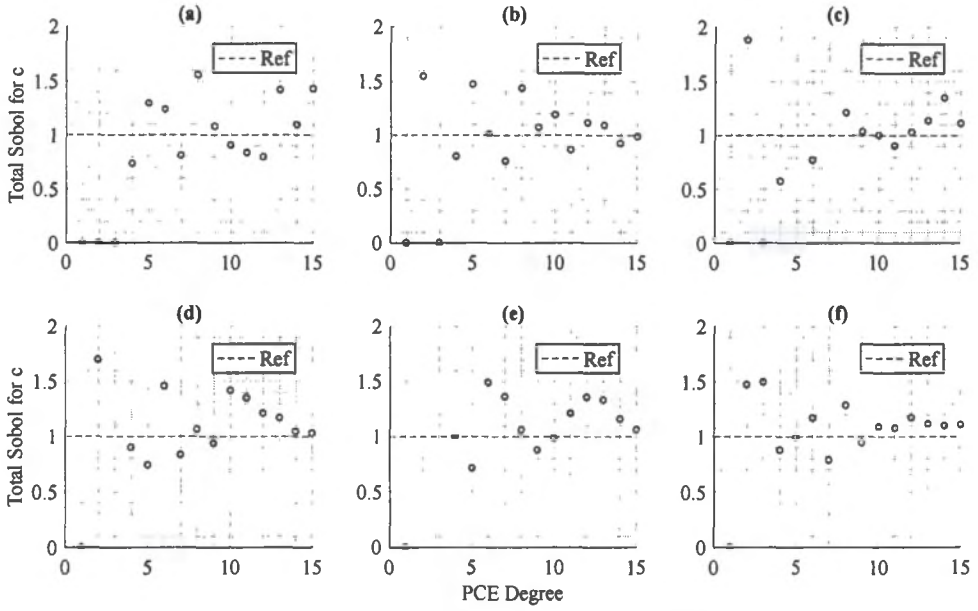

Figure 4-14: Total Sobol indices estimation on c

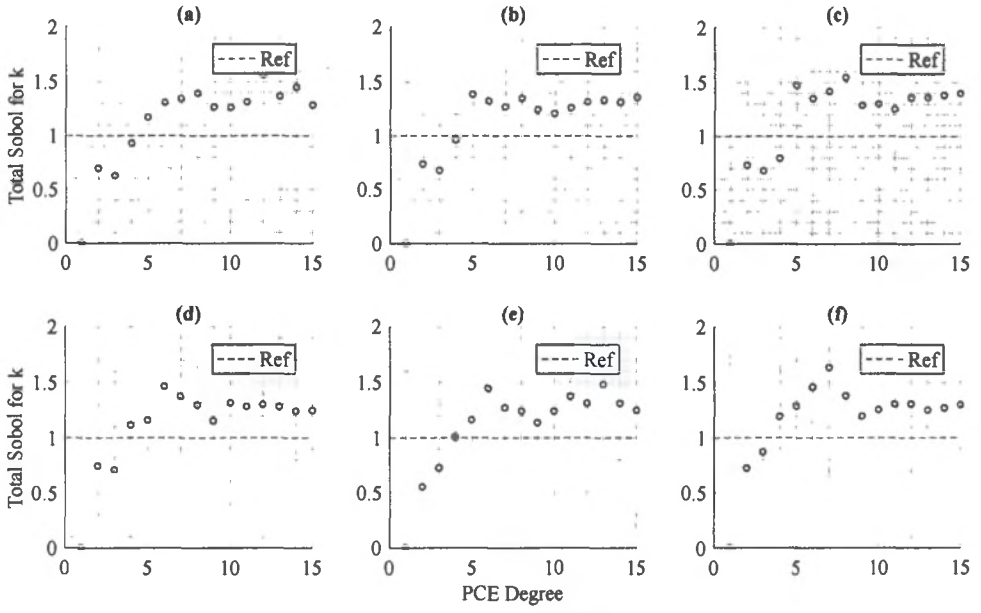

Figure 4-15: Total Sobol indices estimation on k

From the figures above, it can be observed that PCE can give accurate estimation on total Sobol indices of m and can reach convergence around PCE degree of 3 for FSP, LHP and LPP cases. The estimations on total Sobol indices of c and k are less accurate compare to m. The estimation did not reach convergence on total Sobol indices of c for case (a), (b), (c), (d), (e). Only case (f) reaches convergence around PCE degree of 10. For case (b) and (c), the estimation of total Sobol indices of k reaches convergence around PCE degree of 5, but the value is higher than the result from MC simulation. For case (d) and (f) the estimation of total Sobol indices of k reaches convergence around PCE degree of 10, the estimation is still higher than the results from MC simulation, but the accuracy is higher than the estimation from (b) and (c). Case (a) and case (e) here did not reaches convergence.

From the results of PCE estimation of case (a), (b), (c), (d), (e), (f), it supports that the different nonlinearities have impact on the performance of PCE. PCE method shows better performance on LHP and LPP type nonlinearities since the error of estimations on mean,

standard deviation, first order Sobol indices and total Sobol indices are lower than the FSP cases.

4.3.2 Effect of Natural Frequencies

In this section, the effect of natural frequencies to system is discussed. The FSP systems with different natural frequencies are selected. The table bellows shows the system parameters.

Table 4-4: FSP with different natural frequencies

(b)	FSP	0.1	0.5	1	0.05	1	1 g
(g)	FSP	0.1	0.5	0.5	0.05	1	1 g
(h)	FSP	0.1	0.5	1.5	0.05	1	1 g

Figures below shows the PCE simulation results.

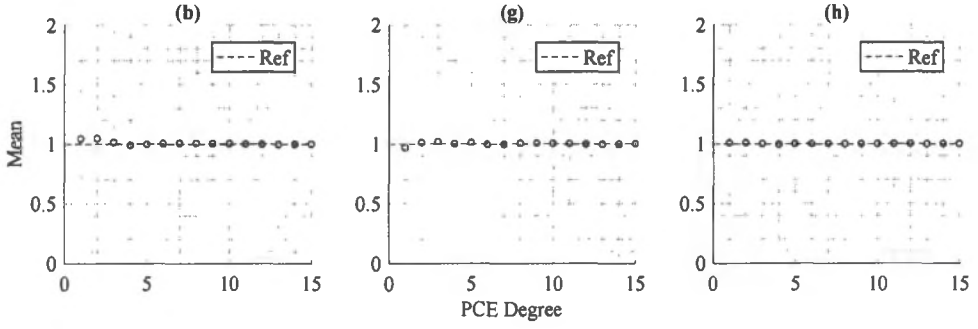

Figure 4-16: Mean

Figure below shows the PCE estimation on mean values. It can be observed that the estimation is accuracy for three different natural periods with a small PCE degree.

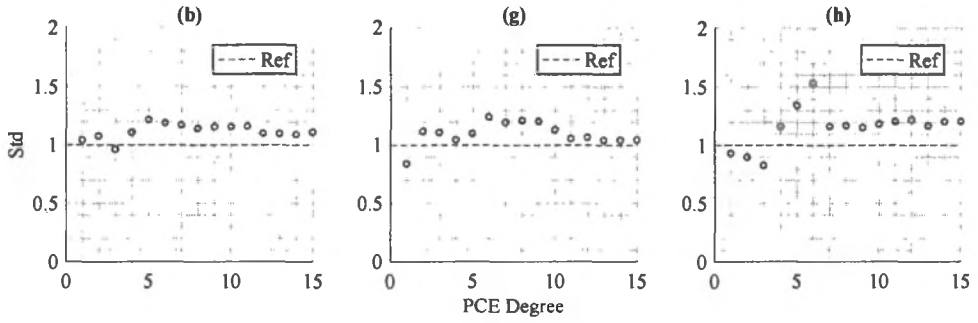

Figure 4-17: Standard Deviation

From figure above, it can be observed that for the estimation on standard deviation, good accuracy can be reach when the PCE degree is higher than 12 for case (b) and case (g). Also, it can be observed that the accuracy decrease with respect to the increase of natural period.

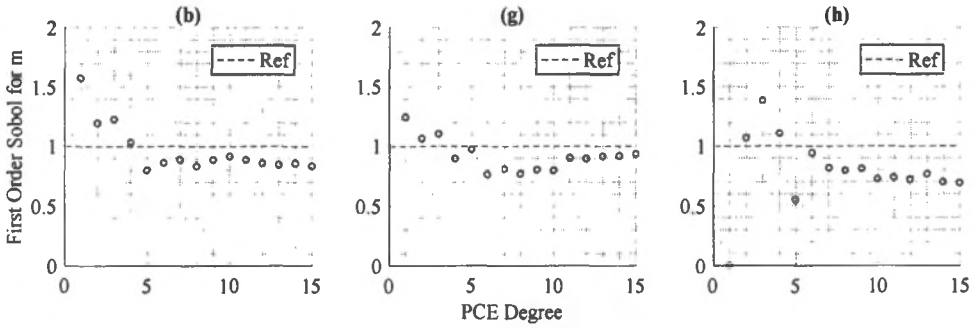

Figure 4-18: First Order Sobol for m

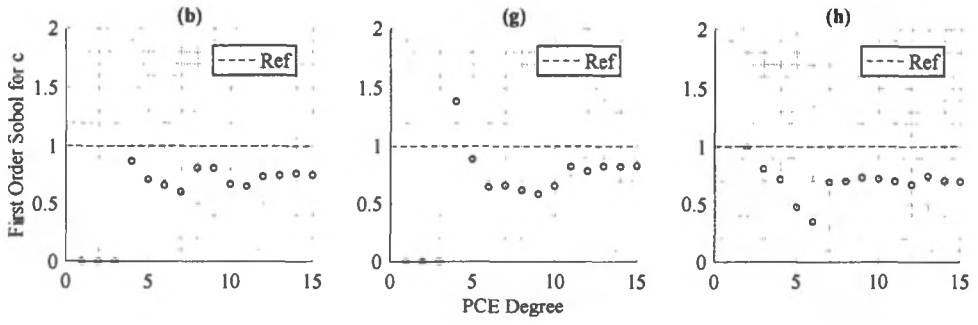

Figure 4-19:First Order Sobol for c

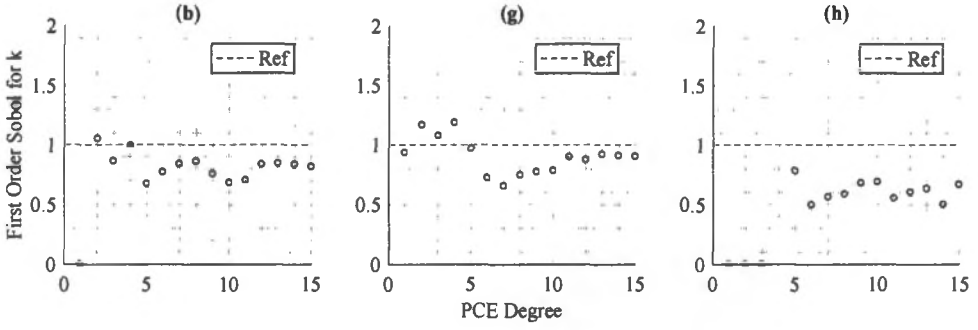

Figure 4-20: First Order Sobol for k

From the first order Sobol indices estimation from figures, similar results can be obtained. These figures show that with the application of PCE degree higher than 12, good accuracy can be reached for case (g), but for other cases have lower accuracy. The increase of natural period leads to lower estimation accuracy.

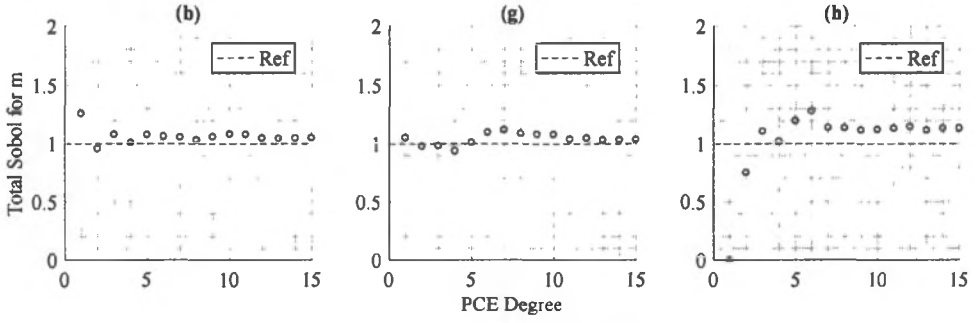

Figure 4-21: Total Sobol for m

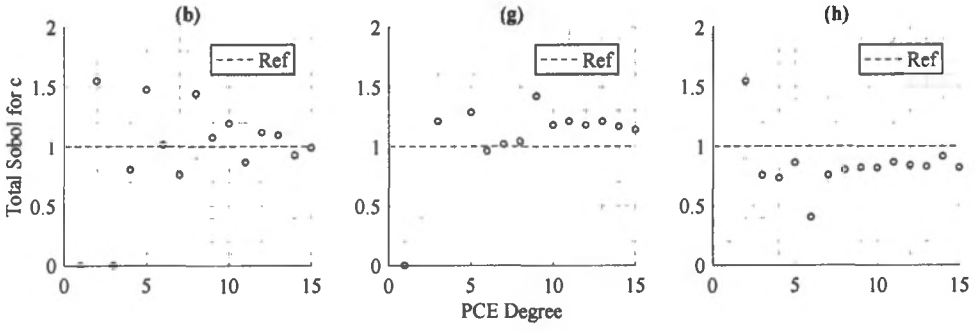

Figure 4-22: Total Sobol for c

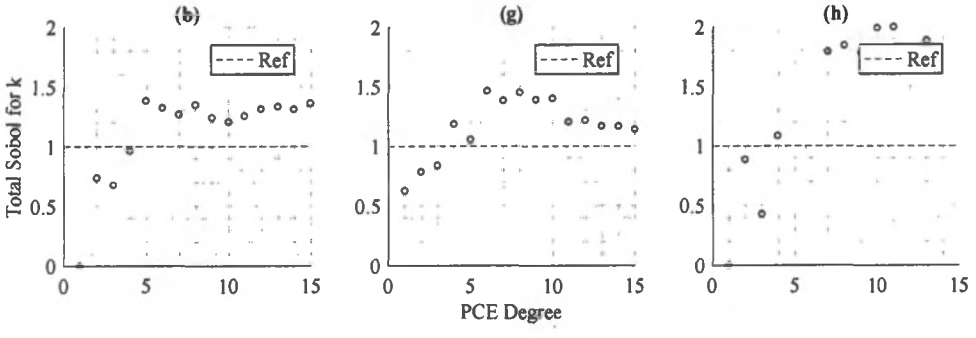

Figure 4-23: Total Sobol for k

For the total Sobol indices, the figures above show that for all three cases, the accuracy of estimation on mass is higher than damping coefficient and stiffness. For the estimation on the stiffness and damping, the larger natural period leads to lower estimation accuracy.

4.3.3 Effect of Damping Ratio

After the discussion of effect of natural period, the effect of damping ratio to the system is then discussed. The FSP systems with different damping ratio are selected. The table bellows shows the system parameters.

Table 4-5: FSP with different damping ration

(b)	FSP	0.1	0.5	1	0.05	1	1 g
(i)	FSP	0.1	0.5	1	0.1	1	1 g

Figures below show the PCE simulation results on mean, standard deviation, first order Sobol indices and total Sobol indices.

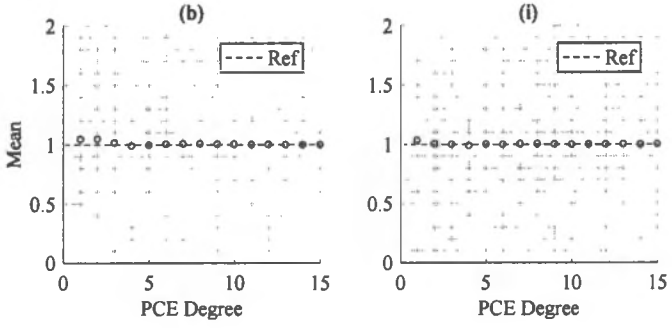

Figure 4-24: Mean

From figure above, it can be observed that for both cases, good estimation on mean value can be reached.

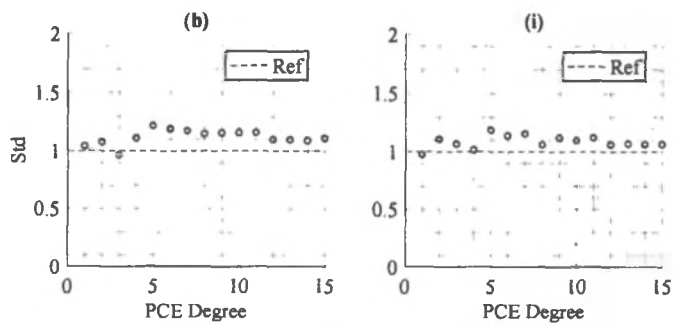

Figure 4-25: Standard Deviation

For the estimation on standard deviation, from figure above it can be observed that with PCE degree around 10, the convergence can be reached, and case (i) with higher damping ratio shows better accuracy than case (b).

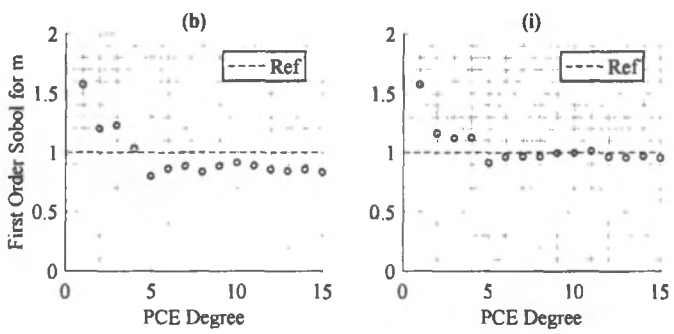

Figure 4-26: First Order Sobol for m

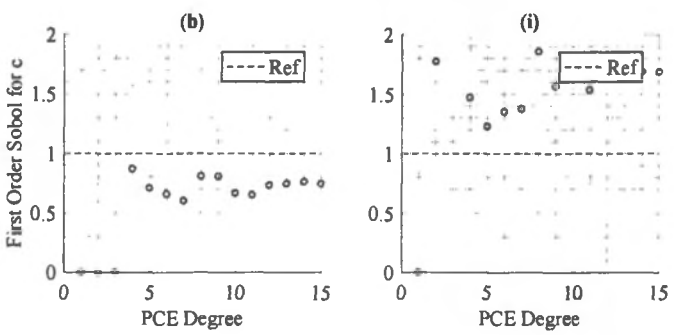

Figure 4-27: First Order Sobol for c

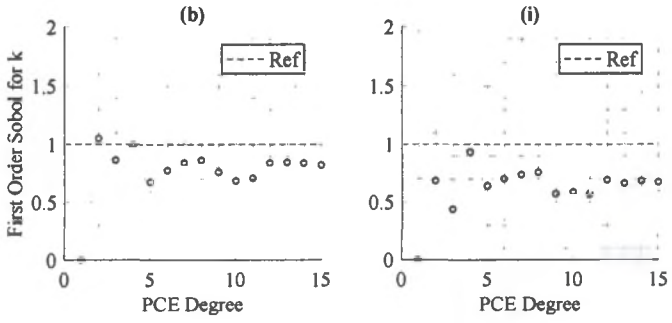

Figure 4-28: First Order Sobol for k

For the estimation on first order Sobol indices, from figures above, it can be observed that for both cases the estimation on mass convergence around PCE degree of 5 and case (i) has smaller error than case (b), and the estimation accuracy on stiffness are close. However, the estimation accuracy on damping decrease with the increase of damping ratio.

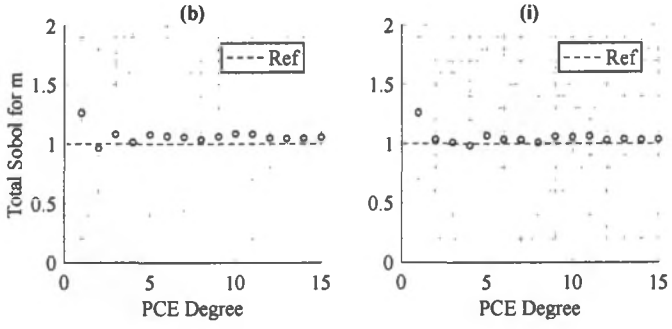

Figure 4-29: Total Sobol for m

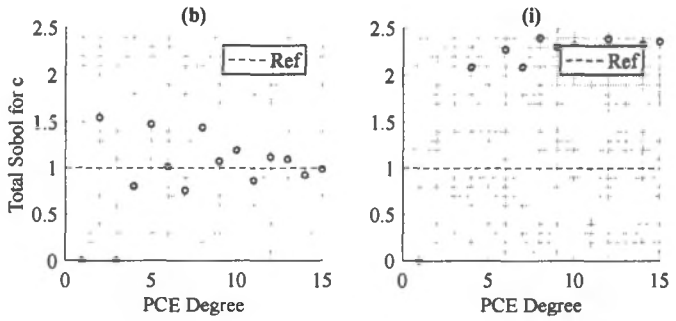

Figure 4-30: Total Sobol for c

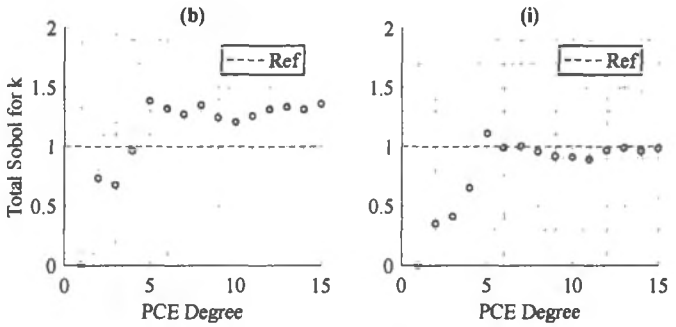

Figure 4-31: Total Sobol for k

For the estimation on total Sobol indices estimation, from figures above, similar observation can be made as the first order Sobol indices estimation. For the estimation on damping coefficient, case with higher damping ratio shows lower accuracy. Also, it can be observed that for the estimation for stiffness, case (i) has better accuracy than case (b).

4.3.4 Effect of Ground Motion and Its Scale

After discussing the impact from structural parameters to the performance of PCE, the effect of ground motion is discussed here. In this section, the effect of different ground motions to system is discussed first, following that the effect of ground scale is discussed. The table bellows shows the system parameters.

Table 4-6: FSP under different seismic excitation

(b)	FSP	0.1	0.5	1	0.05	1	1 g
(j)	FSP	0.1	0.5	1	0.05	2	1 g
(k)	FSP	0.1	0.5	1	0.05	3	1 g

Figures below show the PCE simulation results.

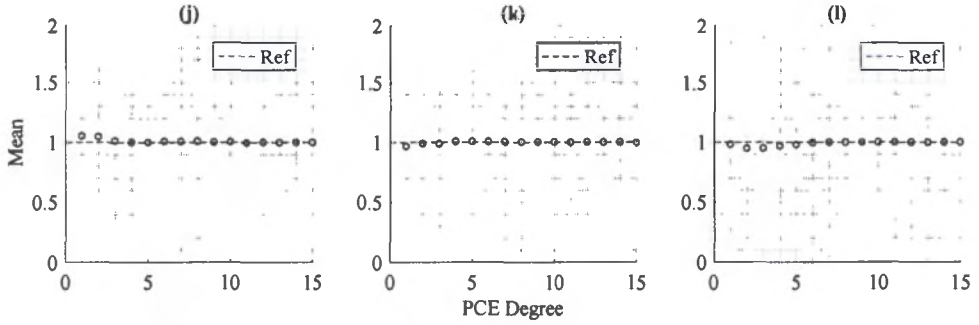

Figure 4-32: Mean

For the estimation on the mean value, it can be observed that for all three cases, good accuracy can be reached.

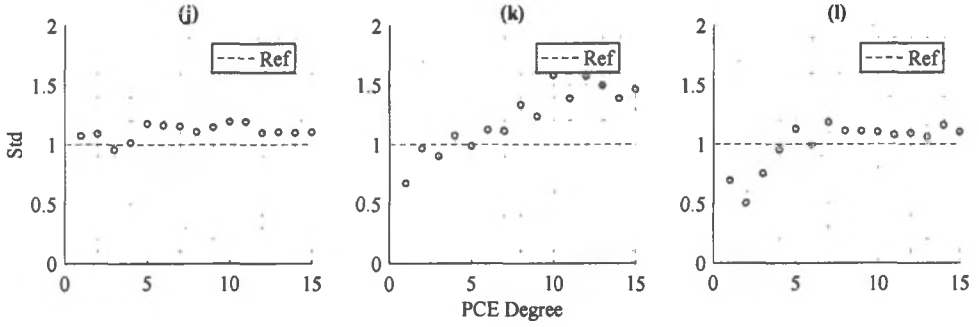

Figure 4-33: Standard Deviation

From the figure above, it can be observed that different from the estimation on mean value, the ground motion selection has effect on the estimation on standard deviation while for case (j) good estimation can be reached around PCE degree of 5 and case (j) with degree around 10, and for case (k), the convergence is not reach with PCE degree of 15.

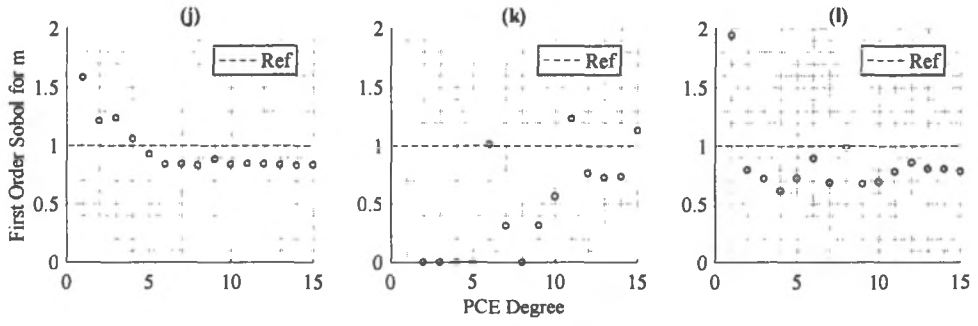

Figure 4-34: First Order Sobol for m

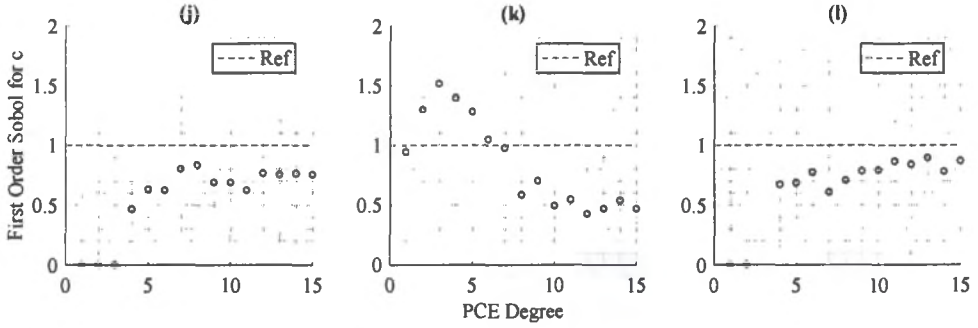

Figure 4-35: First Order Sobol for c

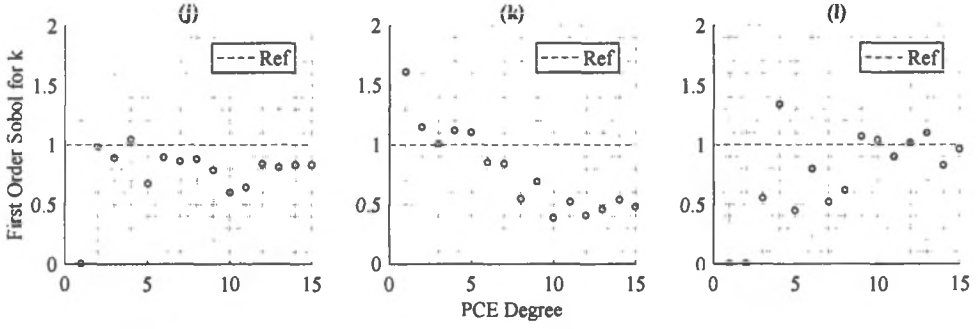

Figure 4-36: First Order Sobol for k

For the first order Sobol indices, it can be observed from figures that case (k) has low accuracy on all estimation for mass damping coefficient and stiffness while case (j) and (l) has better accuracy on estimations. Case (j) can give good estimation on mass around the

PCE degree of 5, but the accuracy on damping coefficient and stiffness is lower. The accuracy of estimation from case (l) is lower than case (j) but higher than case (k).

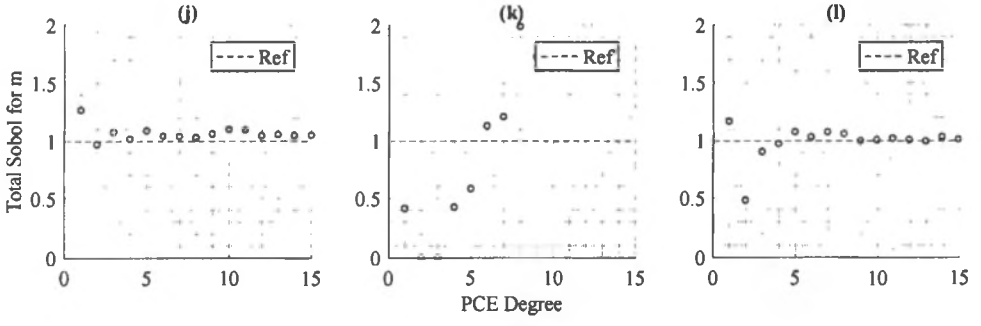

Figure 4-37: Total Sobol for m

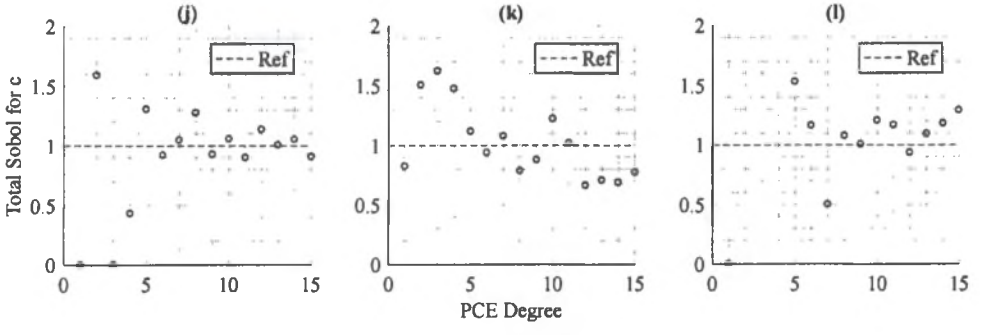

Figure 4-38: Total Sobol for c

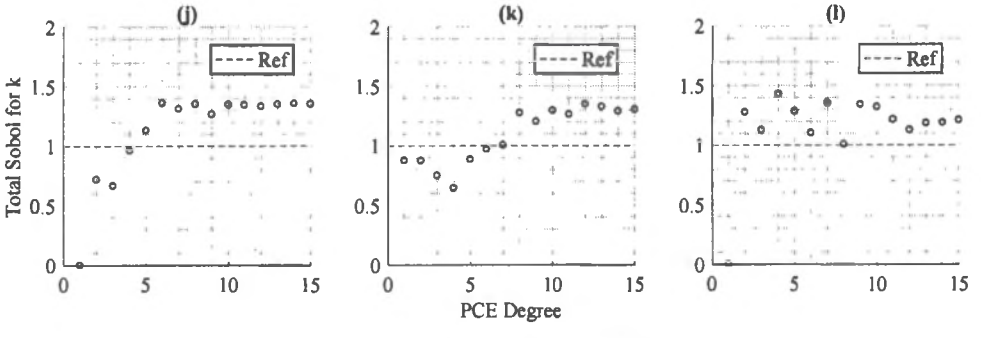

Figure 4-39: Total Sobol for k

For the total Sobol indices estimation, case (k) has lowest accuracy on estimation of mass, while case (j) and case (l) can give good estimation with PCE degree around 5. For the estimation on damping coefficient, all three cases have low accuracy. For estimation of stiffness, case (j) can reach convergence around PCE degree of 7, case (k) is around PCE degree of 10 and case (l) is around PCE degree of 12; however, all of them cannot reach the exact reference value. It can be observed that different ground motion can lead to difference on estimation accuracy.

Following the discussion of effect of ground motions, the effect of ground motion scale to the system is then discussed. The table bellows shows the scale of the ground motion.

Table 4-7: FSP a seismic excitation with different scale

(b)	FSP	0.1	0.5	1	0.05	1	1 g
(l)	FSP	0.1	0.5	1	0.05	1	0.5 g
(m)	FSP	0.1	0.5	1	0.05	1	1.5 g

The figures below show the PCE simulation results.

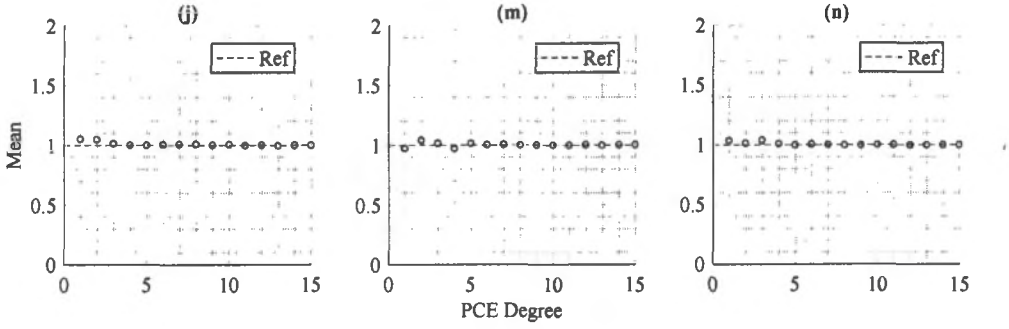

Figure 4-40: Mean

From the figure above, it can be observed that cases with different scale can give accurate estimation on the mean value.

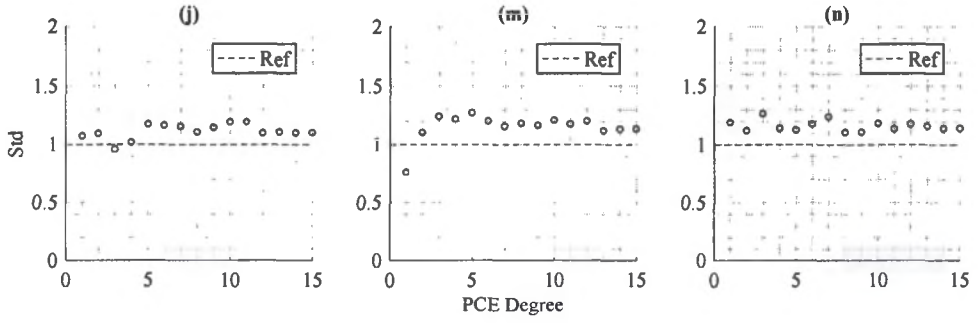

Figure 4-41: Standard Deviation

From the figure above, it can be observed that with different scale, the convergence of estimation on standard deviation can be reached around PCE degree of 4, but the accuracy is lower comparing to the mean value estimations.

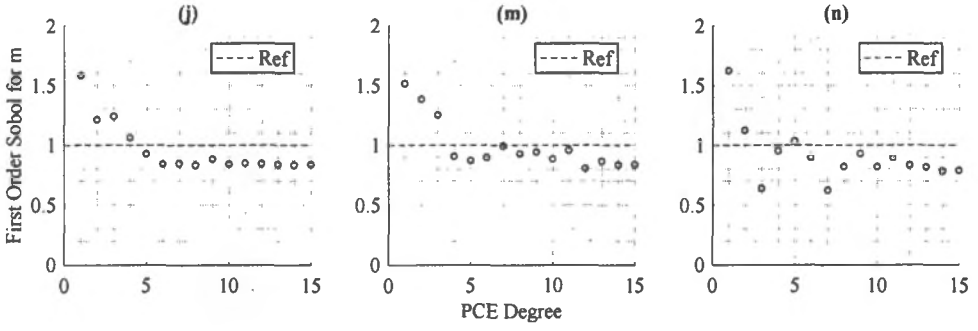

Figure 4-42: First Order Sobol for m

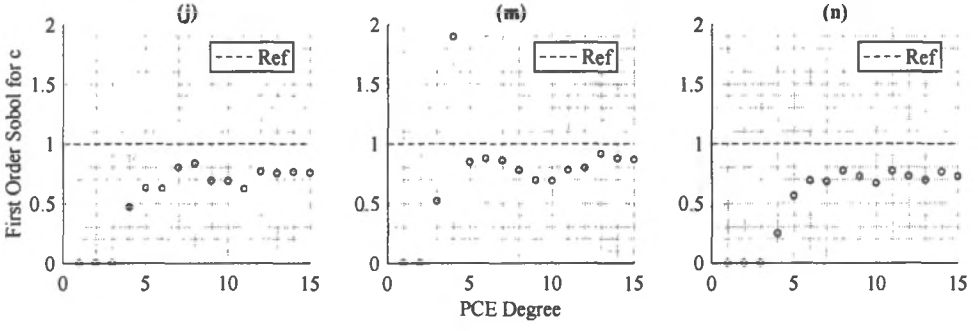

Figure 4-43: First Order Sobol for c

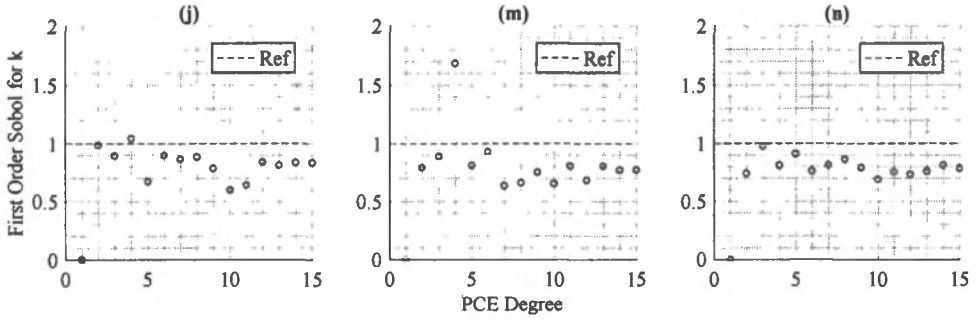

Figure 4-44: First Order Sobol for k

For the estimation on first order Sobol indices, it can be observed from figures above that three cases have similar performance. For mass, damping coefficient and stiffness, three cases reach convergence around sample PCE order, and the accuracy level is close as well.

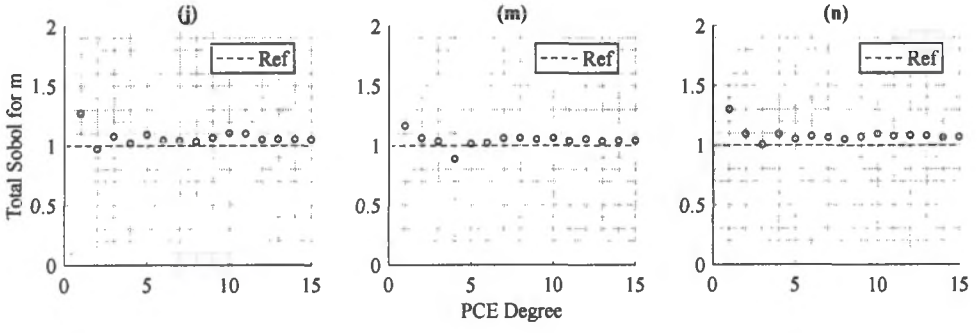

Figure 4-45: Total Sobol for m

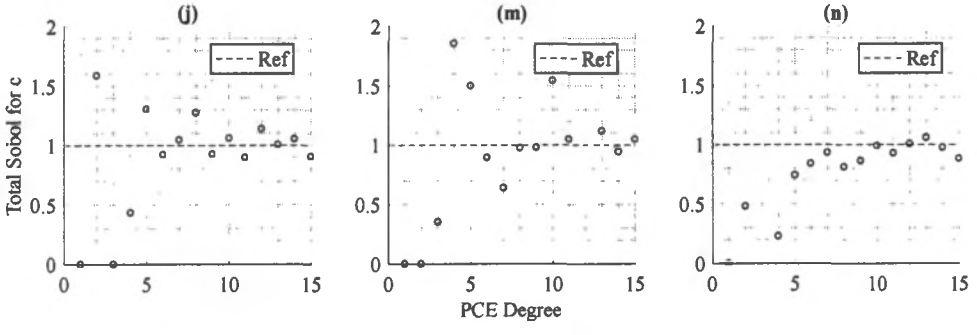

Figure 4-46: Total Sobol for c

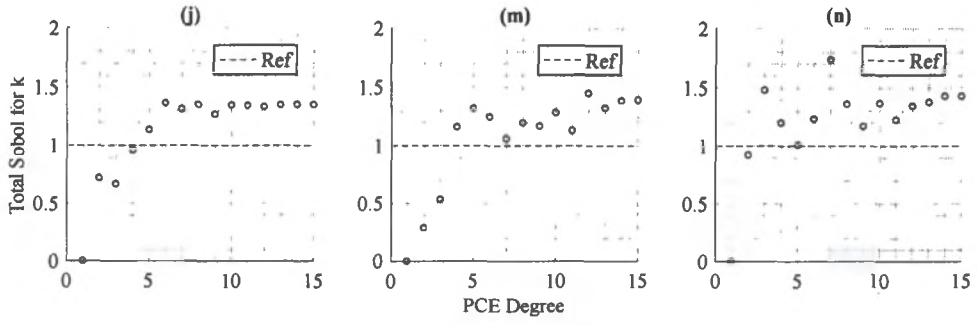

Figure 4-47:Total Sobol for k

Similar observation can be made for estimation on total Sobol indices as well. Three cases with different scale has similar accuracy level as well as the PCE degree needed.

4.4 Uncertainty Quantification of Hybrid Simulation of A SDOF System

4.4.1 Description of the SDOF System

The SDOF system used in this section is the same as the model developed in Chapter 2.

4.4.2 Modelling of Steel Column using Bouc-Wen Model

As mentioned in Chapter 2 the Bouc-Wen material is applied to fiber section in OpenSees to simulate the steel column.

4.4.3 Analysis and Results

PCE model is developed here to evaluate the mean and standard deviation of the SDOF system, and the sample size is selected to be 128 using Sobol sequence.

Table 4-8: PCE estimation

	Mean	Standard deviation
Reference	3.11	0.67
Sobol Sequence	3.04	0.72

It can be observed that, with the PCE method, the mean and standard deviation can be estimated with 2% and 6.9% error compare to reference value.

4.5 Summary and Conclusion

In this chapter, the influence from nonlinearities, natural period, damping, ground motion selection and ground motion scale to PCE model performance are discussed.

For the estimation on mean value of the maximum structural response, PCE for all cases can give accurate estimation with a small PCE degree, but for standard deviation, first order Sobol indices and total Sobol indices the effect from nonlinearities, natural period, damping ratio, ground motion selection is different.

Firstly, the effect of structural properties is discussed. For the estimation on standard deviation, PCE has better performance on LHP and LPP than FSP type nonlinearities. Different natural period does not have significant impact here, but case with large natural period shows less accuracy. Also, case with larger damping ratio has higher accuracy on the estimation, for the estimation on the first order Sobol indices, most of the cases can give accurate estimation on the mass. For the estimation on the damping and stiffness, similar to the standard deviation, PCE has better performance on LHP and LPP type nonlinearities. The cases with larger natural period have lower accuracy on stiffness estimation. Also, the case with higher damping ratio has better performance on mass and stiffness, but the estimation accuracy decreases significantly for the damping. For the estimation on the total Sobol indices, similar conclusion as first order Sobol indices can be made.

Secondly, the effect of ground motion properties is discussed. Ground motion selection can have significant impact on the PCE performance, where in the simulation, case with GM 2 has lower accuracy for almost all criterions. The scale of ground motion does not have

much influence on the performance of PCE, since similar accuracy level can be observed for all criterions.

PCE with higher order can give more accurate estimation on mean, standard deviation, first order Sobol indices and total Sobol indices; however, the computational burden increases as well. The simulation results in this chapter support that when conducted PCE analysis, the different type of nonlinearities, damping ratio, natural period and ground motion selection needs to be considered.

Chapter 5: Model Parameter Identification for Experiment Results

5.1 Introduction

Computational simulation plays an important role in modern engineering applications to predict the behavior of complex systems as well as reduce the finical burden from experiments. Computational simulation always requires the presentation of engineering models, which can be normally categorized into three categories: mathematical models, physical models and empirical models. Mathematical and physical models are always directly derived from a theory with the understanding of the mechanism behind the behavior that the models are going to describe.

Different from these two types of models, empirical models, which known as phenomenological modes or data-driven model are developed based on the collected experiment data. The development of empirical models is under the assumption that the relationship between the observations and target properties extends from past observations; therefore, the empirical models can describe the relationship between the observation and target properties. This type of model has been applied to variant discipline such as computer science, engineering, economic, sociology and chemistry. Here are examples of empirical models in engineering discipline and their function: the modified Ibarra-Median-Krawinkler (IMK) model (Lignos and Krawinkler 2011) for modelling deterioration of structural components, the Bouc-Wen model (Baber and Noori 1985) for nonlinear structural components, the nonparametric algebraic model (Song et al. 2005) for modelling behavior of Magneto-rheological (MR) dampers and the self-centring model (Beck 1989) for modelling the behavior of self-centering energy dissipative (SCED) bracing system.

Since the empirical model is derived from the experimental observation, it is important that the parameters of the model are recognized correctly. In this chapter, one optimization

technique, Practical Swarm Optimization (PSO) is introduced for parameter identification of an empirical model. Another technique, Markov Chain Monte Carlo (MCMC), is introduced for quantify the uncertainty of the empirical model parameters.

5.2 Practical Swarm Optimization (PSO)

The concept of PSO is first introduced by Kennedy and Eberhart (Christopoulos et al. 2008). This method is first developed for optimization of continuous nonlinear functions; more specifically, a simplified social model. The ease of the implementation of PSO to specific problems and its fast converge rate natural make it a popular optimization in many disciplines including model parameter identification, pattern recognition and neural network training.

PSO is a computational method that optimize the problem with target properties and measurement through iterative trial of candidate solutions. The figure below is the flowchart of a typical PSO procedure.

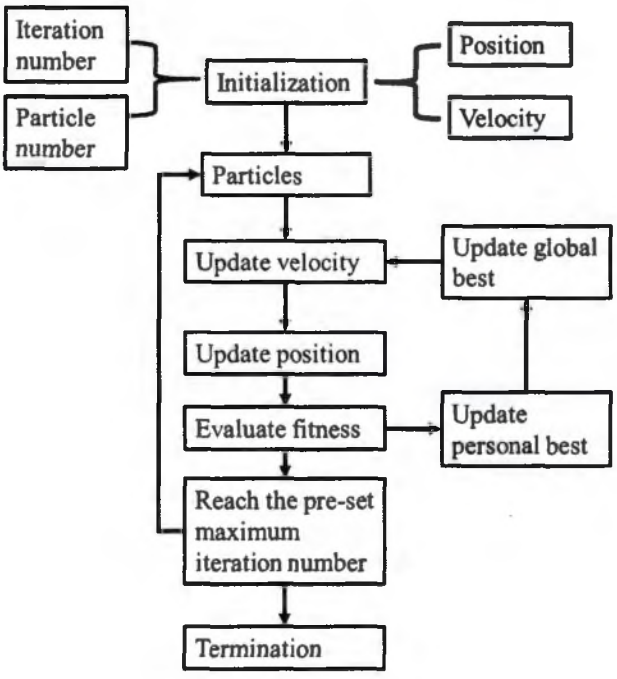

Figure 5-1: Flowchart of PSO

Starting with the initialization step, at the beginning of PSO, researchers need to define the number of iterations and particles. Generally, the larger amount of iterations and particles can lead to more accurate optimization results, as well as the increase of the computation time. Therefore, it is important to select an appropriate set of iterations and particles to balance the accuracy and efficiency. Following that, the researchers need to initializing position and velocity of particles. In this study, the initialization involves two steps. First step is assigning the beginning position of particles with random values under a given range, and the beginning velocity of particles is assigned to be zero. After the position and velocity of all particles has been assigned, the corresponding output from target system will collected, and the fitness of the output to target measurement will be calculated as follow:

$$\text{Fitness(i)} = (\text{Output} - \text{TargetMeasurement})^2 \qquad (5\text{-}1)$$

Where fitness stand for how accurate the output fits the target measurement, and i stands for the $i-th$ interation. After the calculation of fitness, the current position of each particles will be taken as personal best position, and the position of a particle will be taken as global best position, where the fitness is lowest compare to all other particles. After getting the personal and global best positions, the initial velocity of particles is calculated as follow:

$$V_i = w * V_{i-1} + c_1 * r_1 * \left(P_{p_{best}} - P_{i-1}\right) + c_2 * r_2 * \left(P_{g_{best}} - P_{i-1}\right) \quad (5\text{-}2)$$

Where V_i is the velocity of particles at $i-th$ iteration; $P_{i-1}$is the position of particles at $(i-1)-th$ iteration; w is called damping coefficient, and it can be defined as a constant or an equation; r_1 and r_2 are two uniform random variables range from 0 to 1; c_1 and c_2 are two constant coefficients usually set equal to 2; $P_{p_{best}}$ is the personal best position of particles; $P_{g_{best}}$ is the global best position of particles.

And the new position of each particles is calculated as follow:

$$\text{Position} = \text{Previous Position} + \text{Velocity} * 1 \quad (5\text{-}3)$$

After the calculation of new position of each particle, the algorithm will evaluate the fitness of each particle, and repeat the process described above until the pre-defined number of iterations has been reached.

5.3 Markov Chain Monte Carlo (MCMC) Simulation

5.3.1 Theory of MCMC Simulation

Several researches have been done considering the estimation on uncertainties in model parameter as a Bayesian inference problem (Zhang 2004, Collins et al. 1974). In other words, the application of Bayesian statistical framework takes the challenge of estimation on uncertainties in model parameters based on experiential results. More specificity, Markov Chain Monte Carol method is used in this study for numerical model parameter recognizing.

MCMC method is a procedure to sample from a probabilistic distribution. The sample from target distribution can be obtained through construction Markov chain with stationery distribution as desired distribution. Metropolis et al. (1953) proposed a method for Markov chain sampling, and later this method has been generalized by Hasting et al. (1970), which is known as Metropolis-Hasting algorithm.

In Bayesian statistical framework, the conditional probability of realizing a data set D, given observation O, $\mathrm{P}(D|O)$ is recognized as posterior probability is defined as:

$$\mathrm{P}(D|O) = \frac{P(O|D)P(D)}{P(O)} \qquad (5\text{-}4)$$

where $P(O|D)$ is the likelihood, or the probability of realizing a data set O, given data set D; $P(D)$ is the prior probability, or the known information about the data set D, where in this work a Gaussian distribution with infinity variance is applied for all parameters in D; $P(O)$ is called evidence, and is a normalized factor to ensure that the integral of posterior probability is equal to 1.

Beck and Au (2002) have introduced and applied the Markov Chain Monte Carlo (MCMC) simulation procedure to estimate the uncertainties in model parameters, for example, parameter estimation on dynamic response of a large-scale magneto-rheological (MR) damper (Caicedo et al. 2016). The conditional probability of realizing the model parameter

D^i given experimental data make up the posterior probability. By sampling under the posterior probability, the model parameters can be generated. MH algorithm is a procedure to simulate samples based on an arbitrary probability density function (PDF) referred to as target PDF. Samples are simulated as the state of a Markov chain whose stationary distribution is equal to the target PDF, which means after the k^{th} Markov step ($k \rightarrow \infty$), the PDF of simulated samples tends to be the target PDF.

The general procedure of the MCMC approach is as follow:

(1) Estimating the prior information.
(2) Initialization.
(3) Calculate likelihood.
(4) Calculate the posterior.
(5) Propose a new sample.
(6) Accept/ Reject the proposed sample.
(7) Repeat process 3-6 till predefined sample number has been reached.

By applying the MCMC procedure, instead of only get a collection with optimized parameters, a collection with information of probabilistic distribution of parameters, and prediction of error between actual structure response and model prediction can be developed.

5.3.1.1 Methods for MCMC

The calculation of the posterior distribution can involve significant computational burden for multidimensional problems. Markov Chain Monte Carol (MCMC) method provide a solution for calculation of posterior distribution of this type of problems. There are varies type of MCMC can be applied to address this challenge, and in this study the algorithm proposed by Metropolis et al. (1953) and later by Hasting (1970) is selected.

The MCMC method, a chain or a sequence of values are generated. This chain follows a stochastic process, which is also known as Markov Chain. The MH algorithm used in MCMC procedure will generate values of θ, and the distribution of θ will be limited to fit the target distribution $\pi(\theta)$. Therefor, by applying MCMC method, we will be able to sample from the posterior distribution. In this study, a MCMC toolbox developed by is used for MCMC simulation.

The MH algorithm is one of algorithm that can be applied for MCMC simulation. Also, the ease of implement this method, as well as its generalization make it the most general algorithm for MCMC simulation. The main point behind of MH algorithm is replace the calculation of $\pi(\theta)$ by the calculation of $\pi(\theta)/\pi(\theta^*)$. In this way, the calculation of integral in Bayesian formula can be omit.

According to Gamerman (1997) and Marko (2008), by applying MH algorithm a Markov chain is generated with the transition kernel as below:

$$p(\theta,\theta^*) = q(\theta,\theta^*)\alpha(\theta,\theta^*), \theta \neq \theta^* \qquad (5\text{-}5)$$

$$p(\theta,\theta) = 1 - \int q(\theta,\theta^*)\alpha(\theta,\theta^*)d\theta \qquad (5\text{-}6)$$

Where α is the acceptance probability; $(\theta, \cdot)$ is the proposal density; θ is the current data set of the chain. The chain is reversible when the equation below has been satisfied:

$$\pi(\theta)q(\theta,\theta^*)\alpha(\theta,\theta^*) = \pi(\theta^*)q(\theta^*,\theta)\alpha(\theta^*,\theta) \qquad (5\text{-}7)$$

When the chain is reversible, the density π can be the stationary distribution of the chain as equation *(5-8)*, which means when the chain reaches π, rest simulation will follow this distribution.

$$\int \pi(\theta)p(\theta,\theta^*)d\theta = \pi(\theta^*) \qquad (5\text{-}8)$$

Therefore, the acceptance probability α is selected as below:

$$\alpha(\theta, \theta^*) = min\left\{1, \frac{\pi(\theta^*)q(\theta^*, \theta)}{\pi(\theta)q(\theta, \theta^*)}\right\} \quad (5\text{-}9)$$

Therefore, the procedure of MH algorithm can be express as below:

(1) Select an initial value set, select a proposal distribution.
(2) Propose a new value set from distribution.
(3) Accept the new value set if $\pi(\theta^*)q(\theta^*, \theta) > \pi(\theta)q(\theta, \theta^*)$. If the previous condition was not satisfied, accept this set based on the acceptance probability α calculated in equation *(5-9)*.
(4) If θ^* is rejected, set $\theta^i = \theta^{i-1}$
(5) Back to step (2), until the pre-set chain number has been reached.

Once again, the MH algorithm is designed to make the target distribution π the same as the stationary distribution of constructed Markov chain. Therefore, the values in the chain follows the posterior distribution.

5.3.1.2 Results of MCMC

After the MCMC analysis, a chain with input parameter set will be generated, and it can be taken as samples generated from posterior distribution from these parameters. From the chain value of parameters, the moments of parameters can be calculated, and the correlation between parameters can be found as well.

5.3.2 MCMC Toolbox

In this study, a Matlab based MCMC toolbox developed by Laine (2008) is used to conduct MCMC simulation.

5.4 Moment Method

5.4.1 Description of Moment Method

Zhao et al. (2007) proposed the moment method, and the moment method is a method to convert variables with unknow cumulative distribution functions into standard normal distribution. To do the transformation, an explicit fourth-moment equation is used as follow:

$$x_s = S_u(u) = -l_1 + k_1 u + l_1 u^2 + k_2 u^3 \quad (5\text{-}10)$$

Where x_s is the standardized variable, u is the standard normal variable, and l_1, k_1 and k_2 is as follow:

$$l_1 = \frac{\alpha_{3X}}{6(1+6l_2)} \quad (5\text{-}11)$$

$$l_2 = \frac{1}{36}\sqrt{6\alpha_{4X} - 8\alpha_{3X}^2 - 14 - 2} \quad (5\text{-}12)$$

$$k_1 = \frac{1-l_2}{(1+l_1^2-l_2^2)} \quad (5\text{-}13)$$

$$k_2 = \frac{l_2}{(1+l_1^2+12l_2^2)} \quad (5\text{-}14)$$

Where α_{3X} is the third central moment (skewness) and α_{4X} is the fourth central moment (kurtosis). Also, the equations below should be satisfied when doing transformation:

$$\alpha_{4X} \geq (7 + 4\alpha_{3X}^2)/3 \quad (5\text{-}15)$$

5.4.2 Converting Non-Regular Distribution for Sampling

Through equation *(5-10)*, the distribution got from MCMC simulation result can be transformed into standard normal distribution, and later been applied for PCE simulation.

However, it is worth mention that the fourth-moment functional area is limited, if moments fall-into the non-functional area, the fourth-moment method cannot be applied.

5.5 Parameter Identification of Modified IMK Model Parameters from Experiments on Steel Beam-Column Moment Connection

5.5.1 Modified IMK Model

The modified IMK model, was developed from the Ibarra-Krawinkler (IK) model, is an energy-based phenomenological model that incorporates the ability to capture the deterioration, which is critical for response prediction of highly inelastic systems. The modified IMK model establishes strength bounds based on a monotonic backbone curve with rules on define the characteristic of hysteretic behavior between the bounds. For bilinear hysteretic response, the backbone curve is defined by three strength related parameters namely effective yield moment (M_y), post yield strength ratio (M_c/M_y), residual moment ratio (k_{res}), and four deformation related parameters namely yield rotation (θ_y), pre-capping plastic rotation for monotonic loading (θ_p), post-capping plastic rotation (θ_{pc}), and ultimate rotation capacity (θ_u). The rate of cyclic deterioration is control by the reference cumulative rotation capacity (Λ). Figure 5-2 from Lignos and Krawinkler (2011) shows the deterioration model and associated definitions. This IMK model has been implemented in the OpenSees for structural collapse simulation. This model is intended for any force-deformation relationship, and this study focuses on the moment and rotation relationship of steel beam-column connections. The parameter θ_y in this study is calculated by dividing the effective yield moment M_y by the flexure stiffness (K). A vector D is used to describe these parameters as shown below:

$$D^i = [K, \theta_p, \theta_{pc}, \theta_u, \Lambda, M_y^+, M_y^-, \frac{M_c{}^+}{M_y}, \frac{M_c{}^-}{M_y}, k_{res}]$$

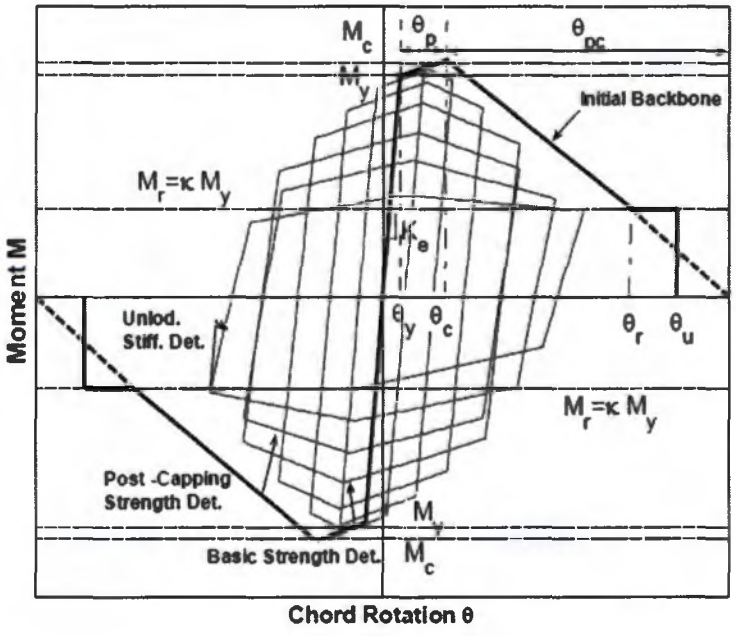

Figure 5-2: Modified IMK model and definition of parameters

5.5.2 Steel Beam-Column Connection Test

Experiment data of three specimens by Zhang (2004) are selected in this study, namely SPCE-1, SPEC-3, and SPEC-6. The experimental data is downloaded from a steel database (Lignos 2013). Table 1 provides the subassembly geometry and material properties of three specimens.

Table 5-1: Properties of SPEC-1, SPEC-3, and SPEC-6:

	SPEC-1	SPEC-3	SPEC-6
Beam section	W36X150	W36X150	W30X108
Column section	W36X230	W27X194	W24X131
Beam-to-column connection	RBS	RBS	RBS
Flange reduction for RBS	50%	50%	50%
Slab presence	Yes	Yes	No
Beam length to centerline of column	177.0 in	177.0 in	177.0 in

Beam effective length from load or support point to idealized plastic hinge location	136.56 in	140.44 in	142.25 in
Distance to closest lateral brace	120 in	120 in	120 in
Nominal yield stress	50 ksi	50 ksi	50 ksi

Specimen SPEC-1 has W36x230 for column and W36x150 for Beam. It was observed that SPEC-1 first yielded in the beam bottom flanges at the RBS at 0.5% story drift cycles. During the 1% story drift cycles, the concrete slab crushed and the panel zone yielding occurred. Beam web local buckling in the RBS happened in the 2% story drift. During the 3% story drift, the specimen reached its maximum capacity, and the beam bottom flange move laterally in the RBS. Column twist was visible at the 4% story drift cycle. Fracture and low fatigue cracks was also observed in the beam flange at the RBS in the first 5% story drift cycle. The plastic moment is 29216 kip-in for east beam, 29203 kip-in for west beam. Specimen SPEC-3 has W27x194 for column and W36x150 for beam. During the test, cracking of the concrete floor slab occurred at the end of the 0.375% story drift cycles. Yielding was observed in the beam bottom flanges at the RBS and near the column face at 1% story drift. Concrete slab crushed at the 1% story drift cycles. Panel zone yielded during 1.5% story drift cycles. Similar to SPEC-1, beam web local buckling occurred in the RBS during first cycles of 2% story drift. Beam flange local buckling happened at 3% story drift cycles. During 5% drift cycles, low cycle fatigue cracks were found and as it reached at the end of first 6% story drift cycle, ductile material tearing of the bottom RBS flange occurred. SPEC-6 has W24x131 for column, W30x108 for beam and has no concrete slab. Yielding was observed at 1% story drift in the beam web at the RBS and at 1.5% story drift in the beam region between RBS flanges and column flange. No visible beam flange buckling, and beam flange lateral movement were found before it reached 4% story drift cycles. Yielding in connection was observed during 4% story drift cycles and small column twisting. Different from SPEC-1 and SPEC-3, SPEC-6 successfully

underwent the first half cycle of 5% story drift. Figs. 2(a), 2(b) and 2(c) present the moment and rotation relationship at beam plastic hinge locations of these three specimens. Both strength and stiffness deterioration can be observed in Figs. 2(a) and 2(b) forSPEC-1 and SPEC-3, while not for SPEC-6.

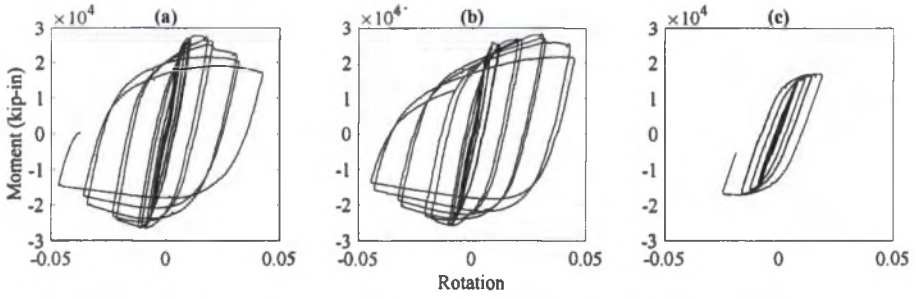

Figure 5-3: Moment-rotation relationship at beam plastic hinge locations for (a) SPEC-1, (b) SPEC-3, (c) SPEC-6

SPEC-1 and SPEC-3 are with concrete floor slab, while there is no concrete floor slab for SPEC 6. Therefore, composite action is expected in SPEC-1 and SPEC-3 during testing. As shown in figure 2, the maximum moment when the top beam is in compression is slightly bigger than the maximum moment when the beam bottom flange is in compression from the non-symmetric hysteresis curves in figure 2(a) and 2(b). This is due to the composition action from the concrete slabs of these two specimens, and the beam moment deteriorate quicker at the bottom flange in compression than top flange in compression. Because there is no concrete slab in SPEC-6, the maximum moments when the beam top flange in compression and the beam bottom flange is in compression are about the same, as indicated in the symmetric hysteresis curve of figure 2(c). SPEC-6 has a weaker panel zone, compared to SPEC-1 and SPEC-3, therefore, smaller moments are developed, as shown in figure 2(c).

According to Zhang (2004), the concrete began to crush against the column flanges, during the 1.5% story drift cycles during testing for SPEC-1. While the concrete slab began to crush during the cycle of 1.0% story drift cycle for SPEC-3.

It can also be observed that although all three specimens had concrete slab, composite action is much stronger in SPEC-3 than that in SPEC-1.

The moment-rotation hysteresis behavior of these three specimens are expected to be emulated using the IMK model for collapse prediction. The backbone curve parameters of the IMK model can be determined following the suggestion by Lignos and Krawinkler (2011) and are presented in Table. 2. These parameters are used as the initial values of D in this study.

Since all specimens use RBS connection, the initial values for θ_p , θ_{pc} and Λ are determined using the predictive equations developed by Lignos and Krawinkle (2011).

where F_y is the expected yield strength of the flange of the beam in Mpa, and it is normalized by 355 MPa (typical nominal yield strength of European structural steel and equivalent with nominal yield strength of around 50 ksi in U.S. steel); L is the shear span (distance of plastic hinge location to point of inflection); L_b is the distance from the column face to the nearest lateral brace; r_y is the radius of gyration about the y-axis of the beam; t_w, t_f, d are thickness of web, thickness of flange, and section depth; c^1_{unit} and c^2_{unit} are coefficients for unit conversion, where $c^1_{unit} = 1$, and $c^2_{unit} = 1$ if international units are used, and $c^1_{unit} = 25.4$, and $c^2_{unit} = 6.895$ if imperial units are used.

Table 5-2: Deterministic parameter values for SPEC-1, SPEC-3, and SPEC-6

	K(kip-in/rad)	$\theta_p(rad)$	θ_{pc}(rad)	Λ(rad)	$\theta_u(rad)$	k_{res}	$\frac{M_c}{M_y}+$	$\frac{M_c}{M_y}-$	$M_y + (kip - in)$	$M_y - (kip - in)$
SPEC-1	8738667	0.016	0.163	0.885	0.2	0.4	1.3	1.05	22870	22870
SPEC-3	8738667	0.016	0.163	0.885	0.2	0.4	1.3	1.05	22870	22870
SPEC-6	4321000	0.019	0.154	0.862	0.2	0.4	1.3	1.3	13603	13603

5.5.3 PSO Analysis Results

In this section, the PSO of IMK model parameter identification from experiment measurement of rotation and moment is conduct. An OpenSees model is developed here for PSO process. Figure below shows the scheme of the model.

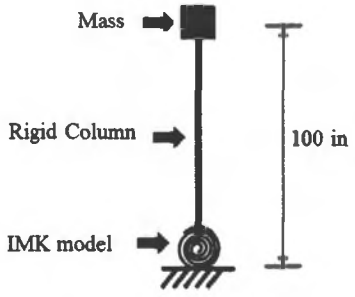

Figure 5-4: Scheme of OpenSees Model using IMK model

This model is developed IMK material applied on zero-length element in OpenSees. The different between OpenSees model output and experiment measurement of moment is applied for PSO simulation. Table below shows the parameters identified by PSO.

Table 5-3: PSO identification of IMK parameters

	K	θ_p	θ_{pc}	Λ	M_y+	M_y-
PSO results	3689546	0.011	0.177	0.625	24793	-23503
	3350309	0.019	0.200	1.05	23495	-23550
	1806136	0.038	0.318	0.831	14998	-14998

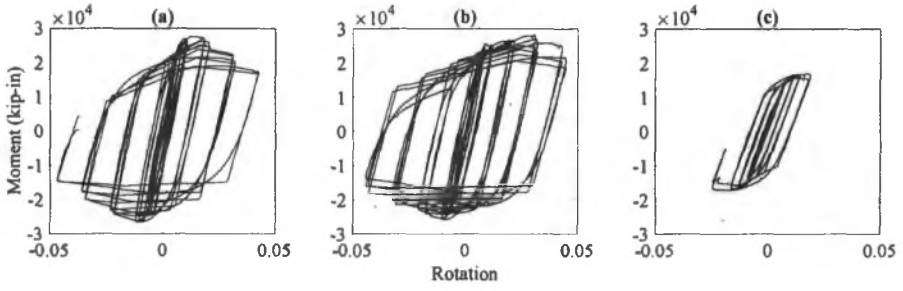

Figure 5-5: Comparison between experiment measurement and OpenSees output using PSO identified parameters, (a) SPEC 1, (b) SPEC 3, (c) SPEC 6

Figure above shows the comparison between experiment measurement and IMK model output given identified parameters, it can be observed that good agreement between the OpenSees model with PSO identified parameters and experiment measurement. It supports that with the application of PSO, the model parameters can be identified.

5.5.4 MCMC Analysis Results

For three specimens, three MCMC simulations are conducted. Figures below shows the density plot developed based on the MCMC chain data.

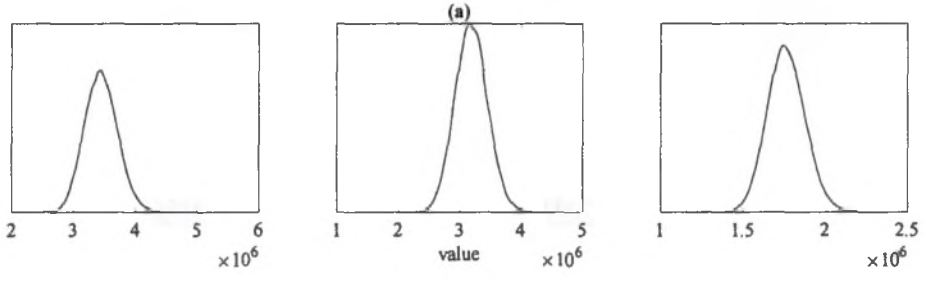

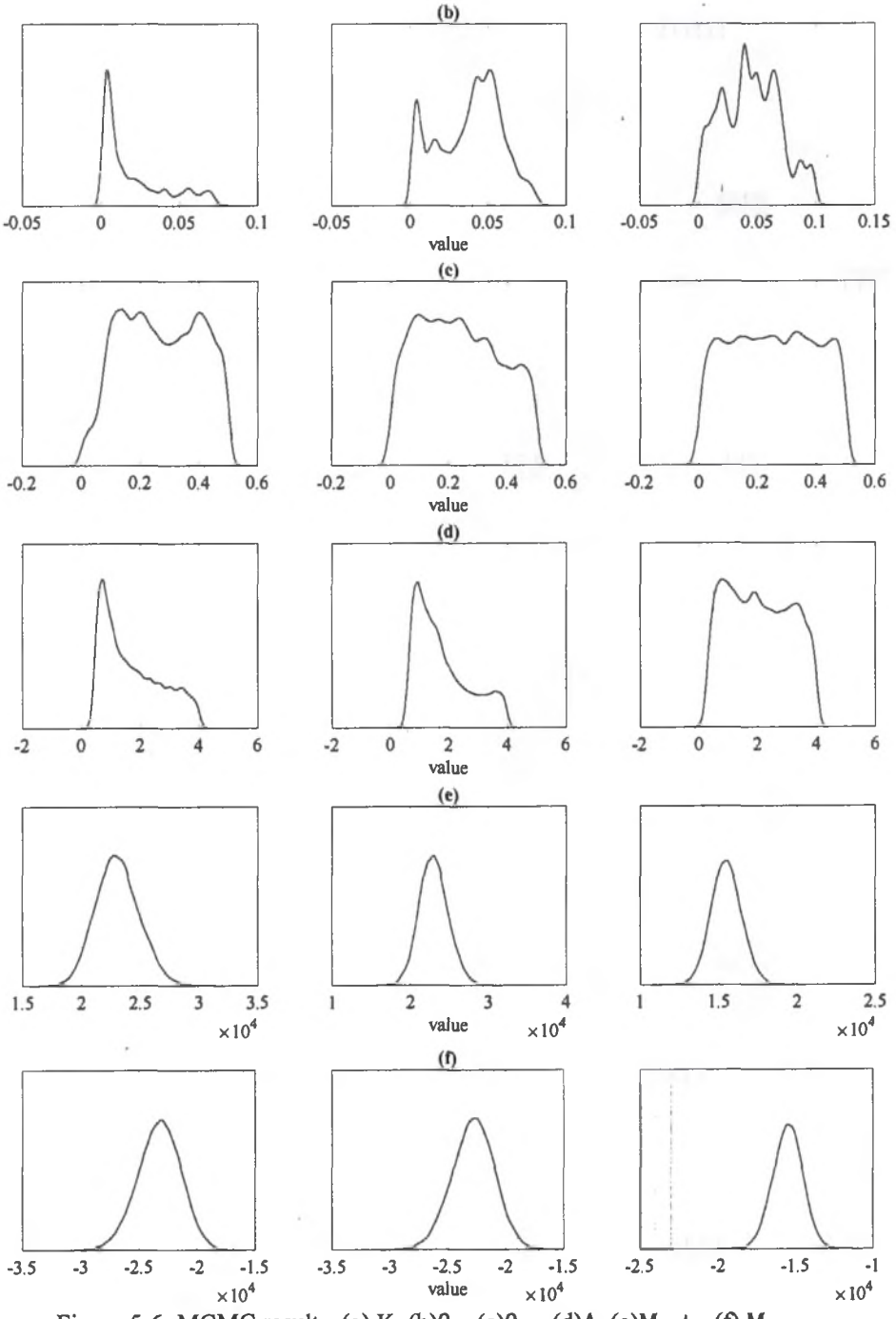

Figure 5-6: MCMC results, (a) K, (b)θ_p, (c)θ_{pc}, (d)Λ, (e)M_y+, (f) M_y-

From figure above, it can be observed that the density plot of stiffness, and positive and negative yield moment similar to gaussian distribution, and others follows unknow types of distributions. Then, the chain data are used to conduct the cyclic analysis, and the dissipated energy is evaluated.

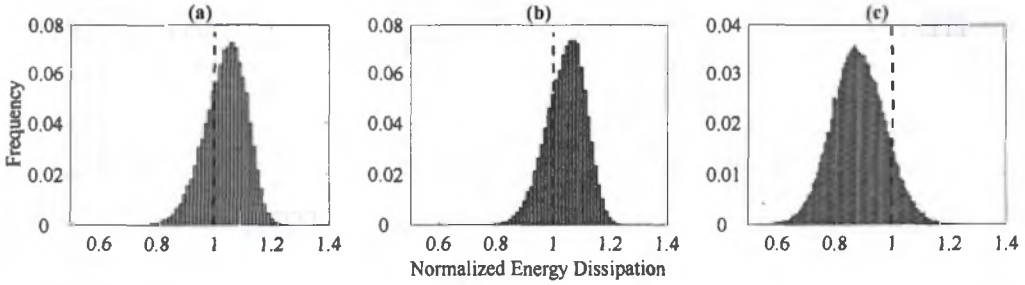

Figure 5-7: Comparison of energy dissipation for (a) SPEC-1, (b) SPEC-2, and (c) SPEC-6

From the figure above, it can be observed that with the uncertainty from input parameters, the dissipated energy varies as well. The red dash line is the energy measured from experiment, and it can be observed that the reference energy dissipation falls into the MCMC results, and instead of getting one value, the uncertainty in energy dissipation can be captured.

After the PSO and MCMC simulation, the experimental substructure parameters in hypercube can be identified as equation below:

$$PSP_{k,HC}^{i(J)} = PSP_{k,CDF}^{i(J)}(PSP_{k,PSO}^{i(J)}) \tag{5-16}$$

The probability of model parameters identified through PSO given CDF developed through MCMC is selected to be the hypercube parameter of this experimental substructure.

5.5.4.1 Rejection Rate

It is recommended to have rejection rate between 15% to 50% (Gelman et al. 1996). The rejection rate is 50%, 49% and 42% for three specimens. The rejection rate is related to σ, larger σ leads to smaller rejection rate and smaller σ leads to bigger rejection rate.

5.5.4.2 Effect of Prior

The prior is the level of knowledge of the target value before the simulation. Non-informative prior is applied here since the assumption here is no information about the target value before the simulation.

5.5.5 Converting PDFs from MCMC Analysis using Method of Moments

Through the application of *(5-10)*, the MCMC analysis samples in unknow cumulative distribution function can be transformed into standard normal distribution when the moments of the MCMC samples fall into the functional area of fourth-moment method.

5.6 Low Discrepancy Sampling from MCMC Analysis of Modified IMK Model

After the conversion of PDFs from MCMC analysis results to standard normal distribution, one can conduct low discrepancy sampling using methods proposed in Chapter 3 to get sample from the standard normal distribution. After the samples are selected, the samples from distribution identified by MCMC simulation can be obtained by converting the samples in standard normal distributing back to the distribution identified by MCMC simulation.

5.7 Summary and Conclusion

In this chapter, the optimization technique PSO and MCMC are applied for IMK model parameter identification. Through the application of PSO, a best fit sample set can be obtained under the given experiment measurement, while using MCMC a chain of possible

sample set can be obtained under given experiment measurement and error variance. The energy dissipation of MCMC simulation samples are evaluated using cyclic test and compared to experiment measurement. After that, the unknown CDF from MCMC sample are converted using forth-moment method. These results support that PSO and MCMC can be applied for model parameter identification.

Chapter 6: Framework of Hybrid Simulation to Account for Numerical Substructure Uncertainties

6.1 Introduction

In this chapter, the uncertainty quantification and experiment design for hybrid simulation accounting for numerical substructure uncertainties is introduced. Two types of experiment design strategies are introduced here namely the sequence experiment design and the adaptive experiment design. Also, two types approaches are used for uncertainty quantification. The first approach is based on meta-modeling and the second approach is based on samples. The proposed methods are illustrated using the SDOF structure developed in chapter 4.

6.2 MC Simulation of Hybrid Simulation with Numerical Substructure Uncertainties

6.2.1 Definition of Uncertainties for Substructures

In this section the SDOF flag-shape model (b) developed in previous chapter is selected, refer to Chapter 4 for detailed description. In this case, the mass, damping coefficients and stiffness is considered to have uncertainties. Table below shows the mean and standard deviation of these three parameters under the lognormal distribution assumption.

Table 6-1: Uncertainties in mass, stiffness and damping coefficients

Case	m		c		k_a	
	Mean	Std	Mean	Std	Mean	Std
(b)	1.00	0.20	0.63	0.13	39.48	7.90

6.2.2 MC Simulation Results

From Chapter 4, the mean, standard deviation, skewness and kurtosis of maximum response of the system subject to the earthquake are as table below:

Table 6-2: Case (b) MC simulation results

Case	Mean	Standard deviation	Skewness	Kurtosis
(b)	7.52	2.45	-0.27	1.48

The MC simulation results will be applied as the reference to evaluate the performance of proposed methods.

6.3 Meta modeling-based approach

For meta modeling-based approach, the mean, standard deviation, skewness, kurtosis is estimated through the meta-model outputs.

6.3.1 Sequential Approach

6.3.1.1 Procedure and Flowchart

The procedure of the Sobol based approach is as following:

(1) Define maximum sample number n.

(2) Start with initial sample set P_{ini} ($P_{ini} \ll ED$) and evaluate the model response Y_{ini}.

(3) Train meta-model using P_{ini} and Y_{ini}.

(4) Enrich sample set with one new sample x_{k+1} through Sobol sequence and evaluate the model response y_{k+1}. $P_{k+1} = P_k \cup x_{k+1}$, $Y_{k+1} = Y_k \cup y_{k+1}$

(5) Train new meta-model using current $P_{current}$ and $y_{current}$.

(6) Repeat procedure (2)-(5) if the maximum sample number is not reached.

6.3.1.2 Computational Simulation Results using PCE and Kriging

Follows the procedure proposed in the previous section, the mean and standard deviation of maximum restructure response under seismic excitation is evaluated using PCE and Kriging methods. Figures below show the simulation results:

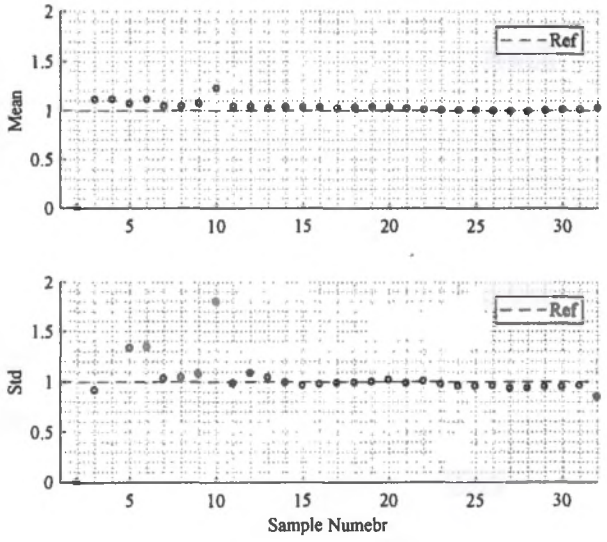

Figure 6-1: PCE Simulation Results

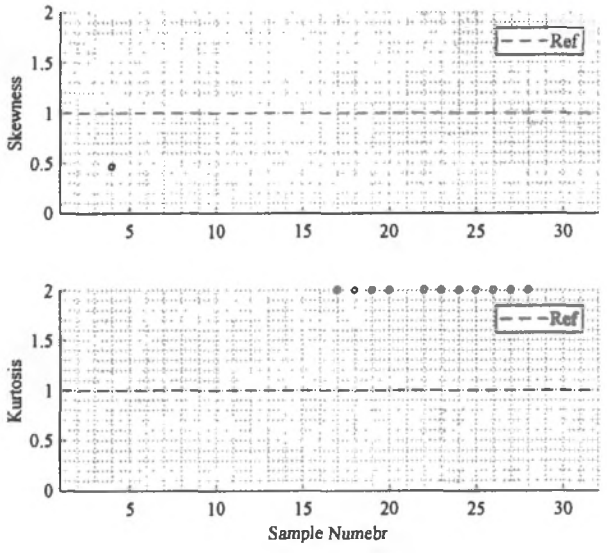

Figure 6-2: PCE Skewness and kurtosis

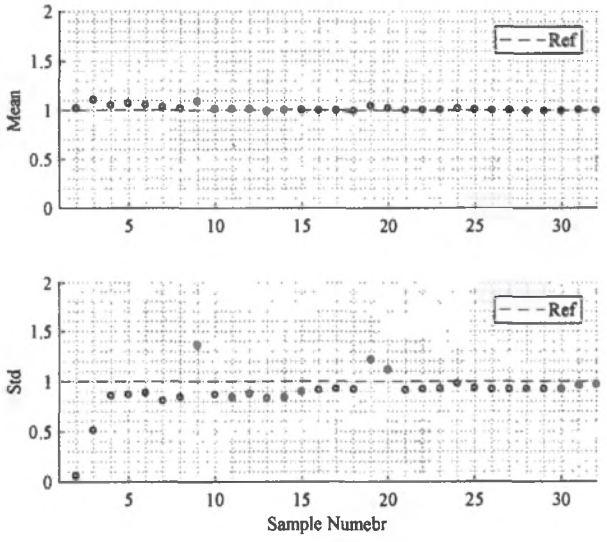

Figure 6-3: Kriging Results

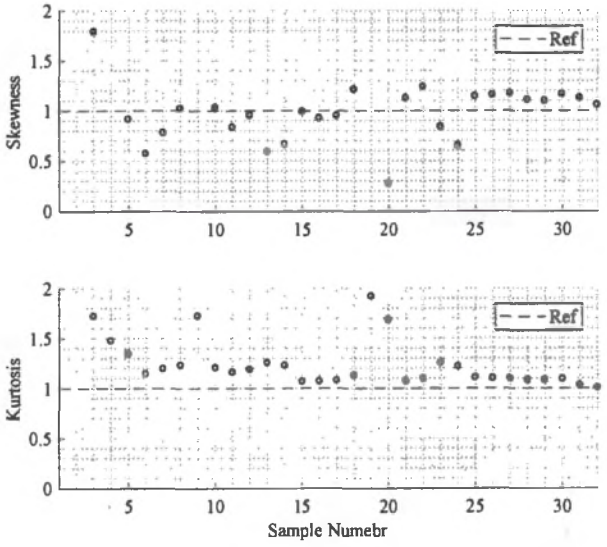

Figure 6-4: Kriging skewness and kurtosis

From figures above, it can be observed that both Kriging and PCE method has good accuracy on estimating mean and standard deviation. Also, it can be observed that for the estimation on mean value, Kriging method reaches convergence earlier compare to PCE method. For the estimation on standard deviation, Kriging and PCE method have similar convergence rate.

6.3.2 Adaptive Approach

6.3.2.1 Procedure and Flowchart

The procedure of the Space-filling based approach is as following:

(1) Define maximum sample number n.

(2) Start with initial sample set P_{ini} ($P_{ini} \ll ED$) and evaluate the model response Y_{ini}.

(3) Train meta-model using P_{ini} and Y_{ini}.

(4) Enrich sample set with one new sample x_{k+1} through space-filling and evaluate the model response y_{k+1}. $P_{k+1} = P_k \cup x_{k+1}$, $Y_{k+1} = Y_k \cup y_{k+1}$

(5) Train new meta-model using current $P_{current}$ and $y_{current}$.

(6) Repeat procedure (2)-(5) if the maximum sample number is not reached.

6.3.2.2 Computational Simulation Results using PCE and Kriging

In this section, the adaptive approach using space-filling method is used, and the simulation results using PCE and Kriging methods are as follow:

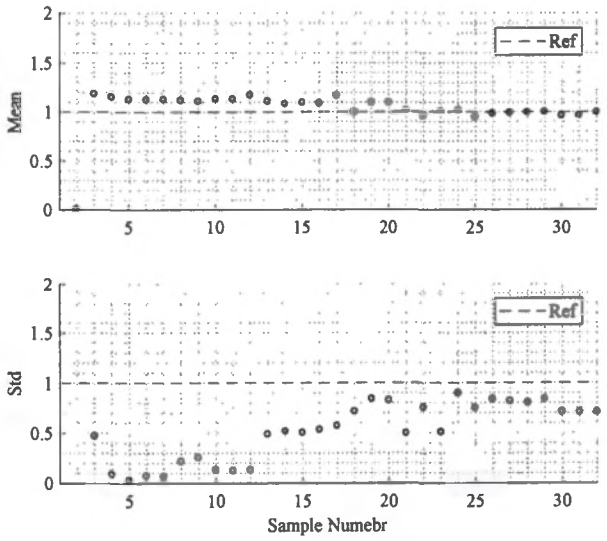

Figure 6-5: PCE Mean and Standard Deviation

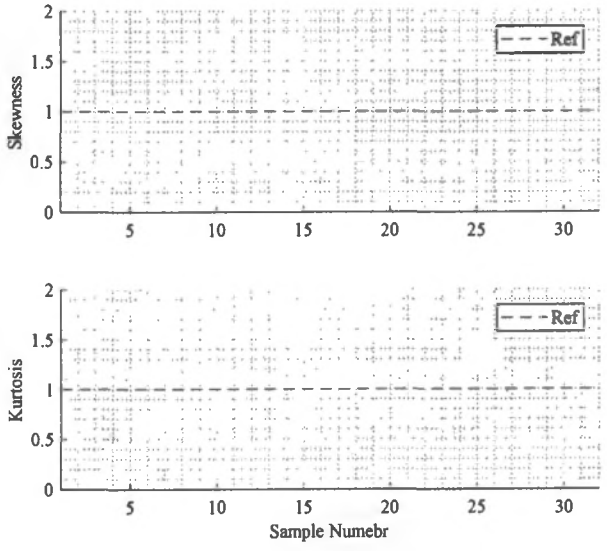

Figure 6-6: PCE Skewness and Kurtosis

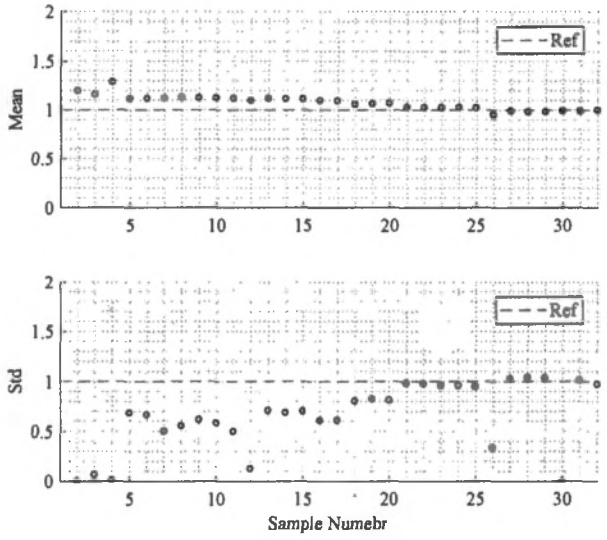

Figure 6-7: Kriging Mean and Standard Deviation

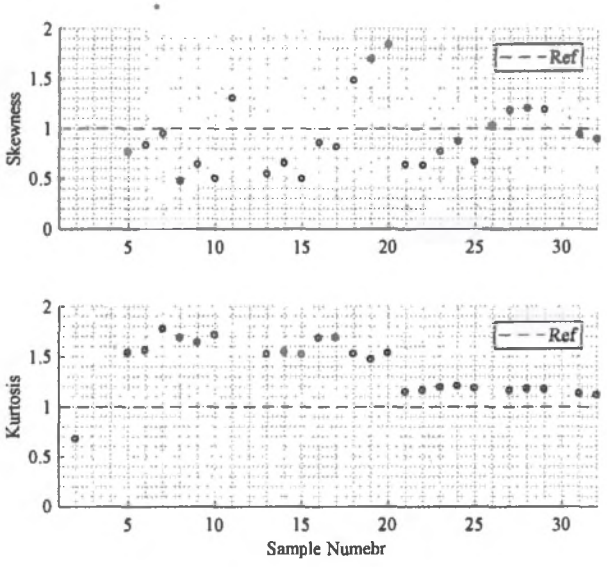

Figure 6-8: Kriging Skewness and Kurtosis

From figures above, it can be observed that, different from sequence approach PCE method does not have good performance on estimating standard deviation of maximum structural

response under seismic excitation. For both PCE and Kriging method, the sample required to have good accuracy on standard deviation is larger comparing to sequence approach. For the mean value, both PCE and Kriging method have good estimation with 20 samples, which is larger compare to sequence approach. The increase of sample number can be explained that the sampling procedure of adaptive approach is 'greedy', the sample are selected based on max-min criterion to give candidate under the different sample size and the previously selected sample cannot be withdrawal. Comparing the sequence approach where a pre-defined sample number is given, and the optimal sample of that number can be generated.

6.4 Sample-based approach

For sample-based approaches, two scenarios are considered, (1) sample with equal assigned probability and (2) sample with different assigned probability. For sample-based approach, the mean, standard deviation, skewness, kurtosis is estimated through the samples.

6.4.1 Sequential Approach

6.4.1.1 Sample with Equal Assigned Probability

6.4.1.1.1 Procedure and Flowchart

The procedure of the Space-filling based approach is as following:

(1) Define maximum sample number n.

(2) Start with initial sample set P_{ini} ($P_{ini} \ll ED$) and evaluate the model response Y_{ini}.

(3) Enrich sample set with one new sample x_{k+1} through Sobol Sequence and evaluate the model response y_{k+1}. $P_{k+1} = P_k \cup x_{k+1}$, $Y_{k+1} = Y_k \cup y_{k+1}$

(4) Repeat procedure (2)-(3) if maximum sample number is not reached.

6.4.1.1.2 Computational Simulation Results

In this section, the mean and standard deviation of the maximum structure response under seismic excitation is estimated without using meta-modeling technique, and the simulation results are as follow:

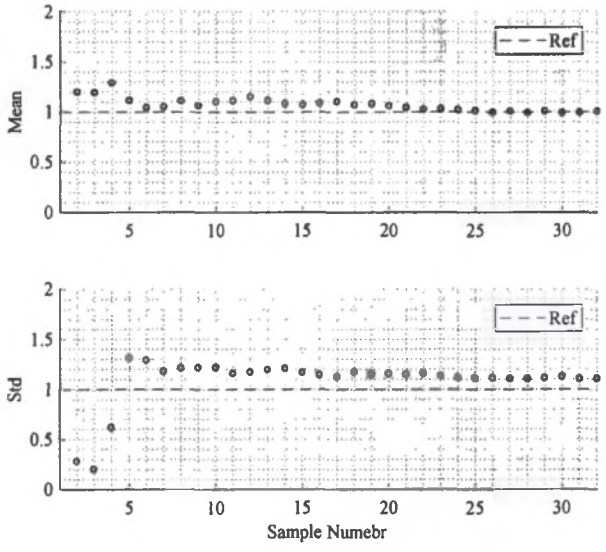

Figure 6-9: Sample Based Mean and Stadnard Deviation

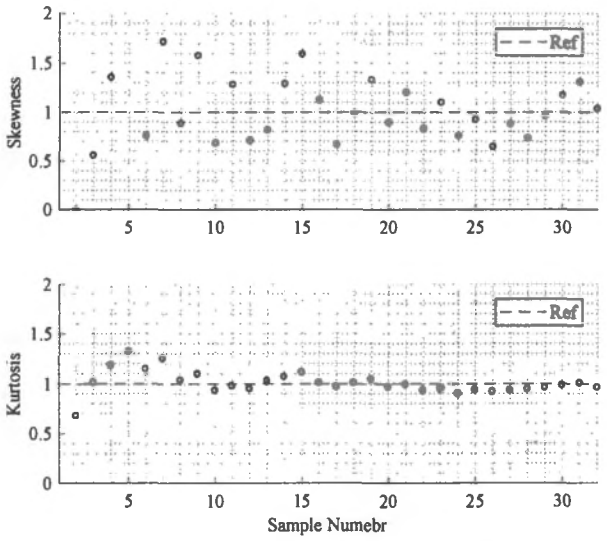

Figure 6-10: Sample Based Skewness and Kurtosis

From figure above, it can be observed that for sample-based approach, the convergence rate for standard deviation is high, while for mean value the simulation results waving back and forward. Also, the good accuracy on estimating the mean and standard deviation can be observed.

6.4.1.2 Sample with Different Assigned Probability

6.4.1.2.1 Procedure and Flowchart

The procedure of the Space-filling based approach is as following:

(5) Define target sample number n.

(6) Start with initial sample set P_{ini} ($P_{ini} \ll ED$) and evaluate the model response Y_{ini}.

(7) Train meta-model using P_{ini} and Y_{ini}.

(8) Enrich sample set with one new sample x_{k+1} through Sobol Sequence and evaluate the model response y_{k+1}. $P_{k+1} = P_k \cup x_{k+1}$, $Y_{k+1} = Y_k \cup y_{k+1}$

(9) Train new meta-model using current $P_{current}$ and $y_{current}$.

6.4.1.2.2 Computational Simulation Results

In this section, the estimation of mean and standard deviation using sample generated following the proposed procure is conduct. In the figure below, similar to the PCE method, Kriging method and sample with equal assigned probability, good accuracy can be reached with a small sample number for both mean and standard deviation.

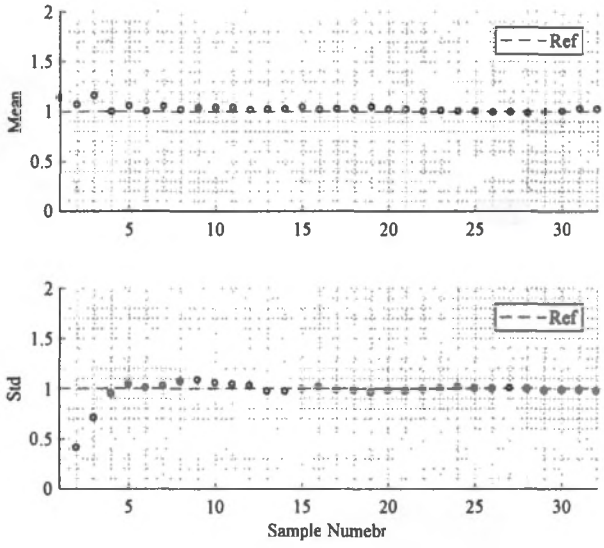

Figure 6-11: Sample Based Mean and Standard Deviation

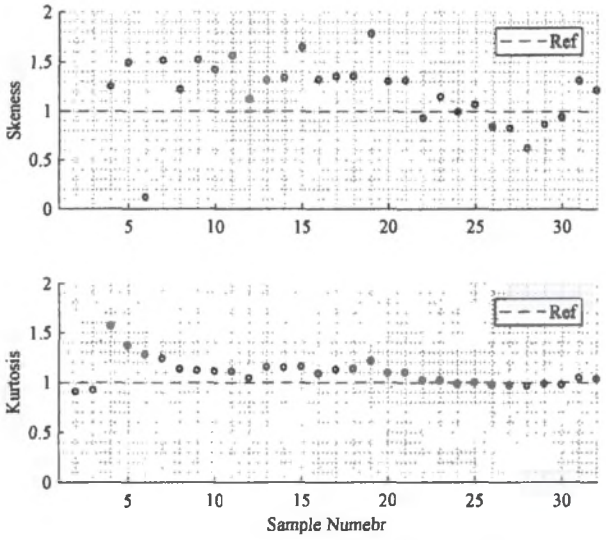

Figure 6-12: GF sequence Skewness and Kurtosis

6.4.2 Adaptive Approach

6.4.2.1 Sample with Equal Assigned Probability

6.4.2.1.1 Procedure and Flowchart

The procedure of the Space-filling based approach is as following:

(1) Define maximum sample number n.

(2) Start with initial sample set P_{ini} ($P_{ini} \ll ED$) and evaluate the model response Y_{ini}.

(3) Enrich sample set with one new sample x_{k+1} use max-min procedure and evaluate the model response y_{k+1}. $P_{k+1} = P_k \cup x_{k+1}$, $Y_{k+1} = Y_k \cup y_{k+1}$.

(4) Repeat procedure (2)-(3) if maximum sample number is not reached.

6.4.2.1.2 Computational Simulation Results

The sample-based approach simulation is conducted for adaptive approach as well. Figure below shows the simulation results on estimating the mean and standard deviation of maximum structural response under seismic excitation. It can be observed that good estimation can be reached for both mean and standard deviation around sample number of 10.

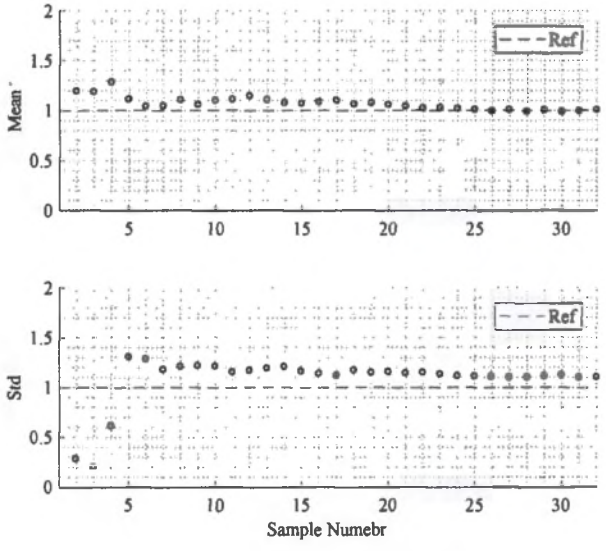

Figure 6-13: Sample Based Mean and Standard Deviation

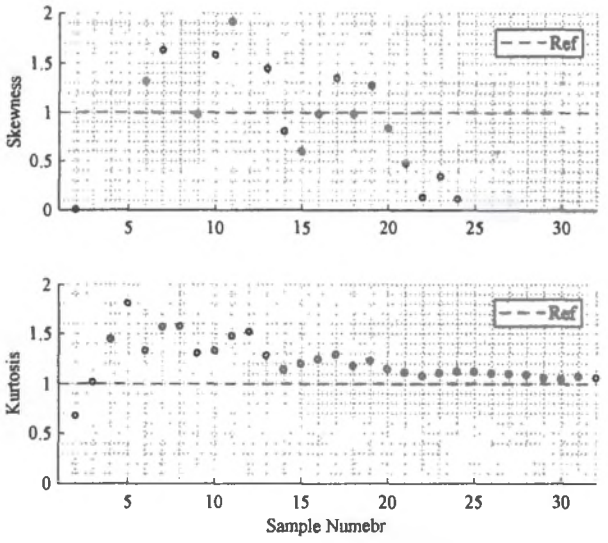

Figure 6-14: Sample Based Skewness and Kurtosis

Similar to Kriging method, figure of sample-based simulation results shows that larger number of samples are required for adaptive approach compare to sequence approach. Also, the mean value is waving back and forward, and the standard deviation reaches convergence around 35 samples, and the accuracy of estimation on standard deviation is lower than sequence approach.

6.4.2.2 Sample with different assigned probability

6.4.2.2.1 Procedure and Flowchart

The procedure of the Space-filling based approach is as following:

(1) Define maximum sample number n.

(2) Start with initial sample set P_{ini} ($P_{ini} \ll ED$) and evaluate the model response Y_{ini}.

(3) Enrich sample set with one new sample x_{k+1} with lowest GF discrepancy and evaluate the model response y_{k+1}. $P_{k+1} = P_k \cup x_{k+1}$, $Y_{k+1} = Y_k \cup y_{k+1}$

(4) Repeat procedure (2)-(3) if maximum sample number is not reached.

6.4.2.2.2 Computational Simulation Results

In this section, the estimation using samples generate by the procedure proposed in the previous section is conduct. From the figure below, it can be observed that the good accuracy can be reached for both mean and standard deviation estimation; however, convergence rate of estimation on standard deviation is lower compare to the estimation using samples with equal assigned probability since good estimation of standard deviation requires the sample number around 22.

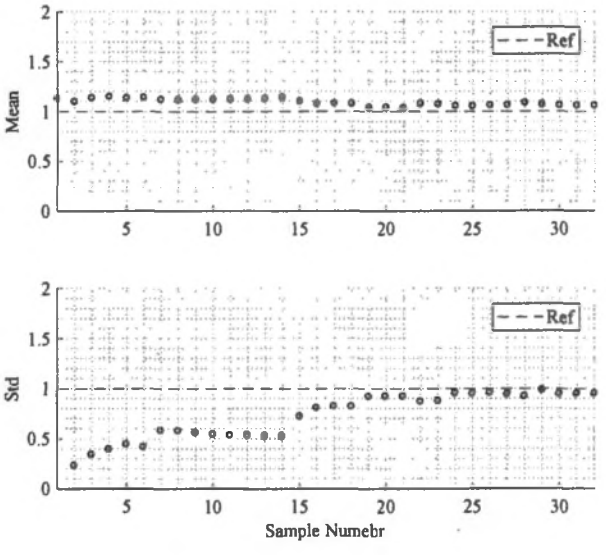

Figure 6-15: Sample based

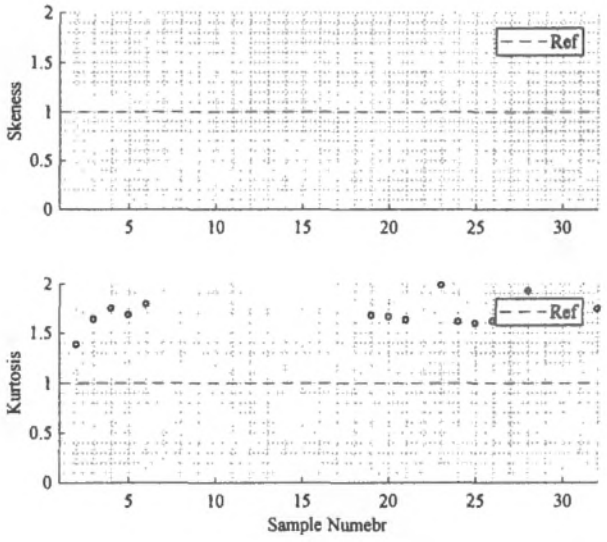

Figure 6-16: GF sequential Skewness and Kurtosis

6.5 Summary and Conclusion

In this chapter, different experiment design procedures are proposed, and different methods are introduced to estimate the mean and standard deviation of the maximum structural response of a SDOF system. From the results it can be observed that sequence approaches have better performance on estimation the mean and standard deviation compare to adaptive approaches. When using sequence approaches, similar observations can be made that PCE method, Kriging method, estimation use sample with equal assigned probability and estimation use sample with different assigned probability all gives good estimation with a small sample number. While for adaptive approach, all approaches require larger sample number to give good estimation. Estimation using samples with equal assigned probability gives good performance on mean and standard deviation with smallest sample number compare to PCE method, Kriging method and sample with different assigned probability. The estimation given by PCE method, Kriging method and samples with different assigned probability give better estimation on mean value than standard deviation.

In conclusion, under the different optimization criterion the sample selection is different, and the estimation based on these sample sets differs as well. Sequence approach has better performance compare to adaptive approach and estimation using samples with equal assigned probability has better performance compare to the estimations using PCE method, Kriging method and samples with different assigned probability.

Chapter 7: Framework of Hybrid Simulation to Account for Numerical and Experimental Substructure Uncertainties

7.1 Introduction

In Chapter 6, the framework of hybrid simulation account for numerical substructure is introduced. In this chapter, the uncertainty quantification and experiment design for hybrid simulation accounting for both numerical and experimental substructure uncertainties is introduced. Based on the results from Chapter 6, the sample-based approach is selected here. Since the PSO and MCMC simulation is applied to quantify the PSP uncertainties and the selection of NSP is based on the PSP, the sequence approach cannot be applied. Therefore, only adaptive approaches are used in this chapter. Three adaptive experiment designed procedures are proposed namely the space-filling max-min, star discrepancy adaptive and GF discrepancy adaptive design procedures. To evaluate the proposed procedures. Examples using space-filling max-min approach and GF discrepancy adaptive approach are performed. However, due to the computational limitation the star discrepancy adaptive approach is not performed and only gives the procedure. The example is based on the SDOF structural developed in chapter 2.

7.2 MC Simulation of Hybrid Simulation with Numerical Substructure Uncertainties

7.2.1 Definition of Uncertainties for Substructures

The target structure is the structure developed in Chapter 2, the mass and damping coefficient are considered to be NS and the β and γ value of Bouc-Wen model are considered to be PS. Refer to Chapter 2 for more detailed information about the structure. The PS parameters are identified through the PSO and MCMC analysis of the modified IMK model. The values of K, Λ, My and M_c/M_y are selected. Including the NSP and PSP, a total of six parameters are used during the experiment design procedure.

7.2.2 MC Simulation Results

First, the MC simulation using 100000 sample is conducted, and the mean, standard deviation, skewness and kurtosis of the corresponding maximum structural response is calculated through the simulation outputs. The results from MC simulation are as table below:

Table 7-1: MC simulation results

	Mean	Standard deviation	skewness	kurtosis
Reference	3.11	0.67	0.95	3.30

The MC simulation results will serve as a benchmark to evaluate the performance of methods proposed in this chapter.

7.3 Sample Based Adaptive Sampling Approach

In this section, three sample based adaptive experiment design procedures are proposed. These procedures guide the selection of NSP based on the PSP identification. After an experiment, the rotation and moment relationship at the bottom of the structure can be measured, and the modified IMK model is used by PSO and MCMC simulation to fit the measured moment under the measured rotation. From MCMC simulation result, the distributions of possible IMK model parameters $PSP_{k,PDF}^{i(j)}$ can be generated, and from PSO simulation result a set of best fit IMK model parameters $PSP_{k,PSO}^{i(j)}$ can be found. The $PSP_{k,HC}^{i(j)}$ can be determined as the probability of $PSP_{k,PSO}^{i(j)}$ in $PSP_{k,PDF}^{i(j)}$. After the PSP is identified, the NSP can be selected based on Space-filling Max-min, star discrepancy adaptive and GF discrepancy adaptive procedures.

7.3.1 Max-Min Based Enrichment

7.3.1.1 Procedure and Flowchart

The procedure of space-filling based approach is as follow:

(1) Select maximum sample number n.

(2) $NSP_{1,HC}^{i(J)}$ are defined to be 0.5. Convert $NSP_{1,HC}^{i(J)}$ to $NSP_1^{i(J)}$ and conduct a hybrid simulation.

(3) Conduct MCMC and PSO analysis to identify $PSP_{1,HC,1}^{i(J)}$.

(4) Select $NSP_{2,HC}^{i(J)}$ based on $PSP_{1,HC,1}^{i(J)}$ through space-filling procedure. Convert $NSP_{2,HC}^{i(J)}$ to $NSP_2^{i(J)}$ and conduct a hybrid simulation.

(5) Conduct MCMC and PSO analysis to get $PSP_{2,HC,1}^{i(J)}$. Change $PSP_{1,HC,1}^{i(J)}$ to $PSP_{1,HC,0}^{i(J)}$, and then update to $PSP_{1,HC,1}^{i(J)}$ based on $PSP_{2,PDF}^{i(J)}$.

(6) Repeat (4) – (5) if current sampler number is smaller than n.

7.3.1.2 Computational Simulation Results using Samples

From figures below, it can be observed that the space-filling max-min approach can give accurate estimation on the mean and standard deviation of the maximum structural response when the sample number is around 12. However, the accuracy on estimating the skewness and kurtosis is lower. From Figure 7-2 it can be observed that the error of skewness and kurtosis estimation both greater than 50%, and the increase of sample number do not have significant improvement on the estimation accuracy.

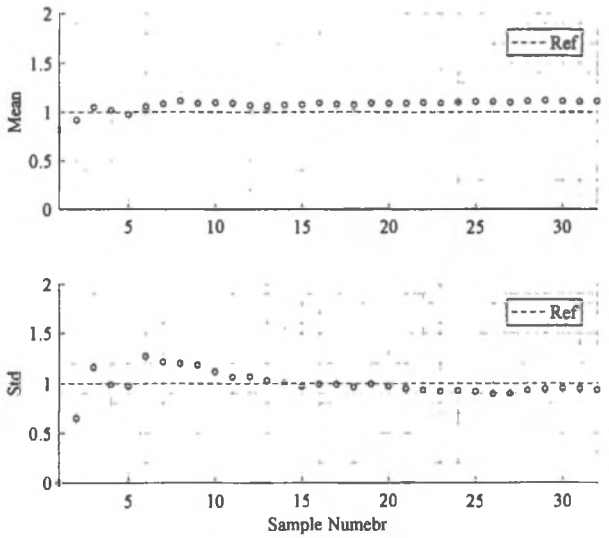

Figure 7-1: Mean and standard deviation

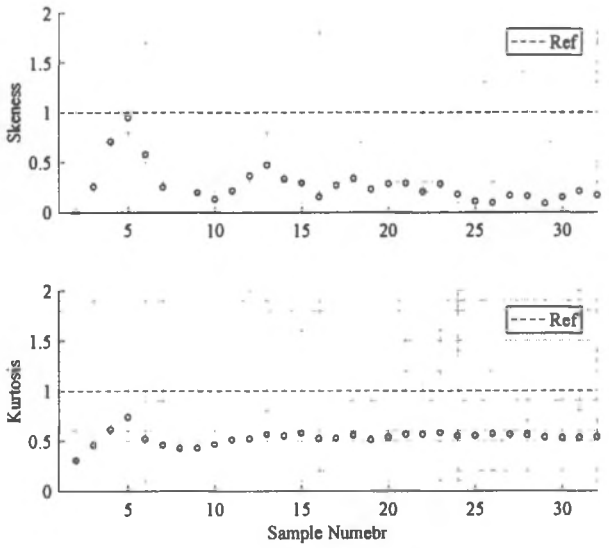

Figure 7-2: Skewness and kurtosis

7.3.2 Star Discrepancy Based Approach

7.3.2.1 Procedure and Flowchart

The procedure of star discrepancy-based approach is as follow:

(1) Select maximum sample number n.

(2) $NSP_{1,HC}^{i(J)}$ are defined to be 0.5. Convert $NSP_{1,HC}^{i(J)}$ to $NSP_1^{i(J)}$ and conduct a hybrid simulation.

(3) Conduct MCMC and PSO analysis to get $PSP_{1,HC,1}^{i(J)}$.

(4) Select $NSP_{2,HC}^{i(J)}$ based on $PSP_{1,HC,1}^{i(J)}$ through star discrepancy adaptive approach. Convert $NSP_{2,HC}^{i(J)}$ to $NSP_2^{i(J)}$ and conduct a hybrid simulation.

(5) Conduct MCMC and PSO analysis to get $PSP_{2,HC,1}^{i(J)}$. Change $PSP_{1,HC,1}^{i(J)}$ to $PSP_{1,HC,0}^{i(J)}$, and is updated to $PSP_{1,HC,1}^{i(J)}$ based on $PSP_{2,PDF}^{i(J)}$.

(6) Repeat (4) – (5) if current sampler number is smaller than n.

7.3.2.2 Discussion about star discrepancy-based approach

Since the modified IMK model is used for PSP parameter identification, and a total six parameters are involved for the calculation of star discrepancy, which leads to the heavy computational burden; therefore, the analysis of star discrepancy-based approach is not preformed and only the procedure is proposed. Instead, another discrepancy based approach using GF discrepancy is proposed and performed in the following section.

7.3.3 GF Discrepancy Based Approach

7.3.3.1 Procedure and Flowchart

The procedure of space-filling based approach is as follow:

(1) Select maximum sample number n.

(2) $NSP_{1,HC}^{i(j)}$ are defined to be 0.5. Convert $NSP_{1,HC}^{i(j)}$ to $NSP_1^{i(j)}$ and conduct a hybrid simulation.

(3) Conduct MCMC and PSO analysis to get $PSP_{1,HC,1}^{i(j)}$.

(4) Select $NSP_{2,HC}^{i(j)}$ based on $PSP_{1,HC,1}^{i(j)}$ through GF discrepancy adaptive approach. Convert $NSP_{2,HC}^{i(j)}$ to $NSP_2^{i(j)}$ and conduct a hybrid simulation.

(5) Conduct MCMC and PSO analysis to get $PSP_{2,HC,1}^{i(j)}$. Change $PSP_{1,HC,1}^{i(j)}$ to $PSP_{1,HC,0}^{i(j)}$, and is updated to $PSP_{1,HC,1}^{i(j)}$ based on $PSP_{2,PDF}^{i(j)}$.

(6) Repeat (4) – (5) if current sampler number is smaller than n.

7.3.3.2 Computational Simulation Results using Samples

From figures below, similar observation as max-min approach can be made. It can be observed that the GF adaptive approach can give accurate estimation on the mean and standard deviation of the maximum structural response, and the convergence can be reached with a small number of samples, but the sample number required to give accurate estimation on standard deviation requires larger sample number compare to max-min approach. Similar to max-min approach, the accuracy on estimating the skewness and kurtosis is low. From Figure 7-4 it can be observed that the error of skewness and kurtosis estimation both greater than 50%, and the increase of sample number do not have significant impact on improving the estimation accuracy as well.

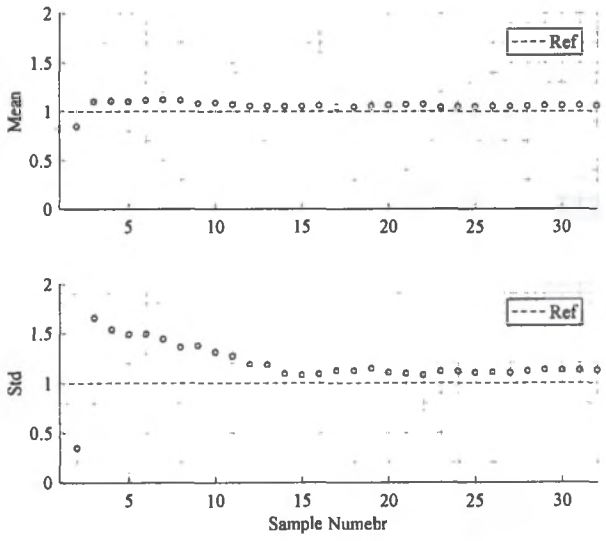

Figure 7-3: Mean and standard deviation

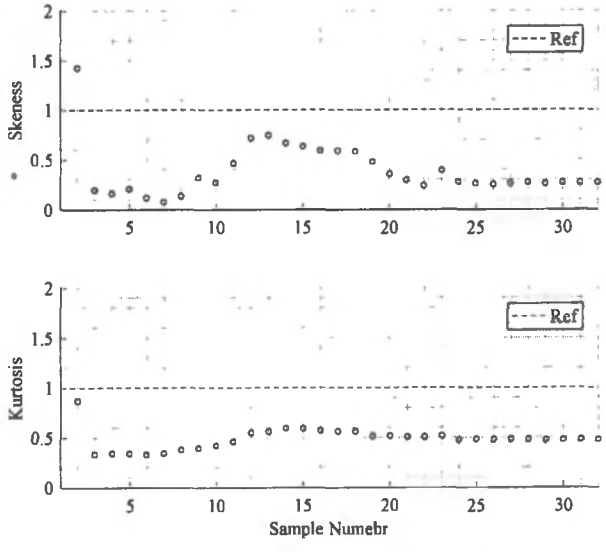

Figure 7-4: Skewness and kurtosis

7.4 Summary and Conclusion

In this section, three sample based approaches are proposed to estimate the mean, standard deviation, skewness and kurtosis of the maximum structural response of the system developed in Chapter 2. The simulation using max-min adaptive approach and GF adaptive are conducted and the results are discussed. Due to the dimensional involved in this example and the computation limit, the Star Discrepancy adaptive approach only gives the procedure and no simulation is conducted. From the simulation results from max-min approach and GF adaptive approach, it can be observed that these two approaches can give accurate estimation on the mean value, and the convergent can be reached in the early stage of the sampling process. The max-min approach can give accurate estimation on the standard deviation with around 12 samples, and the GF adaptive approach requires around 15 samples. For the estimation on skewness and kurtosis estimation, both max-min approach and GF adaptive approach cannot give accurate estimation, and the increase on sample number do not show significant impact on improving the estimation accuracy. It can be concluded that, when the uncertainty from PSP and NSP are involved, the sample required to give accurate estimation on mean and standard deviation increase compare to when only consider the NSP uncertainties. PSO and MCMC methods are applied for selecting the NSP paramours during the sampling process, the dimension may increase significantly based on the selection of model parameters used to identify PSP behavior. The computational effort increases when the dimensions increases, and approach like Star discrepancy based adaptive can become very expensive to simulation.

Chapter 8: Summary and Conclusion

8.1 Summary

In this study, the surrogate modeling techniques are used for uncertainty quantification of hybrid simulations. The different sampling methods are introduced and evaluate to reduce the required sample number for accurate estimation. The influence from different nonlinearities to the surrogate model estimation accurate is proposed, and evaluated though computational simulation results. The model parameter identification of experimental substructure is conducted through PSO and MCMC analysis. Then, the experimental design procedure of the hybrid simulation account for numerical substructure uncertainty and the hybrid simulation account for numerical and experimental substructure uncertainties are proposed. In the sections below, the findings are discussed.

8.2 Findings

In this study, the surrogate modeling techniques are used for uncertainty quantification of hybrid simulations. PCE and Kriging methods are used to predict the maximum structural response, maximum restoring force and maximum acceleration response of a structure, and PCE and Kriging methods can give accurate prediction with properly selected training sample set. Following that, different sampling methods are introduced and the performance of different sampling methods to the uncertainty quantification of system is discussed. Different sampling methods can give different accuracy on estimating the mean and standard deviation of maximum structure response of a structure, and it is important to selected sampling method to balance the computational burden and estimation accuracy. Then, the effects of different nonlinearities, natural period, damping ratio, ground motion and its scale to the uncertainty quantification using PCE are discussed, and it can be observed through computational simulation that these can have influence on PCE

estimation results, and researches need to consider these influences when conduct uncertainty quantification using PCE. After that, the model parameter identification using PSO and MCMC is introduced, and with the presentation of PSO, the model parameters of a phenomenological model can be identified given the experimental measurement, and with the presentation of MCMC the distribution of model parameters can be developed. Then based on these findings, the experimental design procedure of hybrid simulation account for numerical substructure uncertainty and hybrid simulation account for numerical and experimental substructures uncertainty are proposed, and it can be observed through the computational simulation results that with the proposed experimental design procedure, the mean and standard deviation of the maximum response of a structure can be accurately estimated with a small number of samples.

8.3 Future Work

8.3.1 Exploration of Correlation between Parameters

In this thesis, all the numerical substructure and experimental substructures are considered to be independent; however, in reality, some of the parameters can have correlation with each other, the exploration of accounting for these correlations between parameters and put into the experimental design procedure are needed in the future work.

8.3.2 Reduction of Number of Parameters for Uncertainties

During the simulation, one challenge is the heavy computational burden. When the number of parameters is considered during experiment design procedure increases, the computational burden increases dramatically as well. One solution to address this hardiness is reduction of the number of parameters for uncertainties, for example, through sensitivity analysis to remove the parameters that do not have significant impact on the system outputs of interest.

8.3.3 Extension the Framework to Multiple Experimental Substructures

In this thesis, only one experimental substructure is considered. The extension of the framework to multiple experimental substructure needed to be considered as well.

8.3.4 Inclusion of Uncertainties from Ground Motions

As mentioned in chapter 1, there are uncertainties from ground motions as well. Also, from the simulation in chapter 4, it can be observed that the ground motion can have influence on the estimation results. In the future work, these uncertainties from ground motions will be included as well.

8.3.5 Expansion of Computational Simulation to Complex Structures

In this study, the proposed methods are validated through simple structures, for example the SDOF structure and the column only FEM structure. The future work on conducting simulation to more complex structures like frames will be explored.

8.3.6 Experimental Implementation

In this study, the proposed methods are evaluated based on computational simulation. This is an idealization of actual test condition where, for example, there will be no noise involved during the simulation. To validate the proposed method, the next step will be extended the proposed methods into a real-time hybrid simulation conducted in laboratory. The proposed method will be implemented in laboratory and the performance of the methods can be then evaluated.

8.3.7 Extension to Real-Time Hybrid Simulation through Accounting for Uncertainties from Servo-Hydraulic Systems

Also, in the future, the uncertainties from Servo-Hydraulic systems will be considered into the frame work as well. Therefore, the uncertainty from numerical substructure, experimental substructure, ground motion and servo-hydraulic system are considered when doing the experimental design.

References

[1] Abbiati, G., Marelli, S., Sudret, B., Bursi, O., and Stojadinovic, B. (2015). "Uncertainty Propagation and Global Sensitivity Analysis in Hybrid Simulation using Polynomial Chaos Expansion." CIVIL-SOF-COMP (CSC) 2015, Prague.

[2] Asmussen, S., and Glynn, P. W. (2007). Stochastic Simulation: Algorithms and Analysis, *Springer*.

[3] Baber, T. T., and Noori, M. N. (1985). "Random vibration of degrading, pinching systems." *Journal of Engineering Mechanics*., 111(8), 1010-1026.

[4] Baber, T. T., and Noori, M. N. (1985). "Random vibration of degrading, pinching systems." *Journal of Engineering Mechanics*, 111(8), 1010-1026.

[5] Bayer, V., Dorka, U.E., Füllekrugc, U., and Gschwilmd, J. (2005). "On real-time pseudo-dynamic substructure testing: algorithm, numerical and experimental results." *Aerospace Science and Technology*., 9(3), 223-232.

[6] Beck, J. L. (1989) ''Statistical system identification of structures.'' *Proc.,5th Int. Conf. Structural Safety and Reliability*, ASCE, New York,1395–1402.

[7] Beck, J. L., and Au, S.-K. (2002). "Bayesian updating of structural models and reliability using Markov chain Monte Carlo simulation." *J. Eng. Mech.*, 10.1061/(ASCE)0733-9399(2002)128:4(380), 380–391.

[8] Beck, J. L., and Katafygiotis, L. (1998). "Updating models and their uncertainties. I. bayesian statistical framework." *J. Eng. Mech.*, 10.1061/ (ASCE)0733 9399(1998)124:4(455), 455–461.

[9] Byrd, R. H., Hribar, M. E., Nocedal, J. (1997). "An interior point algorithm for large scale nonlinear programming." *SIAM Journal on Optimization*, 9(4), 877-900.

[10] Caicedo, J. M., Jiang, Z., and Baxer, S. C. (2016). "Including Uncertainty in Modeling the Dynamic Response of a Large-Scale 200 kN Magneto-Rheological Damper." *ASCE-ASME J. Risk Uncertainty Eng. Syst., Part A: Civ. Eng.* doi: 10.1061/AJRUA6.0000873.

[11] Cameron, R. H., and Martin, W. T. (1947). "The orthogonal development of non-linear functionals in series of Fourier-Hermite functionals." *Annals of Mathematics.*, 48(2), 385-392.

[12] Chen, C., and Ricles, J. M. (2008). "Development of direct integration algorithms for structural dynamics using discrete control theory." *Journal of engineering mechanics.*, 134, 676.

[13] Chen, C., and Ricles, J. M. (2009). "Improving the inverse compensation method for real-time hybrid simulation through a dual compensation scheme." *Earthquake Engineering & Structural Dynamics.*, 38(10), 1237-1255.

[14] Chen, C., and Ricles, J. M. (2011). "Analysis of implicit HHT-α integration algorithm for real-time hybrid simulation." *Earthquake Engineering & Structural Dynamics.*, 41(5), 1021-1041.

[15] Chen, J., Yang, J., and Li, J. (2016). "A GF-discrepancy for point selection in stochastic seismic response analysis of structures with uncertain parameters." *Structural Safety.*, 59. 20-31. 10.1016/j.strusafe.2015.11.001.

[16] Christopoulos, C., Tremblay, R., Kim, H.-J., and Lacerte, M. (2008). "Self-Centering Energy Dissipative Bracing System for the Seismic Resistance of Structures: Development and Validation", *Journal of Structural Engineering ASCE*, 134(1), 96-107.

[17] Collins, J. D., Hart, G. C., Hasselman, T. K., and Kennedy, B. (1974). "Statistical identification of structures." *AIAA J.*, 12, 185–190.

[18] Crestaux, T., LeMaitre, O., and Martinez, J. M. (2009). "Polynomial chaos expansion for sensitivity analysis." *Reliability Engineering & System Safety.*, 94(7), 1161-1172.

[19] Deng, P., Pei, S., Lindt, J., and Zhang, Chao. (2018). "Experimental Investigation of Seismic Uncertainty Propagation through Shake Table Tests." *Journal of Structural Engineering.* 10.1061/(ASCE)ST.1943-541X.0001975.

[20] Dermitzakis, S. N., and Mahin, S.A. (1985). "Development of sub-structuring techniques for on-line computer controlled seismic performance testing." Report to the National Science Foundation, Earthquake Engineering Research Center, Report No. UCB/EERC-85/04.

[21] Doh, J., Kim, Y., and Lee, J. (2018). "Reliability-based robust design optimization of gap size of annular nuclear fuels using kriging and inverse distance weighting methods." *Engineering Optimization*, 50(12), 2161–2176.

[22] Dorka, U. E. (2002). "Hybrid experimental - numerical simulation of vibrating structures." International Conference WAVE2002. Okayama, Japan.

[23] Dubourg, V., Sudret, B., and Bourinet, J. M. (2011). "Reliability-based design optimization using kriging surrogates and subset simulation." *Structural and Multidisciplinary Optimization.*, 44(5), 673–690.

[24] Fajraoui, N., Marelli, S., and Sudret, B. (2017). "On optimal experimental designs for Sparse Polynomial Chaos Expansions." *SIAM. J. Sci. Comput.*, 38(1), 385–411.

[25] Fang, K. T., Wang, Y. (1993). Number-theoretic methods in statistics. *CRC Press,* Florida.

[26] Gamerman, D. (1997). Ma*rkov Chain Monte Carlo – Stochastic simulation for Bayesian inference*. Chapman & Hall.

[27] Ghanem., R. (1999). "Stochastic Finite Elements with Multiple Random Non-Gaussian Properties." *Journal of Engineering Mechanics.*, 125(1), 26-26.

[28] Gidaris, I., Taflanidis, A. A., and Mavroeidis, G. P. (2015). "Kriging metamodeling in seismic risk assessment based on stochastic ground motion models: Seismic Risk Assessment Through Kriging Metamodeling." *Earthquake Engineering & Structural Dynamics*., 44. 10.1002/eqe.2586.

[29] Hakuno, M., Shidawara, M., and Hara, T. (1969). "Dynamic Destructive Test of a Cantilever Beam, Controlled by an Analog-Computer." *Proceedings of the Japan Society of Civil Engineers*, 171, 1-9.

[30] Halton, J. (1960). "On the efficiency of certain quasi-random sequences of points in evaluating multidimensional integrals." *Numerische Math*., 2(1), 84–90.

[31] Halton, J. (1964). "Algorithm 247: Radical-inverse quasi-random point sequence." *ACM*., 701, doi:10.1145/355588.365104

[32] Han, Y. Z., Gao, X. S., and Li, L. Z. (2007). "Kriging model-based Multi-disciplinary Design Optimization for Turbine Blade." *Journal of Aerospace Power*., 22(7), 1055-1059 (in Chinese).

[33] Hastings, W. K. (1970) "Monte Carlo sampling methods using Markov chains and their applications." *Biometrika*, 57, 97–109.

[34] Hilber, H. M., Hughes, T. J., and Taylor, R. L. (1977). "Improved numerical dissipation for time integration algorithms in structural dynamics." *Earthquake Engng. Struct. Dyn*., 5, 283-292.

[35] Horiuchi, T., Inoue, M., and Konno, T. (1999). "Development of a real-time hybrid experimental system using a shaking table," *JSME Int'l J., Ser. C*., 42(2), 255-264.

[36] Hughes, T. J. R. (1983). "Analysis of transient algorithms with particular reference to stability behavior." *Computational Methods for Transient Analysis.*, 67-155.

[37] Hughes, T. J. R., Pister, K.S., and Taylor, R. L. (1979). "Implicit-explicit finite elements in nonlinear transient analysis." *Computer Methods in Applied Mechanics and Engineering*, 17/18 (1), 159-182.

[38] Hwang, H., Pezeshk, S., Lin, Y. W., He, J., and Chiu, J. M. (2001). "Generation of Synthetic Ground Motion." Center for Earthquake Research and Information and Department of Civil Engineering, The University of Memphis.

[39] Isukapalli, S. S., Roy, A., and Georgopoulos, P. G. (1998). "Stochastic Response Surface Methods (SRSMs) for Uncertainty Propagation: Application to Environmental and Biological Systems." *Risk Analysis.*, 18(3), 351-363.

[40] Kaymaz, I. (2005). "Application of Kriging method to structural reliability problems." *Structural Safety.*, 27(2), 133-151.

[41] Kaymaz, I. (2005). "Application of kriging method to structural reliability problems." *Structural Safety.*, 27(2), 133-151.

[42] Kennedy, J., and Eberhart, R. (1995). "Particle Swarm Optimization." *Proceedings of IEEE International Conference on Neural Networks*, 1942–1948.

[43] Krige, D. G. (1951). "A statistical approach to some basic mine valuations problems on the Witwatersrand." *Journal of the Chemical, Metallurgical and Mining Engineering Society of South Africa.*,52(6), 119-139.

[44] Laine, Marko. (2008) "Adaptive MCMC methods with application in environmental and geophysical models." Phd dissertation, Lappeenranta University of Technology, Lappeenranta, Finland.

[45] Lataniotis, C., Marelli, S., and Sudret, B. (2017). "UQLab user manual – Kriging (Gaussian process modelling)." *Report UQLab-V1.0-105,* ETH Zurich.

[46] Li, J. (2013). "Study of Surrogate Model Approximation and Surrogated-enhanced structural reliability analysis." Doctoral dissertation, Shanghai Jiao Tong University.

[47] Li, X., Cheng, J., Liu, Z., and Wu, Z. (2014). "Robust Optimization for Dynamic

Characteristics of Mechanical Structures Based on Double Renewal Kriging Model." *Journal of Mechanical Engineering.*, 50(3), 165-173.

[48] Lignos, D. G. (2013). Web-Based Interactive Tools for Performance-Based Earthquake Engineering Steel W Shape Database. Retrieved from http://dimitrios-lignos.research.mcgill.ca/databases/steel/

[49] Lignos, D.G., and Krawinkler, H. (2011). "Deterioration modeling of steel components in support of collapse prediction of steel moment frames under earthquake loading." *Journal of Structural Engineering.*, 137 (11), 1291-1302.

[50] Liu, J., Han, Z. H., Song, W. P. (2012). "Efficient Kriging-based optimization Design of Transonic Airfoils: Some Key Issues." *AIAA-2012-0967*, Reston.

[51] Liu, Z., Zhang, J., Wang, C., Tan, C., and Sun, J. (2013). "Optimized Kriging model and important sampling based structural reliability assessment." *Acta Aeronautica et Astronautica Sinica.*, 34(6), 1347-1355.

[52] Lophaven, S. N., Nielsen, H. B., and Søndergaard, J. (2002). "DACE - A Matlab Kriging Toolbox." Technical University of Denmark.

[53] Lucor, D., and Karniadakis, G. (2004). "Adaptive generalized polynomial chaos for nonlinear random oscillators." *SIAM J. Science Computation.*, 26(2), 720–735,

[54] Magonette, G. (2001). "Development and application of large-scale continuous pseudo-dynamic testing techniques." *Physical and Engineering Sciences.*, 359, 1771-1799.

[55] Mahin, S.A. and Williams, M. (1981) "Computer Controlled Seismic Performance Testing." *Proceedings, Second ASCE-EMD Specialty Conference on Dynamic Response of Structures*, Atlanta, Georgia.

[56] Marelli, S., and Sudre, B. (2017). "UQLab user manual – Polynomial Chaos

Expansion." *Report UQLab-V1.0-104,* ETH Zurich.

[57] Marelli, S., and Sudret, B. (2014). "UQLab: A framework for uncertainty quantification in Matlab." *Proc. 2nd Int. Conf. on Vulnerability, Risk Analysis and Management (ICVRAM2014)*, Liverpool, United Kingdom, 2554-2563.

[58] Masayoshi, N., Hiroto, k., and Eiji, T. (1992). "Development of real-time pseudo dynamic testing." *Earthquake Engineering & Structural Dynamics.*, 21, 79 – 92.

[59] Matheron, G. (1963). "Principle of geo-statistics." *Economic Geology.*, 58, 1246-1266.

[60] McClamroch, N. H., Serakos, J., and Hanson, R. D. (1981). "Design and Analysis of the Pseudo-dynamic Test Method." UM EE 81R3, University of Michigan, Ann Arbor, 1981.

[61] Mercan, O., and Ricles, J. M. (2007). "Stability and accuracy analysis of outer loop dynamics in real-time pseudodynamic testing of SDOF systems." *Earthquake Engng. Struct. Dyn.*, 36, 1523-1543.

[62] Metropolis, N., Rosenbluth, A. W., Rosenbluth, M. N., and Teller, A. H. (1953). "Equations of state calculations by fast computing machines." *J. Chem. Phys.*, 21(6): 1087–1092.

[63] Mooney, C. Z. (1997). Monte Carlo Simulation. *Sage Publications.*

[64] Morokoff, W. J., and Caflisch, R. E. (1995). "Quasi-Monte Carlo integration." *J. Comput. Phys.*, 122(2), 218-230.

[65] Nakashima, M., Kaminosono, T., Ishida, M., and Ando, K. (1990). "Integration techniques for substructure pseudo dynamic testing." Proc. 4th U.S. Natl. Conf. on Earthquake Eng., Palm Springs, Calif., II, 515-524.

[66] Nakashima, M., Kato, H. and Takaoka, E. (1992). "Development of real-time pseudo dynamic testing." *Earthquake Engineering. Structural. Dynamic.*, 21, 79-92.

[67] Niederreiter, H. (1992). *Random Number Generation and Quasi-Monte Carlo Methods.* Society for Industrial and Applied Mathematics.

[68] Okada, T. (1980). "A Simulation of Earthquake Response of Reinforced Concrete Building Frames to Bi-D directional Ground Motion by IIS Computer-Actuator On-Line System." *Proceedings, 7th Word Conference on Earthquake Engineering*, Istanbul, Turkey.

[69] Onorato, G., Loeven, G., Ghorbaniasl, G., Bijl, H., and Lacor, C. (2010). "Comparison of intrusive and non-intrusive polynomial chaos methods for CFD applications in aeronautics." *Fifth European Conference on Computational Fluid Dynamics (ECCOMAS).*

[70] OpenSees. (2010). "Open system for earthquake engineering simulation." Pacific Earthquake Engineering Research Center (PEER).

[71] Pan, P., Tada, M., and Nakashima, M. (2005). "Online hybrid test by internet linkage of distributed test-analysis domains." *Earthquake Engineering & Structural Dynamics.*, 34(11), 1407-1425

[72] Pan, P., Tomofuji, H., Wang, T., Nakashima, M., Ohsaki, M., and Mosalam, K.M. (2006). "Development of Peer to Peer (P2P) Internet Online Hybrid Test System." *EESD.*,35, 867-890.

[73] Pronzato, L. (2017). "Minimax and maximin space-filling designs: some properties and methods for construction." *Journal de la Societe Française de Statistique, Societe Française de Statistique et Societe Mathematique de France.*,158(1), 7-36.

[74] Rezaeian, S. and Kiureghian, A. D. (2010). "Simulation of synthetic ground motions

for specified earthquake and site characteristics." *Earthquake Eng. Struct. Dyn.*, 39(10), 1155–1180.

[75] Gelman, A., Roberts, G. O., and Gilks, W. R. (1996). *Bayesian Statistics 5*. Clarendon, Oxford.

[76] Sack, J., Welch, W. J., Mitchell, T. J., and Wynn, H. O. (1989). "Design and analysis of computer experiments." *Statistical Science.*, 4(4), 409-423.

[77] Schellenberg, A. H., Mahin, S. A., and Fenves, G. L. (2009). "Advanced Implementation of Hybrid Simulation." PEER Technical Report 2009/104.

[78] Schobi, R., Marelli, S., and Sudret, B. (2017). "UQLab user manual – PC-Kriging." *Report UQLab-V1.0-109,* ETH Zurich.

[79] Shin, Y., and D. Xiu (2016). "Nonadaptive quasi-optimal points selection for least-squares linear regression." *SIAM J. Sci. Comput.*, 38(1), 385–411.

[80] Shing, P.B., and Mahin, S. A. (1983), "Experimental Error Propagation in Pseud-dynamic Testing." UCBIEERC-83/12, Earthquake Engineering Research Center. University of California, Berkeley.

[81] Shing, P.B., Vannan, M.T., and Cater, E. (1991). "Implicit time integration for pseudodynamic tests." *Earthquake Engineering and Structural Dynamics.*, 20(6), 551-576.

[82] Sobol, I. M. (1967). "Distribution of points in a cube and approximate evaluation of integrals." *Zh. Vych. Mat. Mat. Fiz.*, 7, 784-802 (in Russian).

[83] Sobol, I. M. (1993). "Sensitivity Estimates for Nonlinear Mathematical Models." *Mathematical Modelling in Civil Engineering.*, 1(4), 407–414.

[84] Sobol, I. M. (2001). "Global sensitivity indices for nonlinear mathematical models and their monte carlo estimates." *Mathematics & Computers in Simulation,* 55(1–3), 271-280.

[85] Song, X., Aimadian, M., and Southward, S. C. (2005). "Modeling magnetorheological dampers with application of nonparametric approach." *Intell. Mater. Syst. Struct.*, 16(5), 421–432.

[86] Spencer, B., Finholt, T. A., and Foster, I. (2004). "NEES grid: a distributed Collaboratory for advanced earthquake engineering experiment and simulation." *In: Proceedings of the 13th World Conference on Earthquake Engineering*. Vancouver B C: 13 WCEE Secretariat.

[87] Sudret, B. (2008). "Global Sensitivity Analysis Using Polynomial Chaos Expansions." *Reliability Engineering & System Safety.*, 93, 964–979.

[88] Sudret, B., and Mai, C.V. (2013). "Computing seismic fragility curves using polynomial chaos expansions." *Proc. 11th~Int. Conf. Struct. Safety and Reliability (ICOSSAR'2013),* New York, USA.

[89] Takanashi, K. (1975) "Nonlinear Earthquake Response Analysis of Structures by a Computer-Actuator On-Line System." Bull. of Earthquake Resistant Structural Research Center, Institute of Industrial Science, University of Tokyo.

[90] Takanashi. K. (1980). "Inelastic Response of H-Shaped Columns to Two-Dimensional Earthquake Motions." Bull. of Earthquake Resistant Structural Research Center, Institute of Industrial Science, University of Tokyo.

[91] Thewalt, C. R., and Mahin, S. A. (1987). "Hybrid solution technique for generalized pseudo dynamic testing." EERC-87/09, Earthquake Engineering Research Center, UC-Berkeley.

[92] Wan, X., Karniadakis, G. E. (2006). "Multi-element generalized polynomial chaos for arbitrary probability measure." *SIAM Journal on Scientific Computing.*, 28(3), 901-928.

[93] Wang, D. (2012). "Seismic fragility analysis and probabilistic risk analysis of steel frame structural." Harbin Institute of Technology, Master Thesis.

[94] Wang, K., Tsai, K., and Wang, S. (2007). "ISEE: internet-based simulation for earthquake engineering—part II: the application protocol approach." *Earthquake Engineering & Structural Dynamics*., 36(15), 2307-2323.

[95] Wang, Z., and Shafieezadeh, A. (2018). "REAK: Reliability analysis through Error rate-based Adaptive Kriging." *Reliability Engineering & System Safety*., 10.1016/j.ress.2018.10.004.

[96] Wiener, N. (1938). "The homogeneous chaos." *American Journal of Mathematics*., 60(4), 897-936.

[97] Xie, Y., Yu, H., Cheng, J., Ruan, X. (2007). "The Reliability Estimation Based on Kriging Model." *Journal of Shanghai Jiaotong University*., 2. (in Chinese)

[98] Xiu, D. (2010). *Numerical Methods for Stochastic Computations- A Spectral Method Approach.* Princeton University Press.

[99] Xiu, D., and Karniadakis, G. (2002). "The Wiener-Askey polynomial chaos for stochastic differential equations." *SIAM Journal on Scientific Computing*., 24(2), 619–644.

[100] Yang, Y., Hsieh, S., and Tsai, K. (2007). "ISEE: internet-based simulation for earthquake engineering—part I: database approach." *Earthquake Engineering & Structural Dynamics*., 36(15), 2291-2306.

[101] Yao, S. B., Guo, D. L., and Sun, Z. X. (2013). "Multi-objective optimization of the streamlined head of High - speed Trains Based on the Kriging model." *Science China*., 43(2), 186-200 (in Chinese).

[102] Yu, X., and Lu, D. (2012). "Seismic collapse fragility analysis considering structural uncertainties." *Journal of Building Structures*., 33(10), 8-14.

[103] Zhang, X. (2004). "Seismic Performance of Wide Flange Beam to Deep-Column Moment Connections." Ph.D dissertation, Lehigh University.

[104] Zhao, Y., Asce, M and Lu, Z. (2007). "Fourth-Moment Standardization for Structural Reliability Assessment." *Journal of Structural Engineering.*, 10.1061/(ASCE)0733-9445(2007)133:7(916).